STEREOCILIA MORPHOGENESIS AND MAINTENANCE IS DEPENDENT ON THE DYNAMICS OF ACTIN CYTOSKELETAL PROTEINS

by

Pallabi Roy

A Dissertation

Submitted to the Faculty of Purdue University

In Partial Fulfillment of the Requirements for the degree of

Doctor of Philosophy

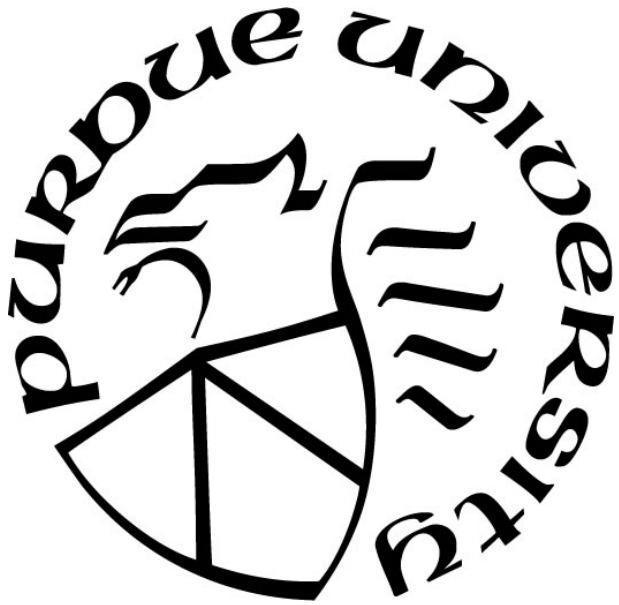

Department of Biology

Indianapolis, Indiana

May 2019

THE PURDUE UNIVERSITY GRADUATE SCHOOL
STATEMENT OF COMMITTEE APPROVAL

Dr. Benjamin J. Perrin, Chair
Department of Biology
Dr. Simon Atkinson
Department of Biology
Dr. Teri Belecky-Adams
Department of Biology
Dr. A.J. Baucum
Department of Biology
Dr. Eri Hashino
Department of Otolaryngology

Approved by:

Dr. Theodore R. Cummins
Head of the Graduate Program

Dedicated to my Husband, my parents and my sister

ACKNOWLEDGMENTS

I would like to extend my deepest gratitude towards my Ph.D. mentor, Dr. Benjamin J. Perrin. I am indebted to him for believing in me and accepting me in his lab. This thesis would not have been possible without his constant help, cooperation, motivation, encouragement and trust. He not only let me work on the projects ongoing in his lab, but also encouraged me to work in collaborative projects outside his lab. That has really helped me to grow professionally and personally during my graduate life. I thank Ben for keeping his doors always open for questions, doubts and queries even beyond regular lab hours. He has been extremely supportive in each step of my Ph.D. tenure in his lab. I consider myself extremely lucky to have been trained under such a wonderful mentor. I bear deep rooted respect for him.

I extend my heartfelt gratitude to Dr. Simon Atkinson without whose priceless cooperation, support and guidance I possibly wouldn't have achieved this degree. I am also thankful to him for being on my Ph.D. thesis Committee. I would also like to extend my gratitude and reverence towards Dr. Teri Belecky-Adams, Dr. A.J. Baucum and Dr. Eri Hashino, the other esteemed members on my Ph.D. thesis Committee. My Committee members have always been extremely supportive and helpful, providing me with constructive ideas and precious feedback towards my thesis.

I thank department of Biology faculty members, especially Dr. Kathy Marrs who has been immensely helpful and supportive during my graduate studies and Dr. Theodore Cummins for his academic and administrative cooperation and beyond. I also thank the department for giving me this wonderful platform for carrying out my graduate studies and help me develop scientifically. I am indeed thankful to the excellent core facilities including state of the art vivarium setup, without which this work would have been impossible.

I am grateful to my wonderful lab mates Jamis McGrath, Garrett Brickens, Chun-Yu Tung, Jeongwon Lee and Matthew Anderson for their wholehearted support during my PhD research and for keeping the lab environment extremely friendly.

I would like to express my gratitude to my husband, Dr. Shubham Chakravarty, for being by my side through thick and thin and providing me with constant care, love, support and guidance that helped me survive over here.

I am extremely grateful to my parents for their blessings and for believing in me and sending me so far away from home. I am thankful to my dad, Mr. Prabir Kumar Roy for being my inspiration and for constantly motivating me for higher studies. I thank my mom, Mrs. Ruma Roy for always being highly supportive and constantly providing me with positive energy that kept me going forward. I also thank my dearest sister, Namrata Roy, for her constant support, love, encouragement and best wishes.

I would also like to thank my parents-in-law, Dr. Kalyan Chakrabarti and late Mrs. Archana Chakravarty for their blessings.

Finally, I thank the Almighty, for helping me achieve my goals.

TABLE OF CONTENTS

LIST OF TABLES

LIST OF FIGURES

LIST OF ABBREVIATIONS

OC	organ of Corti
IHC	Inner hair cell
OHC	Outer hair cell
AHL	Age-related hearing loss
MET	Mechanoelectrical transduction
ABR	Auditory Brainstem Response
SEM	Scanning electron microscopy
MIMS	Multi-isotope imaging mass spectrometry
FRAP	Fluorescence recovery after photobleaching
$t_{1/2}$	Half-maximal recovery
UTLD	Upper Tip link density
LTLD	Lower Tip link density
TALEN	Transcription activator-like effector nucleases
THD1	Tail homology domain1
ABM	Actin Bundling Module
PAB	Parallel Actin Bundles

ABSTRACT

Author: Roy, Pallabi. PhD
Institution: Purdue University
Degree Received: May 2019
Title: Stereocilia Morphogenesis and Maintenance is Dependent on the Dynamics of Actin Cytoskeletal Proteins
Committee Chair: Benjamin J. Perrin

Age-related hearing loss is an acute health problem affecting people worldwide, often arising due to defects in the proper functioning of sensory hair cells in the inner ear. The apical surface of sensory hair cells contains actin-based protrusions known as stereocilia, which detect sound and head movements. Since hair cells are not regenerated in mammals, it is important to maintain the functioning of stereocilia for the life of an organism to maintain hearing ability. The actin filaments within a stereocilium are extensively crosslinked by various actin crosslinking proteins, which are important for stereocilia development and maintenance. Multiple studies have shown that the stereocilia actin core is exceptionally stable whereas actin is dynamic only at the tips of stereocilia. However, whether the actin crosslinking proteins, which are nearly as abundant as actin itself, are similarly stable or can freely move in and out of the core remains unknown. Loss or mutation of crosslinkers like plastin-1, fascin-2, and XIRP2 causes progressive hearing loss along with stereocilia degeneration while loss of espin prevents stereocilia from even developing properly. Do these phenotypes stem from an unstable stereocilia core? Does crosslinking confer stability to the core? To address these questions, we generated novel transgenic reporter lines to monitor the dynamics of actin in mice carrying fascin-2^{R109H} mutation and espin null mice and also to study the dynamics of actin crosslinkers, *in vivo* and *ex-vivo*. We established that actin crosslinkers readily exchange within the highly stable F-actin structure of the stereocilia core. In addition, we determined that stereocilia degeneration in mice carrying fascin-2^{R109H} mutation and espin null mice could possibly occur due to a less stable actin core. These studies suggest that dynamic crosslinks stabilize the core to maintain proper stereocilia functioning. Future work warrants understanding the reason behind the importance of dynamic crosslinks within a stable stereocilia core. Actin stability not only depends on actin crosslinkers, but also on actin filament composition as evident from distinct stereocilia degeneration and progressive hearing loss patterns in hair-cell specific knockout of actin isoforms. Although β- and γ- actin polypeptide sequences differ by only

four amino acids, whether the latter determine the unique function of each cytoplasmic actin isoform was previously unknown. Here we determined that these four critical amino acids determine the unique functional importance of β-actin isoform in sensory hair cells. Taken together, our study demonstrates that actin cytoskeletal proteins are important for the morphogenesis and maintenance of stereocilia.

CHAPTER 1. INTRODUCTION

The inner ear has the ability to detect sound-induced vibrations, head movement and gravity. The two distinct organs located inside the inner ear are responsible for carrying out these specific functions: the cochlea and the vestibular canals. While the cochlea is responsible for detecting sound waves, vestibular canals detect changes in head position and gravity. The cochlea houses the organ of Corti which consists of 3 rows of mechanosensory outer hair cells (OHCs) and 1 row of mechanosensory inner hair cells (IHCs) surrounded by support cells. Each hair cell on its apical surface has numerous actin-based protrusions called stereocilia that are the key players in converting sound waves to electrical signals to be received by the brain. The IHC and OHC stereocilia are arranged into bundles with 3 rows of stereocilia (designated as row 1, 2 and 3) orchestrated in an increasing height giving the appearance of a staircase (Figure 1.1). Stereocilia are deflected in response to sound vibrations and they tug on the tip links, filamentous structures that join the tip of a lower stereocilium to the side of a taller neighboring stereocilium. Tip links convey force to the mechanotransduction channels of hair cells, which are localized at the tips of shorter row stereocilia. The tension generated opens the mechanically gated ion channels, located at the tips of shorter row stereocilia, allowing ion influx and resulting in depolarization of the hair cells. Precise regulation of the length of each row of stereocilia is critical for hearing as loss of stereocilia or changes in their lengths disrupts the mechanotransductive function of the cell. Since hair cells are not renewed in mammals, it is crucial that these intricate microscopic structures are maintained for the entire life of an organism to preserve hearing ability. Thus, understanding stereociliary hair bundle structure and composition, along with their development and maintenance is pivotal to understanding the pathophysiology of deafness.

1.1 Age-related hearing loss

Hearing loss in humans has congenital, progressive, and often age-related forms. Age related hearing loss (AHL) is common, affecting approximately 1/3rd of the world population belonging to the age group of 65-75 years [1, 2]. AHL has a mixed etiology, arising from various factors such as loud noise, chemical exposure, ototoxic medications, oxidative stress, and genetic reasons. While studying the genes underlying deafness in inbred murine models, considerable knowledge

has been gained regarding many aspects of hair cell biology, including their development, cytology and how they behave as mechanosensors. Murine models are extensively used in hearing research because they are short-lived with well-characterized genetics and provides researchers with an ability to adjust environmental factors as per experimental conditions.

Some of the inbred strains used in hearing research include C57BL/6J (B6), CBA/CaJ (CBA) and DBA/2J. The most widely used strain for studying early onset AHL is B6 because of its high-frequency hearing loss by 5-6 months of age along with degeneration and loss of cochlear hair cells [3-9]. In contrast, CBA mice are not prone to AHL until 15 months of age and thus are often used as controls in age-related hearing loss research [3, 10] [11].

The onset of hearing loss in DBA/2J mice occurs at an earlier age than that observed in B6 mice [12]. Both the DBA/2J and B6 inbred murine models harbor the ahl allele of cadherin 23, which produces a truncated variant of Cadherin 23 protein (tip link transmembrane protein Cadherin 23, described in detail below). This mutation is frequently associated with reports of AHL. Additionally, DBA/2J strain is also mutated at the ahl8 locus on chromosome 11. This mutation, when present in conjunction with the $Cdh23^{ahl}$ mutation, results in hearing loss that begins at a very early age [13]. The causative gene for ahl8 is fascin-2, which is an actin crosslinking protein abundant in hair cells [14].

Structural and morphological properties of stereocilia are subject to noise-induced damage. The proteins encoded by $1/3^{rd}$ of all the deafness-related genes localize to the stereocilia bundle [15]. These proteins are predominantly cytoskeletal proteins, mutations in the same result in morphological and functional defects. These proteins include actin cross-linking proteins like espin, fascin-2 and plastin1, and actin filament capping proteins like CapZ, twinfilin, Eps8, Eps8L2 and gelsolin, actin-binding scaffold protein like harmonin-b and motor proteins.

Before we address the pathology of hearing loss, we must first understand how the system functions normally**.**

1.2 Mechanism of hearing

Hearing occurs when sound waves enter the outer ear and travel through the ear canal, vibrating the eardrum. These vibrations are then received by the malleus, incus and stapes (three bony structures inside middle ear). These structures convert the air pressure to fluid pressure that travels through the cochlear duct (inside the snail shaped cochlea) and vibrates the basilar membrane.

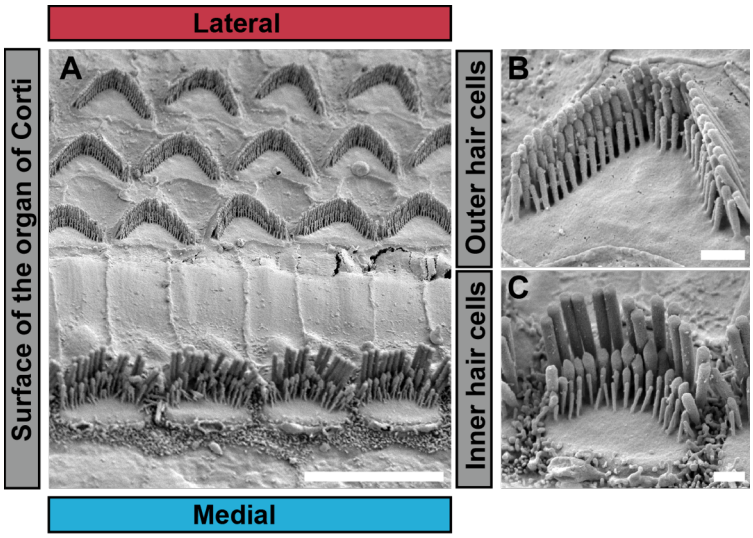

Figure 1.1 Inner and outer hair cell stereocilia. A) Scanning electron micrograph of the surface of the organ of Corti from an adult mouse. The tectorial membrane was removed to expose the stereocilia that protrude from the apical surface of the organ of Corti. A single row of inner hair cells (IHC) is located at the medial side while three rows of outer hair cells (OHC) are found towards the lateral side. Bar is 10 μm. B) Higher magnification of an outer hair cell stereocilia bundle showing the three rows of stereocilia within each bundle. The tallest row ordinarily anchors into the overlying tectorial membrane and does not contain functional mechanoelectrical transduction (MET) channels. The shorter two rows have MET channels that are gated by tip links. Bar is 1 μm. C) Higher magnification image of a typical inner hair cell stereocilia bundle, which often have an incomplete 4th row of thin stereocilia. Scale Bar is 1 μm. Image and figure legend from [16]. http://dx.doi.org/10.1016/j.semcdb.2016.08.017

Basilar membrane is an acellular membrane that extends along the entire cochlear region that vibrates in response to any fluid movements and relays that information to the organ of Corti (OC) (Reviewed in [16]). The cochlea houses the OC, specialized machinery that detects sound and converts mechanical energy into electrical signals. Situated inside the OC are mechanosensory hair cells which together with support cells (pillar cells, dieter cells, etc) form the sensory epithelium and help in the process of hearing. The OC rests on the basilar membrane, whereas the tectorial membrane, an extracellular matrix on the sensory epithelium, covers the apical surface of the OC. The OC consists of numerous hair cells that are organized into 1 row of IHCs and 3 rows of OHCs, which have distinct functions (Figure 1.1). OHCs are responsible for the amplification of incoming sound waves where the net effect is to provide gain and improve frequency selectivity. These amplified sound waves are then received by IHCs that transmit electric signals to afferent auditory neurons to be detected by the brain (reviewed in [17-19]).

1.3 Stereocilia: key players for sound detection

Each hair cell has numerous protrusions at the apical surface known as stereocilia. Stereocilia are key players in converting sound waves into electrical signals to be detected by brain. Both IHCs and OHCs are stimulated by deflections of stereocilia that are as small as a few nanometers. This provides the basic mechanism of the human ear to detect and respond to sound waves in the audible range of 20 Hz to 20 kHz. High frequency sound is detected at the basal (proximal) region of cochlea while the apical (distal) region detects sound of low frequency. Correspondingly, the apical region has longer and more numerous stereocilia within a bundle compared to that of basal region thus resulting in a frequency gradient (tonotopy) along the entire cochlear spiral. In order to detect these small deflections, hair bundles consist of many stereocilia that are arranged in 3 rows arranged in order of increasing height, together giving the appearance of a staircase. This arrangement is critical because bundle deflections in the direction of the longest stereocilia results in the opening of mechanotransduction channels, which are responsible for depolarizing the hair cell.

Early studies in avian cochlea have provided insights into how a hair bundle forms [20]. Initially, the apical surface of each hair cell is covered with numerous actin-based microvilli and a single microtubule-based cilium called the kinocilium. As development proceeds, most of the microvilli

disassemble, while a few mature into stereocilia. During this time, the kinocilium (which is physically connected to the stereocilia bundle) moves to the cell periphery and the stereocilia located close to it start to elongate. It is during this stage that tip links and many other links (connecting adjacent stereocilia) start to form and actin crosslinking proteins start to crosslink actin filaments. This is followed by elongation of stereocilia from the adjacent rows. Next, stereocilia stop elongating for a period during which they start to widen by increasing the number of actin filaments. After widening, the stereocilia resumes elongation until the mature length is attained. Stereocilia in the cochlear base region complete their final elongation phase earlier than the ones at the apex, giving rise to a base-apical length gradient along the cochlea. The kinocilium disappears after the final development of stereocilia in auditory hair cells, though it persists in mature vestibular hair bundles.

1.4 Vestibular stereocilia: detect change in head movements

Each vestibular sensory epithelium is comprised of hair cells and support cells that help coordinate body movements. The mechanosensory hair cells detect velocity and acceleration when stereocilia located at their apical surfaces are deflected in response to body movements [21]. There are two vestibular epithelia known as maculae and cristae ampullares. Maculae lie within the utricle and saccule whereas cristae ampullares are found on the semicircular canals. Both maculae and cristae have a central and peripheral zone with numerous hair cells. Maculae is comprised of a central striola with reduced hair cell density while extrastriolar region surrounds the striola. Hair cells in maculae detect linear head acceleration and gravity while those in cristae detect rotation movements.

Vestibular hair cells also have two subtypes of hair cells, type I and type II, located within the central and peripheral zones in equal proportions, respectively. Type I hair cells which have comparatively more stereocilia than type II hair cells and are innervated by cup-like calyceal terminals of the afferent vestibular ganglion neurons. In contrast, type II hair cells are innervated by bouton terminals emanating from primary afferent neurons [22]. The functions of these two hair cell subtypes are not clearly understood but it is believed that type I hair cells, which are located centrally within the macula or cristae, might be more capable of detecting high frequency

head movements [21]. Hair cells belonging to these subtypes have different cell shape and different stereocilia dimensions.

Vestibular hair cells also have a staircase pattern of stereocilia arrangement important for detecting motion. These hair cells, unlike auditory hair cells, can be regenerated after damage. Thus, repair and replacement of vestibular hair cells benefits people suffering from vestibular dysfunction.

1.5 Stereocilia actin core

Each stereocilium has a stiff actin core which runs along its length. The length of a stereocilium depends on the regulation of its actin core, which is a bundle of extraordinary stable parallel actin filaments. Actin filaments have barbed and pointed ends, so named based on the decoration of actin filaments by myosin S1 fragments observed by transmission electron microscopy (TEM) [23]. The barbed (+) ends of actin filaments are oriented towards the stereocilia tip while the pointed (-) ends are directed towards the base of stereocilia [24]. Actin filament elongation generally occurs at the stereocilia tips because the barbed ends have higher affinity for actin monomers resulting in uniform polarization of actin filaments. Filamentous actin treadmills in solution as monomers are added to the barbed end of the filament with concurrent disassembly of monomers at the pointed end.

1.5.1 Actin is dynamic at the distal tips of stereocilia

The stereocilia actin core is exceptionally stable, unlike other actin structures such as microvilli, stress fibres or filopodia, where actin treadmills in a tip-to-base gradient and turnover occurs on the order of seconds or minutes. Early work in GFP-actin transfected hair cell explants suggested that the stereocilia actin cores continuously treadmill [25, 26]. According to this model, the steady state stereocilia length is maintained by an equal rate of actin monomer disassembly at the base and assembly at the tip. However, several recent studies have contradicted the actin treadmilling model and instead demonstrate that actin turnover primarily occurs at stereocilia tips with little to no actin turnover occurring along the remaining core [27-29] (Figure 1.2). This tip turnover model has been supported by analyzing protein turnover through multi-isotope imaging mass spectrometry (MIMS), actin isoform ablation studies *in vivo* and studying GFP-actin dynamics *in vivo* [27-29].

Initially, it was the measurement of total protein turnover using MIMS technique that shed light on the tip turnover model [29]. The MIMS technique can assess localized protein turnover by measuring N15 incorporation in spatially defined regions as mice are fed an N15 diet. N15 was incorporated at stereocilia tips suggesting that actin turned over in this region. Protein turnover occurred in the shaft at a much slower rate and plateaued at 40%, which corresponds to the actin content of stereocilia. This suggests that actin in the shaft region is stable.

To more directly monitor actin incorporation, the β-actin or γ-actin isoforms were deleted after development by cre-mediated recombination in young adult mice. This approach also supported the tip turnover model [29]. These actin isoforms are known to colocalize in inner hair cell stereocilia. Following ablation, the stereocilia staining with actin isoform specific antibodies showed that the knocked out isoform was lost from the stereocilia tips but not from the shaft, thus indicating that actin in the core was stable in comparison to that in the tips.

An *in vivo* approach using the FLEx-EGFP-actin reporter system was developed to monitor actin incorporation in auditory (inner hair cells) and vestibular (utricular hair cells) systems in adult mice [28]. FLEx is a genetic switch mediated by cre-recombinase, that initiates transgenic EGFP-actin expression irreversibly in the hair cell. Cre mediated recombination removes a tdtomato sequence and inverts the EGFP-actin coding region so it is downstream of the Cagg promoter. This results in irreversible induction of EGFP-actin. A ubiquitously expressed tamoxifen regulated CreER was used to induce EGFP-actin expression to achieve conditional temporal control. Following induction of EGFP-actin expression, its incorporation into the stereocilia core revealed the dynamic regions. The localization pattern of EGFP-actin was compared in IHC stereocilia 1, 2, 20, 40 weeks after EGFP-actin expression was initiated following tamoxifen administration. At every time point examined, EGFP-actin expression was detected almost exclusively in the tip region localized within 0.5 um from the tips of tallest (row1) stereocilia. Notably, the localization of EGFP-actin did not extend down the stereocilia core suggesting that actin in this region of stereocilia is stable [28].

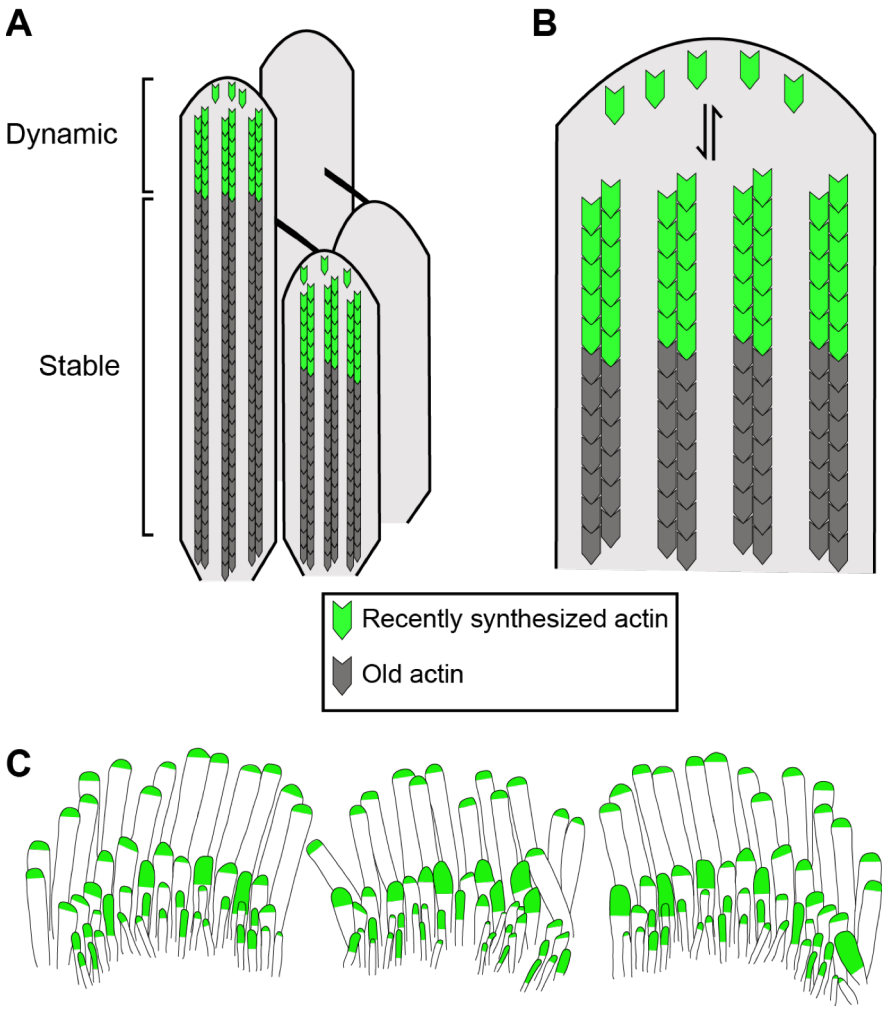

Figure 1.2 The tip turnover model. A) The actin core in the shaft of stereocilia (grey) is exceptionally stable. Actin incorporation in this region is not detected over a months-long timecourse. In contrast, actin incorporation is much more dynamic in the tips of all stereocilia (green). B) Enlarged view of the tip showing actin monomers in dynamic equilibrium with F-actin barbed ends at stereocilia tips. Dynamic equilibrium is posited because mature stereocilia length is constant, suggesting that polymerization must be balanced by an equal amount of disassembly. The equilibrium is likely shifted to net shrinkage or elongation by factors such as regulation of actin polymerization by myosin XVa-whirlin-EPS8, myosin III/espin-1 and actin depolymerizing factor (ADF) as well as the stability of the actin core. C) Mechanotransducing stereocilia incorporate more actin at their tips. A uniform level of actin is incorporated at tips of the tallest stereocilia, which lack functional mechanoelectrical transduction (MET) channels. In contrast, the level of actin incorporation varies amongst mechanotransducing stereocilia, suggesting that tip link mediated membrane tension and ion concentration from MET channel activity influence actin turnover. Image and figure legend from [16].
http://dx.doi.org/10.1016/j.semcdb.2016.08.017

1.5.2 Actin binding proteins

During development, stereocilia lengths are regulated by various myosin motor proteins, crosslinkers and several proteins with capping and severing activity. Myosin XVa, whirlin, Eps8, myosin IIIa and myosin IIIb distinctively localize to stereocilia tips and promote elongation [30-33]. The length of shorter rows of stereocilia are maintained by a long splice isoform of myosin XVa [34]. Capping protein CapZ and proteins with capping activity like TWF2 and Eps8L2 are also known to regulate actin filament elongation and may contribute to the staircase like morphology of the bundle because they localize differentially to each row of stereocilia. For example, Eps8 localizes to the tips of the tallest row of stereocilia whereas TWF2 and Eps8L2 localize to the tips of shorter rows of stereocilia where they may restrict growth to produce the staircase morphology [35-39].

Stereocilia taper near the cell body, with only actin filaments at the middle of the core being able to pass through this region. This taper region is thus characterized by fewer number of actin filaments tightly packed together. The rootlet structure in this stereocilia taper region anchors stereocilia to the cuticular plate lying underneath the cell body with the help of actin binding protein TRIOBP, loss of which results in less rigid stereocilia [40]. Other proteins that are critical in maintaining this specialized stereocilia base structure by anchoring the membrane to the cytoskeleton are radixin, myosin VI, PTPRQ, chloride intracellular channel 5 and Fam65B. Stereocilia lacking any of these proteins tend to fuse [41-46].

1.6 Stability of stereocilia actin core is dependent on tip links and maintenance of mechanotransducive rows

Earlier studies using transgenic reporter to monitor actin dynamics have shown that shorter row stereocilia have variable and increased actin-GFP incorporation at their tips in contrast to row 1, which instead have a uniform incorporation of actin-GFP [28] (Figure 1.2). The increased incorporation at the tips of shorter row stereocilia might stem from stochastic tip link loss followed by stereocilia shortening and subsequent regrowth. This suggests that tip links play an important role in maintenance of the length of shorter row stereocilia.

1.6.1 Structure of tip links

The shorter rows of the bundle are known as mechanotransducing rows because their stereocilia house mechanically-sensitive gated ion channels at their tips, unlike the tallest row stereocilia [47]. The tip of a lower stereocilium is connected to the side of the taller neighboring stereocilium by filamentous structures called tip links. Tip links, which are formed by a heteromeric interaction between CDH23 homodimers and PCDH15 homodimers, convey tensile force to these mechanosensitive ion channels in response to the sound-induced stereocilia deflections, thus resulting in influx of ions [48]. Both transmembrane proteins, CDH23 and PCDH15, are critical to normal hearing and mutation in any of these proteins lead to severing of tip links, disrupted hair bundle structure and ultimately causing hearing loss [49-51]. The loss of function mutations in CDH23 leads to disrupted hair bundle structure. Mice homozygous for null mutations in CDH23 are profoundly deaf with disorganized stereocilia bundle morphology. This emphasizes the critical role played by this complex (PCDH15-CDH23) for the formation and maintenance of tip link structure and bundle morphology in inner ear hair cells.

The upper end of a tip link is anchored into the upper tip link density (UTLD) region[52]. Cadherin 23 through its carboxyl terminus, anchors to the UTLD region by interacting with a tripartite complex (Myosin 7a/Sans/Harmonin-b) that localizes to this region [53]. MYO7A (a motor protein encoded by USH1B), sans (a scaffolding protein product of USH1G), harmonin (a scaffolding protein product of USH1C), and CDH23, are all associated with the Usher type I (USH1) syndrome which leads to deafness, dysfunctioning of vestibules and blindness caused by retinopathy [53, 54]. Harmonin-b is a critical component of the UTLD region as mutations in this protein disrupts UTLD formation, thus reducing sensitivity of hair bundles to mechanical stimulation. The interaction of its PDZ domains with CDH23 and F-actin that controls its localization in stereocilia, is critical for normal hearing, and hence couples the tip link with stereocilia actin core [55, 56]. Harmonin-b localizes to the stereocilia tips but fails to migrate to the UTLD region in absence of CDH23 [55]. Additionally, the presence of harmonin-b is crucial for clustering Myo7a and sans to the UTLD region. The targeting of harmonin-b to the hair bundles is dependent on its interaction with Myo7a, as evident from the improper targeting of harmonin-b to hair bundles in mice lacking Myo7a [57]. Across the LTLD (lower tip link density) region,

where the lower end of a tip link is anchored, is a region where the shorter stereocilia leans upon the taller stereocilia (connected by tip link) known as the contact region [52].

1.6.2 Tip links can be regenerated

Since tip links are fragile structures and prone to disruption by exposure to strong acoustic stimulation or Ca^{2+} free environment, repair is critical for long-term maintenance of hearing. Tip links can be regenerated thus restoring mechano-electrical transduction (MET) current in inner ear hair cells and hearing. Previous studies have shown that tip links can be broken when early postnatal explants are exposed to Ca^{2+} free environment along with BAPTA (1,2-bis(o-aminophenoxy) ethane-N,N,N9,N9-tetraacetic acid), suggesting that tip links are highly sensitive to calcium chelation. CDH23 molecules has been found to largely disappear when tip links are disrupted by BAPTA treatment while PCDH15 migrates across the circumference of stereocilium and becomes available for the formation of the upper and lower ends of regenerating nascent tip links. Initially, regenerating tip links have almost equal amounts of PCDH15 at its both ends. The MET current mediated by these nascent tip links have normal amplitude but there is an abnormal Ca^{2+} dependent decay. This abnormality in the adaptation of MET responses is recovered over a period of 24 hours when the CDH23 molecules replace PCDH15 at the upper end of mature tip links [58]. The replacement of PCDH15 with CDH23 is necessary for the long-term maintenance of MET. The regenerating nascent tip links are shorter compared to the mature tip links illustrating an extended period of tip link remodeling.

1.6.3 Tip links in the maintenance of mechanotranducing rows

Tip link loss or its inability to form properly, has a direct impact on the mechanotransducive (shorter) rows resulting in short and stunted stereocilia with the tallest row stereocilia remaining intact [54]. While monitoring for EGFP-actin incorporation *in vivo*, EGFP-actin levels were found to vary between tips of the tallest row and the mechanotransducive rows of stereocilia within IHC bundles. In the tallest row, EGFP-actin incorporation was found to be uniform among stereocilia within the same IHC bundle. In contrast, the shorter rows had varied levels of EGFP-actin incorporation and the intensity was greater than that found in the tallest row [28]. This pattern of

EGFP-actin incorporation might be due to stochastic tip link loss followed by stereocilia shortening and subsequent growth. This is consistent with shortening of only mechanotranducive stereocilia when tip links are ablated during postnatal development. Similarly, shortening of mechanotranducive stereocilia is also exacerbated by the hypomorphic *Cdh23*^{ahl} allele (a short-truncated variant of CDH23) that leads to age-related hearing (AHL) loss [59]. The molecular mechanism behind this phenomenon is not understood. One reason could be attributed to membrane tension. Intact tip links pull on the membrane at the tips of mechanotransducing stereocilia, reducing the membrane tension force on the stereocilia core. When tip links break, it causes an increase in membrane tension. This increased force could shift the dynamic equilibrium between actin association and dissociation at stereocilia tips towards net disassembly. Additionally, reduced influx of ions such as Ca^{2+} might directly change actin polymerization dynamics or the activities of actin binding proteins. Tip link loss may alter proteins of the link complex, influencing actin regulatory proteins and their localization to modulate stereocilia actin dynamics and length. This results in irregular stereocilia length and disrupted bundle morphology.

The morphology of stereocilia in the shorter rows is sensitive not only to the disruption of tip links but also to the loss or mutations in various actin cytoskeleton proteins like fascin-2, Eps8L2, β-actin and long isoform of myosin XVa [34, 35, 60]. Mutations in actin severing proteins ADF (Actin depolymerizing factor) and AIP1 (which cooperates with ADF/cofilin for actin depolymerization) results in short and missing mechanotransductive stereocilia [28]. None of the above-mentioned mutations affect stereocilia from the tallest rows. This suggests that differential well-coordinated mechanisms regulate stereocilia morphology in an orderly fashion in different rows within a bundle, thus giving rise to the intricate staircase pattern, responsible for the synchronized event of hearing.

1.7 Stability of stereocilia actin core is dependent on actin crosslinking and capping proteins

The exceptional stability of mammalian stereocilia core is attributed to the unique complement of actin binding proteins that regulate the length of stereocilia and thus help in the proper maintenance of stereocilia morphogenesis, perturbation of which leads to deafness. Crosslinking of the actin filaments in stereocilia is known to occur at a frequency of about one crosslinker per 10 actin

subunits [61, 62]. Various crosslinking proteins like fascin-2 (FSCN2), espin (ESPN), plastin-1 (PLS1) and XIRP2 contribute significantly to stereocilia morphogenesis and maintenance. The reason for multiple crosslinkers is not known and in some cases their function is redundant. However, each of these crosslinkers is indispensable and is critical for long term maintenance of stereocilia architecture because mutations in these proteins lead to progressive hearing loss along with degeneration of stereocilia [60, 63-66]. In contrast, ESPN mediated crosslinking is crucial for development of stereocilia as a null mutation of ESPN results in abnormally short, thin and unstable stereocilia [67, 68].

Described below are the major actin crosslinking and capping proteins implicated in hearing loss.

1.7.1 Actin crosslinking proteins

1.7.1.1 Fascin: Structure and function

Fascin is a 55 kDa globular protein known to exist in three isoforms. Fascin-1(FSCN1) and fascin-2 (FSCN2) are expressed in hair cells in addition to sertoli cells and retinal photoreceptor cells, respectively, while fascin-3 (FSCN3) isoform is expressed only in the testis. Fascin has 4 highly conserved β-trefoil domains with very similar actin binding sites. FSCN1 and FSCN2 isoforms have 56% sequence identity and three possible actin binding sites are located within β-trefoil domains 1 and 3. Mutagenesis studies have shown that the major actin binding site located in the β-trefoil domain 1 consists of residue serine 39 (in case of FSCN1) and serine 38 (in case of FSCN2). *In vitro* cosedimentation assays have shown that mutations in the actin binding sites of fascin results in inhibition of actin binding and thus impair actin bundling in filopodia in cells [69, 70]. An amino acid substitution of arginine to histidine at position 109 (R109H) of FSCN2 protein within actin binding site 2 (Arg^{111} in case of FSCN1) results in hair bundle degeneration and progressive hearing loss [64]. Actin bundling and filopodia formation is known to be affected at a much lesser extent when other residues on fascin surface are mutated (for eg; fascin(K22E/K43E/R398E) and fascin(R271E/K353E/K358E)) within actin binding site 1[69]. This suggests that fascin not only has two major actin binding sites but it also makes secondary contacts with actin filaments. Cryo-electron tomographic techniques have demonstrated that actin binding sites 1 and 2 of fascin bind two actin monomers located within the same filament while the actin binding site 3 connects to the actin monomer located on the adjacent filament [71].

Using competition assays, it has been shown that in the absence of any competitive molecule like free fascin molecules, fascin crosslinks actin filaments in a stable fashion by toggling between single and double bound states. When one of its actin binding sites releases, it re-binds the actin filament before the second actin binding site can release. In presence of competitive molecules in solution, this molecule readily occupies the transiently available binding site from the dissociation of the first actin binding site of fascin. Fascin in its singly bound state, having only the second binding site, dissociates rapidly. This is how multiple crosslinkers competing for the same binding site, occupy the site as soon as a pre-existing crosslinker dissociates [72].

Another property of fascin is that it binds F-actin cooperatively as demonstrated by low speed *in vitro* cosedimentation actin bundling assays [73]. All fascin mutants are known to have similar inactive configuration. Studies have shown that when one of the actin binding sites of fascin is affected, there is a change in its conformation which consequently affects the other actin binding sites. This suggests that when one actin binding site of fascin binds F-actin, it facilitates the binding propensity of other actin binding sites.

Fascin also contributes to the packing arrangement of actin filaments. Using cryo-electron tomography of reconstituted fascin/actin bundles from filopodia, it was found that fascin crosslinks promote hexagonal packing of actin filaments in vitro [74]. The OHC and utricular bundles have liquid packing of actin filaments. In contrast, the IHC bundles have a composite packing arrangement with the central core being hexagonally packed while the periphery comprising of liquid packed actin filaments. Mice lacking PLS1 have hexagonal arrangement of actin filaments in OHC and utricular bundles instead of liquid packing that is observed in mice having wild type levels of PLS1 [75]. The composite packing arrangement in IHC bundles was also lost resulting in only hexagonal packing throughout the core in IHC bundles in mice in which PLS1 was knocked out. This suggests that PLS1 promotes liquid packing and that fascin might be more abundant in the IHC stereocilia in contrast to OHC and utricular hair bundles which have predominantly liquid packing of actin filaments.

1.7.1.1.1 Fascin dynamics

While actin dynamics has been increasingly studied and well understood, not much is known about the dynamics of actin crosslinking proteins, including fascin, which are nearly as abundant as actin itself. Recent work in zebrafish and drosophila has shed light on the dynamics of fascin. Turnover of fascin-2b (FASCN2b, one of the FSCN2 paralogs) in zebrafish or fascin in drosophila occurs in seconds unlike the relatively slow turnover of actin [76]. It is the non-phosphorylated form of FSCN2b in Zebrafish stereocilia that exchanges rapidly with F-actin independent of its concentration and without a bias in its movement towards either the top or bottom half of the hair cell bundle. Rapid and random fascin-2b exchange not only promotes F-actin depolymerization but at the same time reforms the paracrystal structure by enabling efficient crosslinking of the newly polymerized actin filaments.

One possibility that remains unexplored is whether the dynamics of mammalian fascin depends on posttranslational modifications. The ability of fascin proteins to bind and bundle F-actin is dependent on the phosphorylation state of their serine 38. It has been reported that the non-phosphorylated form of fascin binds actin [76]. Phosphorylation of serine 38 residue in FSCN2 (serine 39 in case of FSCN1) by protein kinase C (PKC) abolishes actin bundling property of fascin [69]. IKKe in Drosophila has been demonstrated to inhibit PKC signaling during bristle morphogenesis so that fascin is protected from inhibitory phosphorylation and thus can bind actin [77]. It's interesting that mutations on the phosphorylation sites (S38 and S39) of fascin do not significantly affect the turnover of fascin in filopodia and stereocilia suggesting that other post-translational modifications (possibly ubiquitination) in addition to phosphorylation regulate turnover of fascin [78]. Monoubiquitination at the actin binding site 2 of fascin regulates fascin activity and turnover by slowing down actin crosslinking thus enhancing disassembly of actin bundles [78].

1.7.1.1.2 FSCN2 in mammalian stereocilia

FSCN2 is one of the most abundant actin cross-linking proteins in stereocilia, predominantly expressed in the inner hair cells (IHC) during final stages of stereocilia elongation. This developmentally regulated actin cross-linker plays a crucial role in stabilizing stereocilia once

developed. There is a gradual progression of FSCN2 expression as the cochlear hair cells age. By P10 FSCN2 expression becomes detectable in IHC, along the entire length of stereocilia. FSCN2 is abundantly detected in the IHC bundles by P30. Transcript levels of FSCN2 increase from P5 to P10 by 5-fold before decreasing back to the P5 level by P30. In contrast, the protein levels showed a continuous increase from P5 to P30 [64]. The elevated protein levels at P30 suggest that the turnover of FSCN2 is relatively slow at this age compared to an earlier developmental point. The transient increase in FSCN2 expression correlates well with the elongation of the tallest rows of stereocilia of the maturing mouse IHC bundles. In contrast to the cochlear hair cells, FSCN2 expression is almost uniform at all ages in vestibular hair cells and is concentrated mostly at the tips [64].

1.7.1.1.3 Progressive hearing loss caused by mutation in FSCN2 protein

Stereocilia in DBA/2J mice (expressing the $FSCN2^{R109H}$ mutation), which binds but cannot crosslink actin, develop normally but eventually fail to maintain stereocilia length [60]. The degeneration is evident primarily in the OHCs at the basal end of cochlea while the phenotype spreads later towards the apical end. Pronounced degree of variation in degeneration levels is observed in individual stereocilia within a hair bundle. While the R109H mutation causes stereocilia shortening, it does not have much effect on the localization of FSCN2. Though the protein is detected at a reduced level in stereocilia, it is capable of binding F-actin but actin cross-linking is prevented suggesting that one of the actin binding sites is disrupted [60]. Although the stereocilia morphology and function are similar whether $FSCN2^{R109H}$ is on DBA/2J or B6 background, the progression of hearing loss in $FSCN2^{R109H}$ mice on a B6 background is slower compared to that on DBA/2J [60].

Mice in which β-actin is absent are characterized by progressive degeneration of hair cell bundles similar to that in DBA/2J mice. At 16 weeks of age, the length of row 3 stereocilia is significantly shortened with row 1 being unaffected. Stereocilia of mice lacking β-actin or expressing $FSCN2^{R109H}$ mutation are normal during early developmental stages but as mice age, stereocilia in rows 2 and 3 tend to shorten and show irregular heights without altering the total number of stereocilia per bundle [60]. Mice lacking β-actin and expressing $FSCN2^{R109H}$mutation had similar

phenotype but the onset of degeneration occurs even earlier than the single mutants. This suggests a sort of synergism between the two proteins in terms of controlling actin dynamics at stereocilia tips.

Both β-actin and fascin-2 proteins are critical for maintenance of stereocilia structure and function during aging. The phenotype in mice lacking β-actin or expressing mutant fascin-2 protein is dependent on the hypomorphic expression of $Cdh23^{ahl}$ allele, which accelerates progressive hearing loss and the phenotype is suppressed by the expression of dominant $Cdh23^{+}$ allele [60]. The truncated variant of Cdh23 ($Cdh23^{ahl}$) lacks the critical 43 amino acids from the 2^{nd} and 3^{rd} ectodomains and might make the protein less stable, thus affecting its interaction with PCDH15 and its localization to the tip links [79]. This causes defects in tip links and channel activity, resulting in shortening of mechanotransductive stereocilia. Both β-actin and fascin-2 proteins are critical for stereocilia length regulation possibly through a common pathway, reflecting the genetic interaction with Cdh23. For example, the mechanotransduction machinery at stereocilia tips might be regulating actin dynamics in conjunction with actin crosslinking proteins, including fascin-2, to promote stereocilia stability along with other actin capping and severing proteins that promote growth.

1.7.1.1.4 Stereociliary length is influenced by various fascin-2 orthologous proteins.

Overexpression of FSCN2b, results in elongation of stereocilia [80]. It has been proposed that during actin treadmilling, the reduction in the rate of actin depolymerization at the stereocilia base caused due to substantial actin crosslinking by FSCN2b is responsible for the lengthening effect. FSCN2b promotes the formation of highly ordered parallel actin bundles and thus contributes in shaping stereocilia. FSCN2b when coexpressed with ESPN results in the formation of long filopodia in cultured COS-7 cells. This suggests that the length and formation of filopodia is controlled by the combinatorial effect of these two actin-crosslinking proteins [80].

1.7.1.2 Espin: Structure and properties

Espins are a family of actin crosslinking protein, which were first detected in the junctional plaques of the ectoplasmic specializations of Sertoli cells [81, 82]. Multiple isoforms of ESPN differing in size (~25 kDa to ~110 kDa) and having different ligand binding sites exist as a result of different transcriptional start sites and alternative splicing of espin pre-mRNA [83, 84]. The isoforms are different in their N-terminal peptides. Espin 1, the largest of the espin isoforms, has 8 ankyrin repeat (AR) domains on its N-terminus that bind the THDI domain (tail homology domain 1) of Myo3A [81, 85]. Espin 1 and Espin 2 also contain an additional actin filament binding site (xAB), which is absent from the other smaller isoforms [82]. The AR domain, which is specific to espin1, folds back to the Ankyrin-repeat binding (ARB) site, blocking xAB domain, which results in autoinhibition. MYO3 tail homology domain relieves this autoinhibition by binding to the ARB region by competitively inhibiting the AR domain [86]. The actin bundling module (ABM), an ~14 kDa C-terminal peptide, important for actin bundling is shared by all the espin isoforms [82, 87]. The WH2 domain (Wiskott Aldrich Syndrome protein homology 2), that is essential for the ESPN-mediated actin bundling, is also present in all of the espin isoforms [83, 88]. Espins with the help of their WH2 domain bind actin monomers. The smaller isoforms lack one or the other domains. For example, espin 2B lacks the AR domain, espin 3A and espin 4 lack the AR and the xAB domains [86].

1.7.1.2.1 ESPN in hair cell stereocilia

ESPN is detected in the stereocilia of the cochlear and vestibular hair cells during early development and expression increases throughout stereociliogenesis [67]. Espin isoforms are developmentally regulated with espin 2 and espin 3 being dominantly expressed until E20 in embryonic inner ear. After this, espin 2 levels decrease while espin 3 levels keep increasing until P15. Espin 1 isoform is highly expressed during late embryonic development and early postnatal stages reaching its highest concentrations around P6. The smallest isoform, espin 4 is not detected during embryonic development but is instead highly expressed between P6 and P10 [89]. This implies that espin 4 isoform may have a role in postnatal stereocilia elongation important for the staircase pattern within a bundle and for the graded stereocilia height across the cochlear spiral. The large espin isoforms, comprised mostly of Espin 1, localize at the tips while the other isoforms

are detected throughout the stereocilium [86]. Espins play an important role in the growth of hair cell stereocilia by efficiently crosslinking actin filaments promoting the assembly and stabilization of parallel actin bundles (PABs).

1.7.1.2.2 Loss-of-function phenotype

Mutations in espin gene including the jerker mutation in mice, are associated with vestibular dysfunction and deafness. The jerker mutation, named for the head jerking movements of the mice, is a result of a frameshift mutation (caused by a deletion of a guanine residue) on chromosome 4 in the espin gene. Homozygous *jerker* mice are deficient for all espin isoforms [68]. The defects in stereocilia morphogenesis and stability in mice lacking espin varies between different regions in the inner ear. The stereocilia of cochlear IHCs and OHCs of homozygous *jerker* mice ($Espn^{je/je}$), collapse, shorten and disappear around postnatal day 10. The stereocilia are abnormally thin in these mice suggesting that ESPN is required to increase the number of actin filaments per stereocilia to increase stereocilia diameter. Stereocilia progressively degenerate in the cochlear hair cells and by P20 barely any stereocilia can be detected. Apparently, other actin bundling proteins like FSCN2, PLS1, PLS2, ESPNL, XIRP2 that are localized to stereocilia are unable to compensate for the loss of ESPN [60, 64],[66, 90]. Although ESPN null cochlear stereocilia degenerate by P10, extrastriolar utricular stereocilia are maintained well into adulthood. Heterozygous jerker mice ($Espn^{je/+}$) have half the amount of wild type ESPN levels [68]. The stereociliary width of $Espn^{je/+}$ lies in between that of wild type and $Espn^{je/je}$ mice at P0 which then gradually increases to that of wild type by P20. Transient tapering is observed in the stereocilia width from the proximal to the distal end of stereocilia probably due to haploinsufficiency. Even so, jerker heterozygotes recover and develop stereocilia morphology and hair cell abundance similar to that of mice with wild type levels of ESPN.

1.7.1.3 Plastin: Structure and properties

PLS1 (also known as fimbrin) is one of the most abundant proteins of stereocilia based on biochemical studies [61, 91]. Plastin consists of EF-hand Ca^{2+} binding domains at the N-terminus and two actin binding domains each of which consist of a pair of calponin-homology domains.

Each of these domains is critical for actin bundling activity of plastin which is known to be regulated by Ca^{2+} [92]. In immature hair cells, plastin-3 (PLS3) is transiently expressed, while PLS1 is detected in both the developing and mature stereocilia [93, 94]. PLS1 levels are high between P1 and P21 after which its levels start to drop. PLS1 is the next abundant protein in vestibular stereocilia after actin itself, followed by FSCN2 and ESPN [75]. PLS1 promotes liquid packing of actin filaments within stereocilia as loss of PLS1 resulted in hexagonal packing arrangement of actin filaments in utricular and cochlear stereocilia [75].

1.7.1.3.1 Loss of function phenotype

Mice in which PLS1 has been knocked out develop progressive hearing loss. *Pls1* KO mice develop normally with no impairment in the stereocilia morphology and the overall organization of the organ of Corti remains unaltered. In contrast, morphological defects in hair bundles are pronounced in mature hair bundles. This is characterized by thinner and bent stereocilia of different lengths within a row, compared to wild-type stereocilia. In *Pls1* KO IHC, the length of longest stereocilia are frequently found to be reduced by 20% accompanied by reduction in width which becomes more noticeable with age, affecting the rigidity of IHC stereocilia core. This in turn affects the efficiency of mechanotransduction. A mix of normal and defective stereocilia in terms of length and width is observed within the same bundle with the difference being more distinct at the distal ends of stereocilia. Stereocilia in OHC of *Pls1* KO mice are not as severely affected as those of IHC, appearing mostly normal though some defects like stereocilia fusion and shortening have been occasionally visible by 8 weeks of age [63]. Similarly, in absence of PLS1, utricular stereocilia fail to achieve their final matured dimensions, which are instead thin and short [75]. This suggests that the morphology and maintenance of stereocilia in auditory and vestibular bundles depend on PLS1. In mature hair cells, PLS1 helps maintain the correct number of actin filaments and also ensures proper cross linking between actin filaments within the stereocilium, thus preserving the core. PLS1 might contribute to the core maintenance by assisting in adding new β-actin or γ-actin subunits to the existing actin filaments and averting their depolymerization. Future studies will be necessary to determine which mutations in the *PLS1* gene are linked to age-related hearing loss.

1.7.1.4 XIRP2

XIRP2 belongs to the actin binding Xin-repeat containing protein family [95]. Xin-actin binding repeat containing 2 (XIRP2) originally detected in striated muscle [96], is an actin cross-linking protein specifically expressed in the inner ear hair cells colocalizing with the actin-rich structures [65, 66]. The F-actin cross-linking activity of XIRP2 is conferred by its 28 Xin domains [97], which bind and stabilize actin bundles [95]. XIRP2 is produced from the two long isoforms of the six different splice forms of the *Xirp2* gene. Two distinct isoforms of XIRP2 are expressed by hair cells. The short XIRP2 splice form, lacking the Xin repeat domain, is expressed in mouse cochlear and utricular hair cells localizing in the stereocilia actin bundles and apical region of hair cell while the long isoform is restricted to the cuticular plate [65]. The short isoform although cannot cross-link F-actin but does colocalize with F-actin rich structures. The long isoform is excluded from the stereocilia by steric hindrance [95].

XIRP2 helps to maintain the structure and morphology of hair cell stereocilia and its absence causes moderate high frequency hearing loss [65]. Structure and morphology of hair cells are unaltered during early development in *Xirp2*$^{-/-}$ mice. The stereocilia in OHC and IHC starts to degenerate progressively at P9 in the basal end and extends to the middle turn by P13 in mice lacking XIRP2. The degeneration is characterized by reduced height of the shortest stereocilia in both OHC and IHC, disappearance of stereocilia from IHC, thinning of tallest stereocilia in IHC while thickening in OHC. An increased spacing between individual stereocilia within a bundle has also been detected. These show that the actin bundling in XIRP deficient stereocilia are grossly dysregulated and disorganized [65, 66]. XIRP2 has been proposed to play a critical role in the protection and repair of actin bundle structure. The Xin repeats of XIRP2 protect the filament ends from depolymerization [95] and thus, in absence of this protein, the filaments within a stereocilium tend to shorten, generating gaps. XIRP2 might also be acting as a staging protein promoting reformation of the broken filaments. These functions could account for the defects observed in knockout stereocilia.

1.7.2 Barbed-end capping proteins

Actin capping proteins bind to the barbed ends of filaments and prevent both addition of new actin monomers and disassembly of actin filaments from the same end. Several capping proteins have been detected in stereocilia like TWF2, Eps8, Eps8L2 (Epidermal growth factor receptor substrate pathway 8), gelsolin and heterodimeric capping protein CAPZ consisting of subunits like CAPZA and CAPZB2 [33, 35-38]. Each of these proteins is required for a controlled regulation of length and width of stereocilia within a bundle. In contrast, the role of twf2A can be compensated by other cytoskeletal proteins as evident from the normal stereocilia morphology in twf2A KO mice.

Eps8 and Eps8L2 have actin crosslinking as well as capping properties. Eps8 expression remains high only in the longest row of stereocilia while diminishing in the shorter rows with maturation. Correspondingly, in mice lacking Eps8, row 1 stereocilia in cochlear hair bundles are significantly short along with an acute hearing loss at an early age [32, 33, 98]. This suggests that Eps8 is important for initial elongation of stereocilia. In contrast, expression of Eps8L2 is enriched at the tips of shorter rows as the cochlear hair cells age [98]. This is critical for the maintenance of stereocilia in adult cochlear hair cells as Eps8L2 null-mutant mice develop late-onset progressive hearing loss [35]. There is an associated degeneration in the staircase organization of the cochlear hair bundles characterized by few abnormally long shorter row stereocilia in IHCs while some were short or missing. Absence of Eps8L2 is also associated with reduction in stereocilia diameter and a pronounced tapering in the distal ends of stereocilia, reminiscent of that observed in espin jerker heterozygote mice.

TWF2 acts as a barbed end capping protein predominantly in the 2nd and 3rd rows of adult stereocilia, thus possibly restricting their elongation once their mature length is attained. When twf2 is overexpressed in developing hair cells, it results in significantly short stereocilia in the 2nd and 3rd rows [38]. Gelsolin, another barbed end capping protein, is predominantly expressed only in shorter row stereocilia tips of OHC bundles between P0 and P8. Lack of gelsolin results in abnormally long, disheveled stereocilia, though for unknown reasons this phenotype restricted to the apical region of OHC bundles [99]. Additionally, another member of the barbed end capping protein class, CapZB2 localizes along stereocilia shaft during P8 (widening phase) after which it is detected at stereocilia tips at P21 to regulate elongation [98]. Stereocilia in mice lacking CapZB2

have dysmorphic bundles at early postnatal stages which worsens with age and eventually result in hearing loss and vestibular dysfunction [98]. Thus, capping proteins are critical for proper formation and maintenance of hair bundles.

1.8 Actin isoforms and their role in stereocilia maintenance

Actin consists of various distinct isoforms of which alpha-actin (the most acidic isoform) is predominantly expressed in muscle cells. In contrast, the more basic β- and γ-actin isoforms are ubiquitously expressed and differ by only four out of 375 amino-acid residues at the amino-terminus [100]. β-actin and γ-actin are encoded by *Actb* and *Actg1* genes respectively, the coding sequences of which are 89% identical. The subtle differences in the amino acid sequences lead to differences in the biochemical properties of β- and γ-actin. The polymerization properties of the proteins differ *in vitro* with β-actin exhibiting faster polymerization and depolymerization kinetics than that of γ-actin under conditions when the monomers are Ca^{2+} bound [101-103]. In addition, β- and γ-actin distinctly localize to certain cell types and the difference in localization pattern is regulated by their different post-translational modifications [102, 104]. The targeting of *Actb* transcript to the subcellular locations is regulated by the unique 3' UTR zipcode sequence which is absent in the *Actg1* transcript [105-107]. Additionally, the ribosome density and translation rate also differ between the *Actb* and *Actg1* transcripts.

β-actin and γ-actin protein sequences are evolutionarily conserved, and correspondingly both these proteins are essential for normal cellular functioning. These proteins comprise the structural component of stereocilia. Neither of the proteins can compensate for the absence of the other as evident by various developmental defects along with progressive hearing loss resulting due to point mutations in *ACTB* or *ACTG1* in humans. Mice lacking β-actin are embryonic lethal while mice lacking γ-actin survive but suffer from progressive hearing loss along with stereocilia degeneration [108-113]. This suggests that β- and γ-actin are each expendable for stereocilia formation but required for maintenance [111, 114]. That β- and γ-actin have non-redundant biological roles was determined from generating mice in which β-actin or γ-actin were conditionally ablated from hair cells. Mice in which hair cells were devoid of β-actin displayed only high frequency hearing defects and had abnormally short row 3 stereocilia [111]. In contrast, mice with γ-actin deficient

hair cells uniformly displayed defects in all frequencies tested, rapidly progressing with age, and had several missing row 3 stereocilia by 24 weeks of age. Therefore, β- and γ- actin are both important for preventing age-related hearing loss. Understanding the aberrations of these actin isoforms could lead to the elucidation of new mechanisms, shedding light on age-associated onset of human deafness.

1.9 Vital questions

Although stereocilia arise from microvilli which have a continuously treadmilling actin core, actin turnover occurs only at the stereocilia tips while remaining stable along the core. What contributes to this exceptional stability of the stereocilia actin core? What is the significance of a dynamic tip region? Is the actin treadmilling in stereocilia core restricted by the actin crosslinking proteins? Actin crosslinkers are the next most abundant proteins in stereocilia after actin. While actin dynamics has been extensively studied, dynamics of actin crosslinkers important for development and maintenance of stereocilia morphology has not been defined in mammalian stereocilia. The question is how stable is fascin-2 in mammalian stereocilia or does it move rapidly in and out of stereocilia? Furthermore, it is unclear as to why hair cells require two highly similar actin isoforms that differ by only four amino acid residues? Addressing these questions is necessary to understand stereocilia structure and function better.

1.10 Study Aims

The overall goal of this research was to determine the role of actin cytoskeletal proteins in stereocilia morphogenesis and maintenance. This was accomplished by determining if the mutations in actin crosslinkers (FSCN2 and ESPN) that cause deafness decrease the stability of actin core *in vivo*. We further characterized crosslinker dynamics and explored the potential therapeutic utility of modifying crosslinker expression levels. We also determined how actin isoforms regulate stereocilia function at the protein level. The studies done here will shed more light into understanding the importance of stable as well as dynamic regions within the core necessary for maintaining functional stereocilia for the ability to hear.

CHAPTER 2. THE STABLE ACTIN CORE OF MECHANOSENSORY STEREOCILIA FEATURES CONTINUOUS TURNOVER OF ACTIN CROSSLINKERS

This chapter has been published in reference [115].

2.1 Abstract

Stereocilia are mechanosensitive protrusions on the surface of sensory hair cells in the inner ear that detect sound, gravity and head movement. Their core is comprised of parallel actin filaments that are crosslinked and stabilized by several actin-binding proteins including fascin-2, plastin-1, espin and XIRP2. The actin filaments are the most stable known, with actin turnover primarily occurring at the stereocilia tip. While stereocilia actin dynamics have been well-studied, little is known about the behavior of the actin crosslinking proteins, which are the most abundant type of protein in stereocilia after actin and are critical for stereocilia morphogenesis and maintenance. Here, we developed a novel transgenic mouse to monitor EGFP-fascin-2 incorporation. In contrast to actin, EGFP-fascin-2 readily enters the stereocilia core. We also compared the effect of EGFP-fascin-2 expression on developing and mature stereocilia. When induced during hair cell development, we observed increases in both stereocilia length and width. Interestingly, stereocilia size was not affected when EGFP-fascin-2 was induced in adult stereocilia. Regardless of the time of induction, EGFP-fascin-2 displaced both espin and plastin-1 from stereocilia. Altering the actin crosslinker composition, even as the actin filaments exhibit little to no turnover, provides a mechanism for ongoing remodeling and repair important for stereocilia homeostasis.

2.2 Introduction

Stereocilia are actin-based protrusions on the apical surface of sensory hair cells in the auditory and vestibular system that detect sound, movement and gravity. Bundles of auditory stereocilia have three rows of increasing height, giving the appearance of a staircase [62]. This architecture is necessary for function, as deflection of the bundle towards the tallest row gates mechanotransduction channels located at the tips of stereocilia in the shorter rows, thereby depolarizing the hair cell in response to sound [116-118]. Since hair cells are not renewed in

mammals, proper stereocilia homeostasis including precise regulation of their length is critical for maintaining the ability to hear.

Establishment and maintenance of proper stereocilia length depends on regulation of the actin core. The actin filaments within the core are uniformly oriented with their barbed, fast-growing ends towards the stereocilia tip [24]. These filament ends are relatively dynamic, with polymerization at the tip driving stereocilia elongation during the growth phase [27]. Actin continues to incorporate at the tips of mature stereocilia that maintain a constant length, implying that there is ongoing monomer exchange at filament barbed ends [28, 29]. Actin along the mammalian stereocilia shaft is exceptionally stable with little to no detectable actin incorporation [27-29], which contrasts with a previously accepted model where actin was continuously renewed by treadmilling [25, 26]. While several studies have focused on stereocilia actin dynamics, less is known about the behavior of actin crosslinking proteins, which are abundant in stereocilia.

Several different actin crosslinking proteins are found in stereocilia, including fascin-2 (FSCN2), espin (ESPN), plastin-1 (PLS1) and XIRP2, and contribute significantly to stereocilia development and maintenance [60, 63-66, 68]. For example, stereocilia in mice expressing mutant FSCN2 protein are initially normal, but subsequently degenerate and develop progressive hearing loss [64]. PLS1 is required for stereocilia to grow to their normal width, and also for maintaining stereocilia integrity and function [63]. ESPN is also essential for development as null mutants have abnormally short, thin and unstable stereocilia [68]. Each of these actin crosslinkers is developmentally regulated in mouse, with PLS1 and ESPN levels being relatively high as stereocilia are growing, after which their levels decrease. In contrast, the level of FSCN2 increases as stereocilia mature, corresponding to its role in stereocilia maintenance [64, 75].

To characterize FSCN2 incorporation in mouse, we generated a FLEx-EGFP-FSCN2 transgenic line that allows for controlled induction of EGFP-FSCN2 *in vivo*. We found that, in contrast to actin, EGFP-FSCN2 readily exchanges into the stereocilia core. In addition, EGFP-FSCN2 displaced endogenous PLS1 and ESPN from both mature and developing stereocilia and increased the size of developing, but not mature, stereocilia. Together, these data show that FSCN2 is

dynamic and can influence other actin crosslinkers to remodel the highly stable stereocilia actin core.

2.3 Results

2.3.1 EGFP-FSCN2 expression early in hair cell development

To monitor EGFP-FSCN2 incorporation in stereocilia *in vivo*, we developed a new transgenic mouse that allows for conditional EGFP-FSCN2 expression following Cre-mediated recombination. Using a FLEx switch [119, 120], recombination excises the tdTomato gene and inverts EGFP-FSCN2 gene so its expression is now driven by the near ubiquitous CAGG promoter (figure 2.9). We characterized three different EGFP-FSCN2 transgenic founder lines by crossing them to the Atoh1-Cre mice, which express Cre recombinase in inner, outer and vestibular hair cells from an early developmental stage [121]. Each transgenic founder line (Lines C, E and F) expressed EGFP-FSCN2 to different extents in hair cells. Line C had a mosaic expression pattern, with detectable EGFP-FSCN2 in approximately 60% of inner hair cells (IHCs), outer hair cells (OHCs) and utricular hair cells. The other lines showed more penetrant expression with more than 95% of auditory hair cells expressing in line F (table 1). In all founder lines, EGFP-FSCN2 expression resulted in almost exclusive localization of the protein to stereocilia of OHCs, IHCs and utricular hair cells and even distribution along the stereocilia length (Figure 2.1A-F). EGFP-FSCN2 expression was not detected in mice that lacked the Atoh1-Cre transgene. To measure the extent of EGFP-FSCN2 expression, we performed immunocytochemistry on the sensory epithelium of mosaic lines C and E with dye-conjugated FSCN2 antibody and compared the signal in EGFP-FSCN2 expressing and non-expressing IHCs in the same microscopic field (Figure 2.1G-I). We found that EGFP-FSCN2 expression increased total FSCN2 levels by 1.8-fold in line C and 2.4-fold in line E (Figure 2.1J).

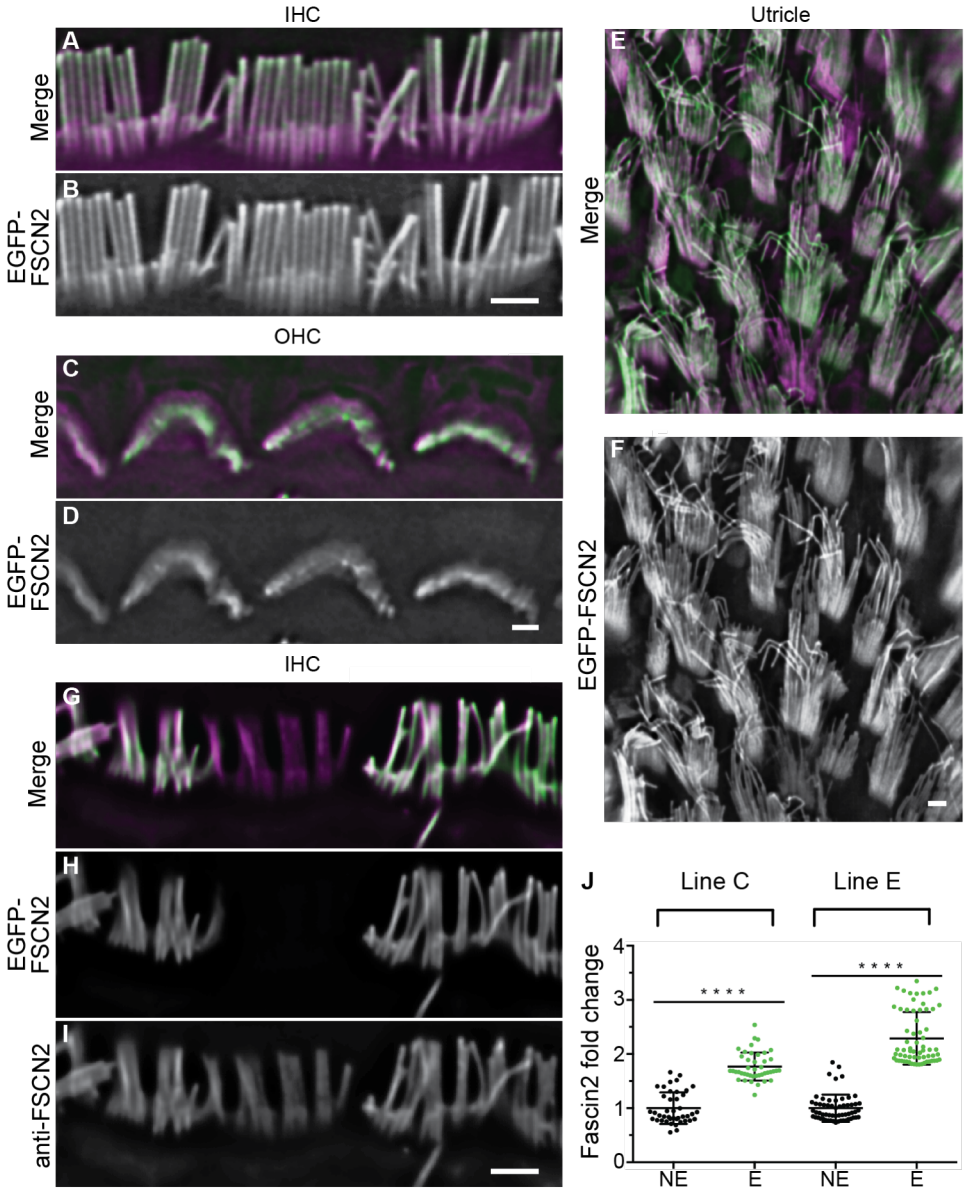

Figure 2.1 EGFP-FSCN2 localized to stereocilia following induction by constitutive Atoh1-cre. EGFP-FSCN2 localization in IHCs (A, B), OHCs (C, D) and utricular hair cells (E, F) from 4-week-old mice. F-actin is counterstained with phalloidin. EGFP-FSCN2 is green and phalloidin is magenta in merged images. EGFP-FSCN2 was detected uniformly along the stereocilia length. G-I) FSCN2 immunostaining in mosaic transgenic line. IHCs from 4-week-old mice were labeled with anti-FSCN2 antibody (I), EGFP-FSCN2 images (H) show expressing and non-expressing cells, merged in (G). The level of total fascin2 detected by immunostaining was increased in expressing cells. J) Plot of the fold change in total fascin2 levels in line C and line E EGFP-fascin2 transgenic lines between expressing cells and non-expressing cells (labeled E and NE). Error bars indicate SD. ****; P<0.0001(student's t-test). Each dot represents one stereocilium (n>=80 for each condition). Data for each plot was generated from three different mice. Scale bar=1 μm.

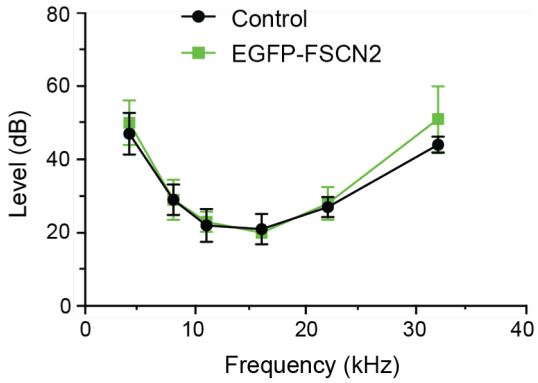

Figure 2.2 EGFP-FSCN2 expression did not perturb auditory function. Auditory Brainstem Response (ABR) thresholds from 5-week-old control mice and transgenic FLEx-EGFP-FSCN2 Atoh1-cre mice. Error bars indicate SD. For 32k, p=0.9506 n.s by Student's t-test. Five mice were analyzed for each genotype.

Finally, we tested hearing by measuring auditory brainstem response (ABR) thresholds in line E and F mice where EGFP-FSCN2 expression was the most penetrant. At 5 weeks of age, ABR thresholds of FLEx-EGFP-FSCN2 Atoh1-Cre mice were comparable to control mice lacking one or both transgenes, with similar ABR thresholds at all the monitored frequencies (Figure 2.2). These data indicate that expression of EGFP-FSCN2 does not disrupt stereocilia development or auditory function in young mice.

2.3.2 EGFP-FSCN2 rapidly incorporates into mature stereocilia

To characterize EGFP-FSCN2 incorporation in stereocilia, we irreversibly induced EGFP-FSCN2 expression at P21 by administering tamoxifen to FLEx-EGFP-FSCN2 Cagg-CreER mice, which ubiquitously express the tamoxifen regulated CreER-recombinase. EGFP-FSCN2 expression was detected uniformly along the entire length of auditory hair cell stereocilia 1 day after induction, which was the earliest timepoint tested (Figure 2.3A, B). EGFP-FSCN2 localized similarly 3 and 7 days post induction (Figure 2.3C-F), and expression was not detected in uninduced control mice (Figure 2.10). For comparison, we used an identical strategy to induce actin-EGFP from a FLEx-actin-EGFP transgene in a separate set of mice. Consistent with previous results, actin-EGFP

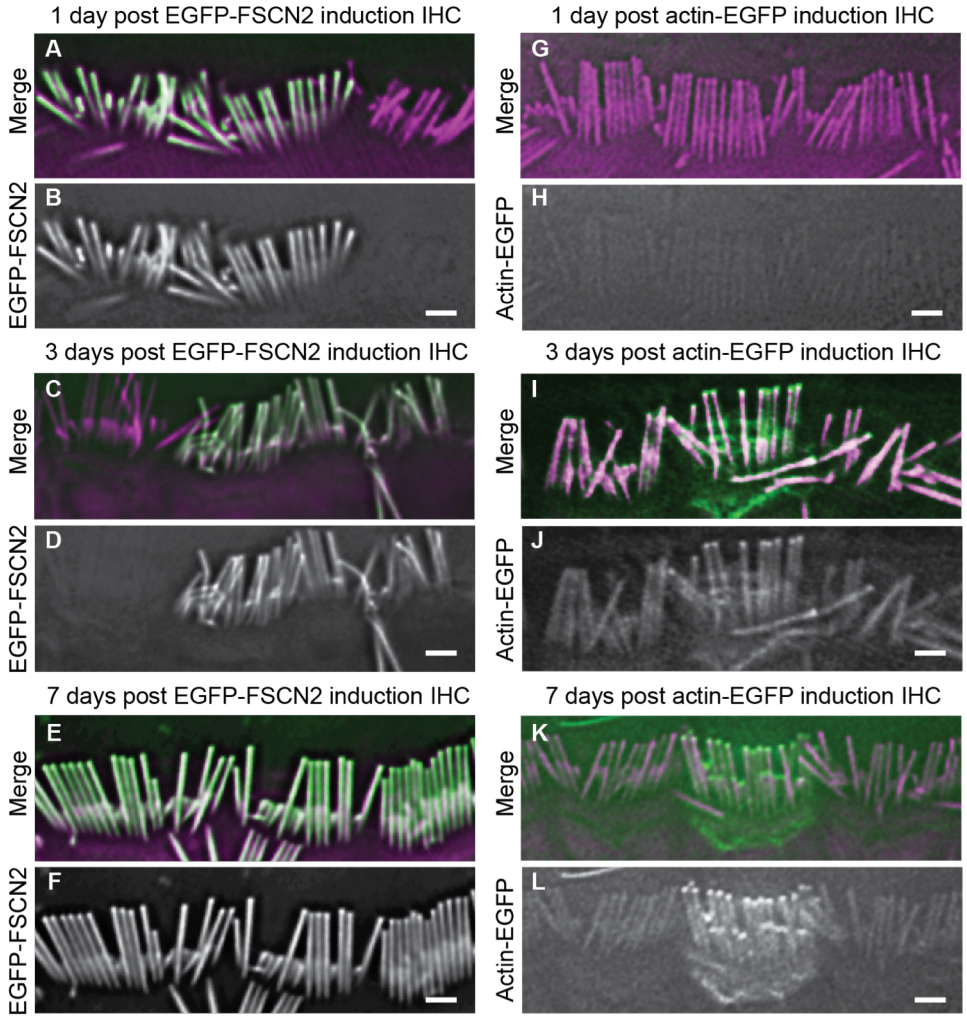

Figure 2.3 Incorporation pattern of EGFP-FSCN2 and actin-EGFP in stereocilia is different. EGFP-FSCN2 (A-F) and actin-EGFP (G-L), merged with phalloidin-stained F-actin 1, 3 or 7 days after tamoxifen was administered to FLEx-EGFP-FSCN2 Cagg-CreER mice. In merged images, EGFP-FSCN2 is in green and F-actin is in magenta. EGFP-FSCN2 incorporated along the stereocilia length while actin-EGFP incorporation was restricted to tips. At least three mice were used for each experiment. Scale bar=1μm.

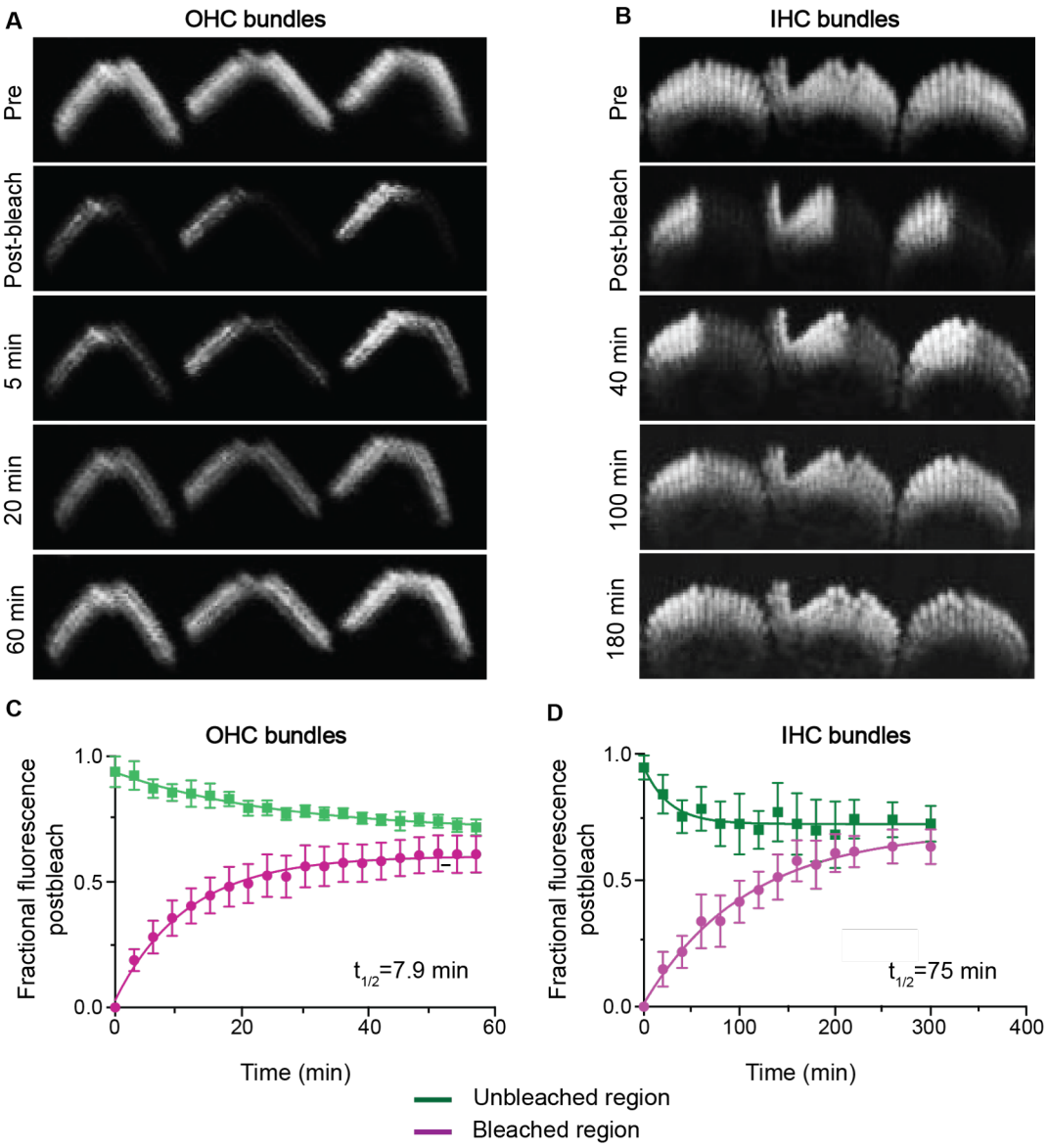

Figure 2.4 EGFP-FSCN2 fluorescence recovery after photobleaching. Small rectangular regions of stereocilia bundles from P7 FLEx-EGFP-FSCN2 Atoh1-cre explants were photobleached and fluorescence recovery was monitored over time. A) OHC bundles. B) IHC bundles. Plot showing changes in fluorescence intensity from pre-bleach values within bleached and unbleached sections in OHC (C) and IHC (D) bundles respectively. Error bars indicate SD. Values were corrected for additional bleaching that occurred during timelapse imaging.

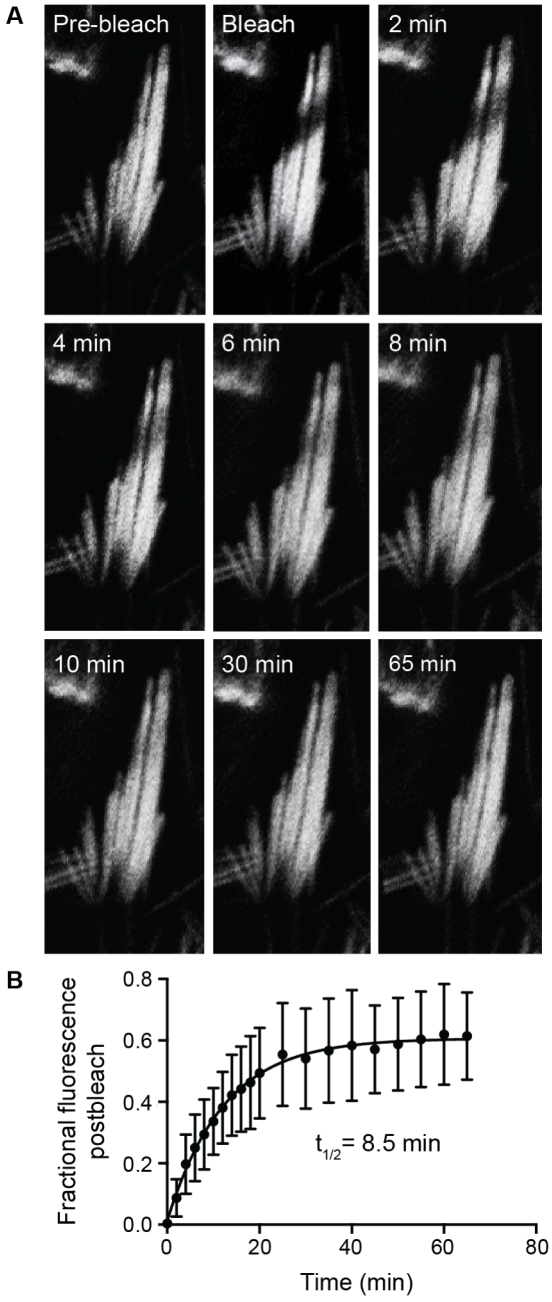

Figure 2.5 Fluorescence recovery of EGFP-FSCN2 after photobleaching in utricular hair cells. A) Small regions were bleached in P7 FLEx-EGFP-FSCN2 Atoh1-cre explants and fluorescence recovery was monitored over time till 65 min. B) Plot showing changes in fluorescence intensity post-photobleaching within the bleached region. Error bars indicate SD.

incorporation in stereocilia was limited to their tips 3 days after induction and could not be detected at earlier timepoints (Figure 2.3G-L) [28]. Together, our data demonstrate that in contrast to actin, FSCN2 readily incorporates into stable, established stereocilia cores.

2.3.3 EGFP-FSCN2 incorporation in postnatal explants

To further define the dynamics of EGFP-FSCN2 in stereocilia, we next measured its fluorescence recovery after photobleaching (FRAP) in early postnatal explants. Sensory epithelium was explanted from P7 FLEx-EGFP-FSCN2 Atoh1-Cre mice. Rectangular regions covering about half of inner and outer hair cell bundles were photobleached and EGFP-FSCN2 fluorescence recovery was monitored over time (Figure 2.4A, B). The time until half-maximal recovery ($t_{1/2}$) was 7.9 minutes in OHC stereocilia and 75 minutes in IHC stereocilia based on plots of the fraction of fluorescence recovered (Figure 2.4C, D). We also quantified fluorescence intensities of the unbleached portion of each bundle. Signal in these regions decreased as fluorescence recovered in the bleached portion (Figure 2.4C, D), likely due to movement of EGFP-FSCN2 within the bundle. Thus EGFP-FSCN2 can enter and exit the stereocilia core, and that $t_{1/2}$ differs between IHC and OHC stereocilia. For comparison, we also analyzed EGFP-FSCN2 FRAP in utricular stereocilia from the extrastriolar region, which has a mixed population of type I and type II cells. Owing to the different morphology of these bundles, we bleached a smaller rectangular region (Figure 2.5A). Half-maximal EGFP-FSCN2 recovery took 8.5 mins (Figure 2.5B), which is similar to that of OHC bundles.

2.3.4 PLS1 and ESPN levels in EGFP-FSCN2 transgenic mice

Since FSCN2 crosslinks are transient, we reasoned that other stereocilia crosslinkers are likely also dynamic and that EGFP-FSCN2 might compete with them for actin binding within stereocilia. To test this idea, we measured relative PLS1 and ESPN protein levels in EGFP-FSCN2 expressing cells and neighboring non-expressing cells in the mosaic lines. We first assessed cells in P21-P28 mice where EGFP-FSCN2 expression was initiated early in development by Atoh1-Cre. Anti-PLS1 antibody and anti-pan-ESPN antibody were used to label stereocilia. With constitutive expression of EGFP-FSCN2, PLS1 levels were decreased ~4 fold and ESPN levels were decreased 2.5-fold in IHC stereocilia expressing EGFP-FSCN2 (Figure 2.6A-F, 2.6 S,T). EGFP-FSCN2 expression reduced PLS1 (Figure 2.6 G-I, 2.6S) and ESPN (Figure 2.6 J-L, 2.6 T) levels ~1.5-fold

in OHC stereocilia, while PLS1 and ESPN levels dropped ~3.6-fold (Figure 2.6 M-O, 2.6 U) and 1.5-fold, respectively, (Figure 2.6 P-R, 2.6 V) in utricular stereocilia.

In order to determine if FSCN2 can displace PLS1 and ESPN in fully developed IHC stereocilia, we induced FLEx-EGFP-FSCN2 CAGG-CreER at P21. One week post induction of EGFP-FSCN2 expression, PLS1 levels decreased 1.4-fold while ESPN levels remained nearly stable (Figure 2.7A-F, 2.7M, 2.7O). Three weeks after EGFP-FSCN2 induction, PLS1 and ESPN levels decreased 3.5-fold and 1.5-fold, respectively, (Figure 2.7G-L, 2.7N, 2.7P), which is similar to their expression levels when EGFP-FSCN2 was constitutively expressed. These results suggest that EGFP-FSCN2 competes for actin-binding with PLS1 and ESPN and is consistent with the idea that actin crosslinkers are remodeled in mature stereocilia.

2.3.5 EGFP-FSCN2 expression during hair cell development results in elongation of stereocilia

Next, we wanted to determine if the altered crosslinker composition resulting from EGFP-FSCN2 expression influences stereocilia architecture. Correlative scanning electron microscopy (SEM) was used to image pairs of expressing and non-expressing cells identified by fluorescence microscopy in mosaic lines (Figure 2.11). Stereocilia length and width was increased when EGFP-FSCN2 was started early in hair cell development by Atoh1-Cre (Figure 2.8A-E). In contrast, initiating EGFP-FSCN2 expression in mature stereocilia at P21 had no apparent effect on stereocilia length or width (Figure 2.8F-J). These data show that EGFP-FSCN2 can promote elongation and widening in stereocilia only while they are still growing but once fully developed the ability for FSCN2 to influence morphology is lost.

2.4 Discussion

Mammalian stereocilia are distinguished by the exceptional stability of the actin filaments that comprise their core. Once formed, these filaments appear to be largely static, which contrasts with actin dynamics in structures such as microvilli, filopodia or lamellipodia, where the actin network turns over rapidly. To gain further insight into the unique behavior of the stereocilia core, we

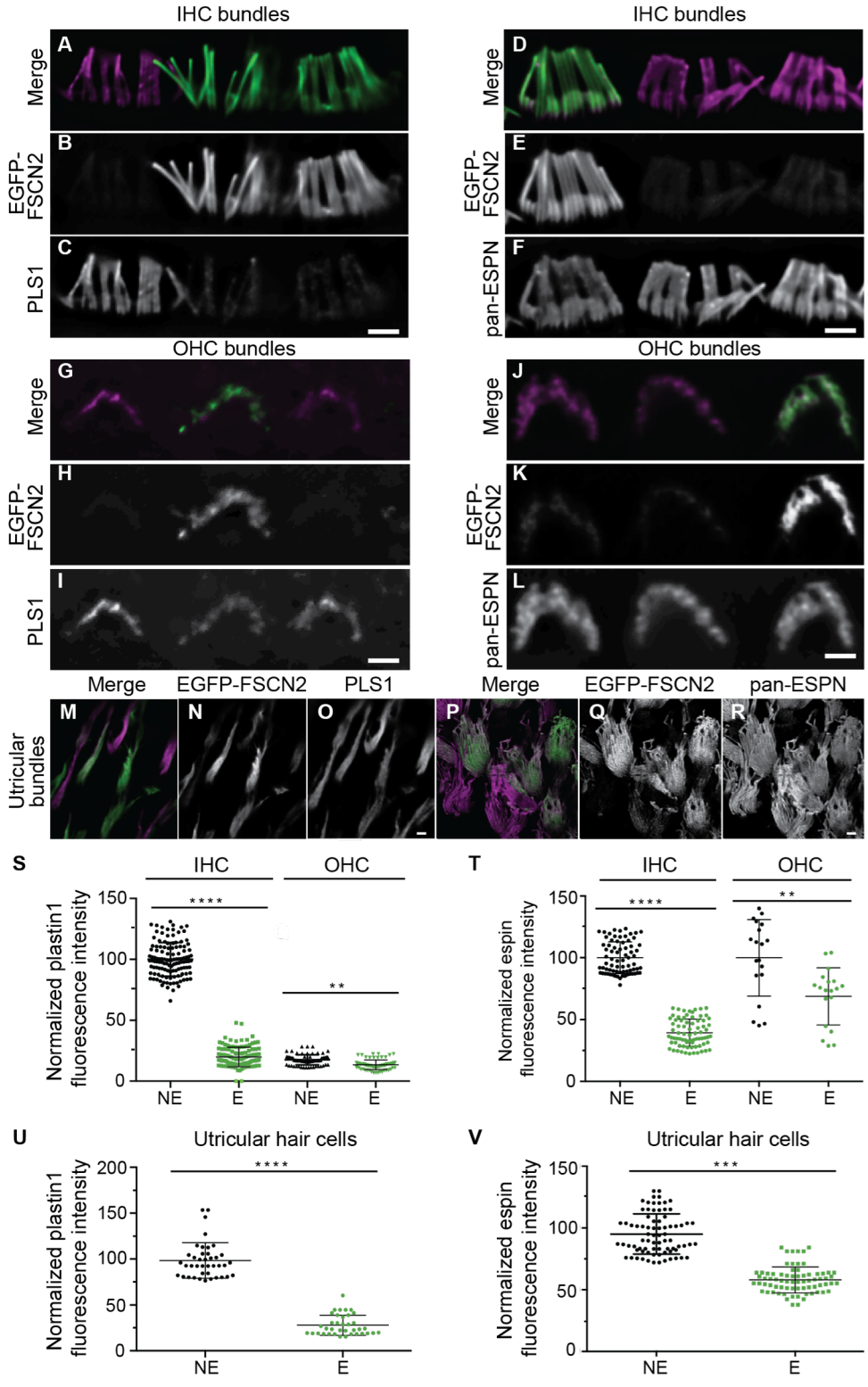
IHC bundles
IHC bundles
Merge
EGFP-FSCN2
PLS1
pan-ESPN
A
B
C
D
E
F
OHC bundles
OHC bundles
G
H
I
J
K
L
Merge
EGFP-FSCN2
PLS1
Merge
EGFP-FSCN2
pan-ESPN
Utricular bundles
M
N
O
P
Q
R
S
IHC
OHC
Normalized plastin1 fluorescence intensity
NE
E
T
Normalized espin fluorescence intensity
U
Utricular hair cells
V

Figure 2.6

Figure 2.6 Constitutive EGFP-FSCN2 decreases PLS1 and ESPN levels in stereocilia. Anti-PLS1 immunostaining of IHC (A-C), OHC (G-I) and utricular (M-O) stereocilia and anti-pan-espin immunostaining of IHC (D-F), OHC (J-L) and utricular (P-R) stereocilia from FLEx-EGFP-FSCN2 Atoh1-cre at 3 weeks of age. Mosaic EGFP-FSCN2 expression allowed for comparison of PLS1 or ESPN levels in neighboring cells with or without EGFP-FSCN2 expression. In merged images, EGFP-FSCN2 is green and anti-PLS1 or anti-pan-ESPN staining is magenta. EGFP-FSCN2 expressing cells (marked as E) had PLS1 and ESPN levels lower than the non-expressing cells (marked as NE) in all the cell types studied here. S-V) Plots of normalized fluorescence intensity of anti-PLS1 staining in IHC and OHC stereocilia (S) and utricular stereocilia (U) as well as anti-pan-espin staining in IHC and OHC stereocilia (T) and utricular stereocilia (V). In (S) and (T), intensity values for non-expressing and expressing cells (marked NE and E, respectively) were normalized to the average non-expressing IHC value and in (U, V) to the average non-expressing utricular value acquired in the same image. Error bars indicate SD; ****, $P<0.0001$; ***; $P<0.001$ and **, $P<0.05$ (one way ANOVA). Each dot represents one stereocilium.

assessed the dynamics of actin crosslinkers *in vivo* using a new mouse model. We found that actin crosslinkers, which are abundant and required for stereocilia formation and maintenance, are readily exchanged within stereocilia even though actin filaments are highly stable.

Early studies suggested that actin in stereocilia was continuously renewed by a treadmilling mechanism [25, 26]. However, recent experiments in mouse and bullfrog using several approaches including multi-isotope imaging mass spectrometry [29], conditional actin isoform ablation [29], live imaging of GFP-actin [27] and conditional expression of GFP-actin *in vivo* [28] instead demonstrated that actin incorporation is largely restricted to stereocilia tips, where the barbed ends of the filaments terminate. Away from the tip, very little actin is gained or lost along the length of the stereocilia core after it is formed, even over months-long experimental time courses (reviewed in [16]).

Mammalian stereocilia actin cores are much more stable than in zebrafish, where actin is reported to turnover on an hourly timescale [76], or of bundled actin filaments that form *Drosophila* bristles, where actin is depolymerized within days of assembly [77] Even though actin stability varies markedly between these structures, GFP-fascin isoforms behave similarly. Each isoform is able to incorporate into the existing actin network suggesting similar mechanisms drive turnover.

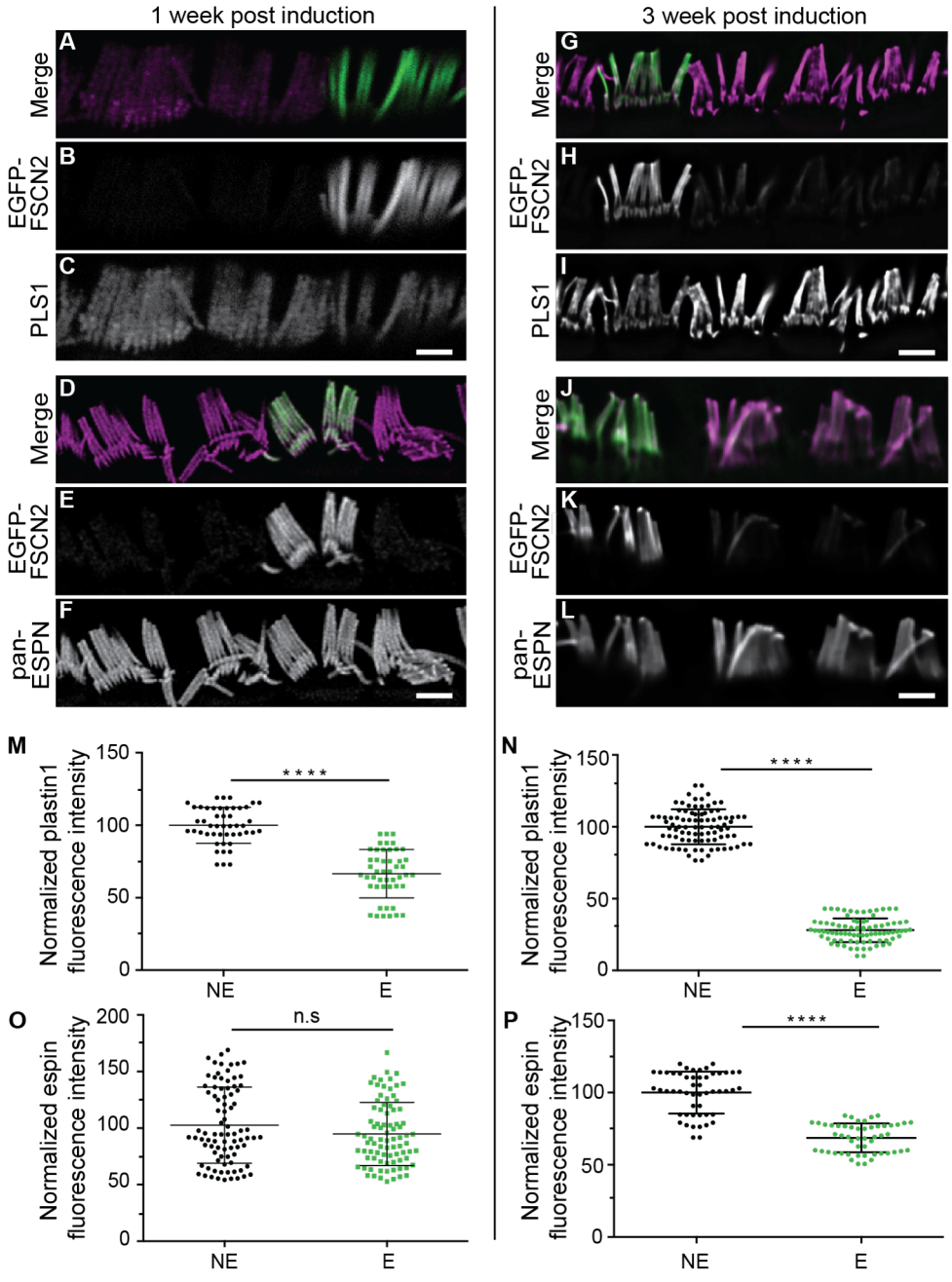
1 week post induction
3 week post induction
A
Merge
B
EGFP-FSCN2
C
PLS1
D
Merge
E
EGFP-FSCN2
F
pan-ESPN
G
Merge
H
EGFP-FSCN2
I
PLS1
J
Merge
K
EGFP-FSCN2
L
pan-ESPN
M
Normalized plastin1 fluorescence intensity
150
100
50
0
****
NE
E
N
Normalized plastin1 fluorescence intensity
150
100
50
0
****
NE
E
O
Normalized espin fluorescence intensity
200
150
100
50
0
n.s
NE
E
P
Normalized espin fluorescence intensity
150
100
50
0
****
NE
E

Figure 2.7

Figure 2.7 Inducing EGFP-FSCN2 expression in mature stereocilia reduces PLS1 and ESPN levels. One week (A-F) and three weeks (G-L) after EGFP-FSCN2 expression was started by Cre mediated recombination. Immunostaining of PLS1 (C,I) and pan-ESPN (F,L) while EGFP-FSCN2 fluorescence marks expressing cells (B,E,H,K). In merged images, PLS1 and pan-ESPN staining is magenta and EGFP-FSCN2 is green. M-P) Fluorescence intensity of PLS1 and pan-ESPN staining was normalized to the average value of non-expressing cells in the same image. Non-expressing and expressing cells are labeled NE and E, respectively, on the x-axes. Plots are PLS1 intensities 1 week (M) and 3 weeks (N) post induction; pan-ESPN intensities 1 week (O) and 3 weeks (P) post induction. Error bars indicate SD; **** $p<0.0001$ and n.s; not significant ($p>0.05$) (student's t-test). Each dot represents one stereocilium and three mice were analyzed for each experiment. Scale bar=1μm

However, the half-life of GFP-fascin isoforms in FRAP experiments varies considerably, ranging from seconds in *Drosophilia* bristles [77] and zebrafish stereocilia [76] to several minutes in mouse stereocilia, where the half-life is 10-fold longer in IHC stereocilia than OHC stereocilia (Figure 2.4 C, D). These differences may be in part due to how the actin filaments are packed, which differs according to the complement of actin crosslinkers that are expressed [75]. For example, IHC stereocilia cores have a central domain of hexagonally packed actin filaments that is lacking in OHC and utricular stereocilia, where filaments instead have a liquid packing arrangement [75]. Fascin promotes hexagonal packing [74] and, considering that fascin-actin binding is cooperative [73], it may dissociate more slowly in the central region of the IHC core.

Interestingly, expression of EGFP-FSCN2 resulted in decreased levels of ESPN and PLS1 localized to stereocilia, indicating that actin crosslinkers may compete for binding (Figure 2.6, 2.7). Besides competitive binding, crowding, decreased antigen accessibility or changes in filament conformation that decreased binding site availability or affinity for ESPN or PLS1 may account for their loss from stereocilia. Inducing EGFP-FSCN2 expression early in development or after stereocilia were mature decreased ESPN and PLS1 levels to a similar extent, suggesting that other crosslinkers besides FSCN2 are dynamic and can enter and leave the actin array independently of filament stability. Furthermore, PLS1 levels continued to decrease between 1 week and 3 weeks following EGFP-FSCN2 induction in mature hair cells, perhaps reflecting slower changes to the packing arrangement of actin filament shifts or normal developmental changes in the endogenous expression levels of crosslinkers [75].

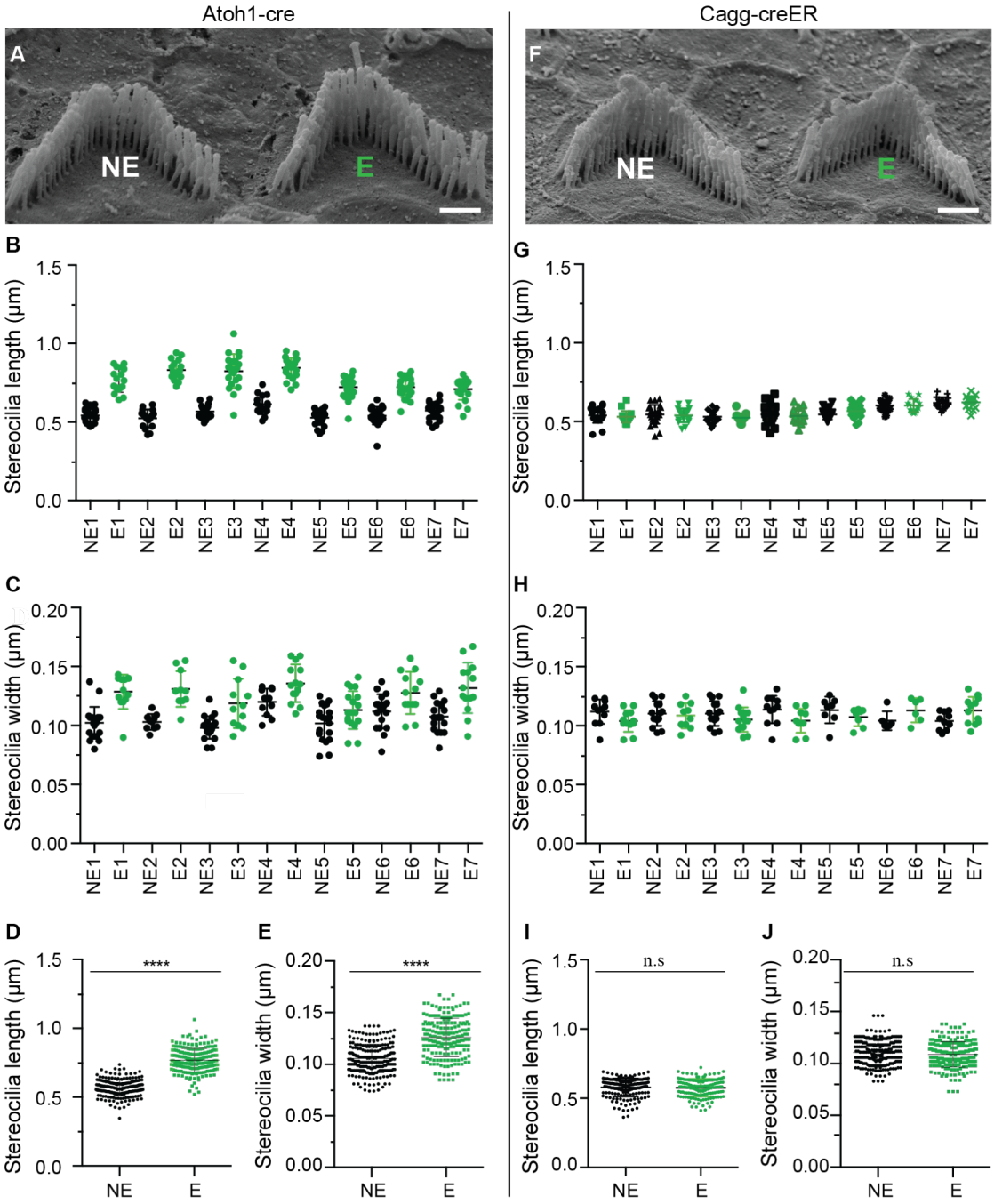
Atoh1-cre
Cagg-creER
A
F
NE
E
B
G
Stereocilia length (µm)
C
H
Stereocilia width (µm)
NE1 E1 NE2 E2 NE3 E3 NE4 E4 NE5 E5 NE6 E6 NE7 E7
D
E
I
J
****
n.s
NE
E

Figure 2.8

Figure 2.8 EGFP-FSCN2 expression promotes growth of developing but not mature stereocilia. A-E) OHC stereocilia from 3-week-old FLEx-EGFP-FSCN2 Atoh1-Cre mice, which express EGFP-FSCN2 from an early developmental stage. F-J) FLEx-EGFP-FSCN2 Cagg-CreER mice 3 weeks after tamoxifen administration to induce EGFP-FSCN2 expression. Pairs of cells where one cell was non-expressing and the other expressing EGFP-FSCN2 (marked NE and E, respectively) were identified by fluorescence microscopy prior to processing the sample for scanning electron microscopy (SEM). The identical pairs of cells were located and imaged by SEM (A, F). Lengths and widths of stereocilia in the shortest row of the bundle were measured from cells induced by Atoh1-Cre (B-E) and Cagg-CreER (G-J). Length (B,G) and width (C,H) of pairs of non-expressing and expressing cells from a single experiment (marked NE and E, respectively). Length (D,I) and width (E,J) collected from three independent experiments. Error bars indicate SD; ****; $P<0.0001$ and n.s; not significant ($p>0.05$) (student's t-test). Each dot represents one stereocilium and three mice were analyzed for each experiment. Scale bar=1μm.

Multiple crosslinkers are required for normal stereocilia maintenance while others are also required for bundle development (reviewed in [16]. We found that EGFP-FSCN2 increased stereocilia length and width only when it was initiated early in development (Figure 2.8 A-E), and had no effect on mature stereocilia (Figure 2.8 F-J). Likely, FSCN2 slightly increases the stereocilia growth rate, but not the developmental timing of growth. After a developmental shift that prevents further growth, crosslinking itself is not sufficient to increase stereocilia size. Instead, FSCN2 crosslinks, though themselves transient, seem to promote stereocilia stability as mice expressing mutant FSCN2 form normal stereocilia which subsequently degenerate [60].

Stereocilia maintenance is important since their integrity is essential for hearing and mammalian hair cells are never replaced. However, potential repair mechanisms are somewhat mysterious considering that the actin filaments are not detectably replaced, yet are almost certainly damaged by years of mechanical stimulation. How are small breaks in the core fixed? Perhaps transient actin crosslinks allow for a small amount of actin depolymerization and assembly at sites of damage while still preserving the overall stability of the structure.

2.5 Materials and Methods

Mouse lines

The FLEx-EGFP-FSCN2 construct was generated by cloning mouse EGFP-FSCN2 sequence into a base FLEx vector. The sequence elements are in the following order: chicken β-actin

promoter/intron, lox2372, tdTomato and lox511 in the forward orientation, followed by β-actin-EGFP, lox2372 and lox511 in the reverse orientation before an SV40 polyA signal in the forward orientation. Linear, gel purified DNA was injected into C57BL/6 pronuclei, which were implanted into pseudopregnant mice by the Mouse Genetics Core at The Scripps Research Institute. Mice carrying the transgene were identified by PCR analysis of genomic DNA from tail snips. Subsequent generations were maintained on the C57Bl/6 background. Atoh1-Cre and Cagg-CreER lines were as previously described [28, 111]. Mouse lines were maintained using standard husbandry practices in AALAC accredited facilities. The Institutional Animal Care and Use Committee of Indiana University – Purdue University School of Science approved all experimental procedures.

Table 2-1 Percentage of outer hair cells, inner hair cells and utricular hair cells expressing EGFP-FSCN2.

FLEx-EGFP-FSCN2 transgenic mouse line	% of expressing cells in Inner hair cells	% of expressing cells in Outer hair cells	% of expressing cells in Utricular hair cells
Line C	68%	64%	62%
Line E	93%	88%	80%
Line F	98%	96%	95%

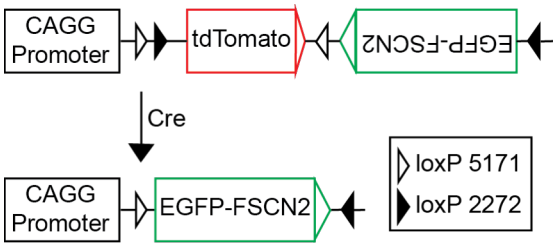

Figure 2.9 Schematic diagram representing Cre-mediated irreversible induction of EGFP-FSCN2. Cre-mediated recombination inverts EGFP-FSCN2 from its antisense to sense orientation, while deleting tdtomato. This results in constitutive expression of EGFP-FSCN2.

Imaging by fluorescence microscopy

Dissected cochleae were fixed in 4% formaldehyde in PBS for 16 hours at 4C before decalcifying in 170 mM EDTA in PBS for 16 hrs at 4˚C. Cochlear turns and the utricle were dissected, incubated in 0.2% Triton X-100 for 10 minutes and stained with phalloidin conjugated to Alexa-647 (ThermoFisher). For immunostaining with anti- PLS1, pan-ESPN (recognizing espin 1, 2B, 3A and 4 [86]) or FSCN2 antibodies, dissected cochleae were fixed in 4% formaldehyde in PBS for 20 minutes. The apical cochlear turn was immediately dissected, incubated in 0.5% Triton X-100 for 10 minutes, blocked in 5% goat serum for 1 hour and incubated with primary antibody

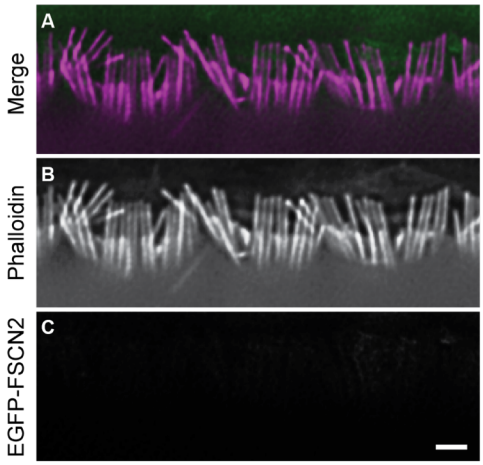

Figure 2.10 Tamoxifen is required for CreER to induce EGFP-FSCN2. A) Merged image of EGFP-FSCN2 and phalloidin stained F-actin. B) Phalloidin staining only. C) EGFP-FSCN2. In merged image, phalloidin is in magenta. Scale bar=1 μm.

overnight at 4˚C. Antibodies were anti-FSCN2 dye conjugated to Alexa-546 (1:50, [60]), anti-PLS1 (1:100, Abnova) raised in mouse, or anti-pan-ESPN (50 μg/ml, a kind gift from Dr. James Bartles) raised in rabbit. Unlabeled primary antibodies were detected with secondary antibodies conjugated to Alexa 546 and F-actin was counterstained with phalloidin-647. Samples were mounted in Prolong Gold and imaged either with a Nikon 90i epifluorescent microscope equipped with a Hamamatsu Orca Flash4-LT CMOS camera, SOLA-SE II LED illuminator and a 100X NA 1.45 objective or with a 63X NA 1.4 objective on a Leica SP8 confocal microscope operating in resonant mode. Images were subsequently deconvolved using Huygens X11 Essentials deconvolution software.

Scanning electron microscopy (SEM)

To compare the effect of EGFP-FSCN2 on stereocilia length, pairs of expressing and non-expressing cells were identified by fluorescence microscopy before tissue was processed for SEM. Pairs of cells were relocated based on comparison of distinctive landmarks in the tissue. Dissected cochlea turns were prepared as for fluorescence microscopy, suspended in a dish of PBS and imaged using either an upright Nikon 90i epifluorescent microscope or with an inverted Leica SP8 laser scanning confocal microscope equipped with a 40x NA 1.1 water immersion objective operating in resonant mode. The turns were then post-fixed in 2.5% glutaraldehyde, 0.1 M sodium cacodylate, 2 mM $CaCl_2$ overnight at 4C. To reduce surface charging, tissue was incubated in 2% each of arginine, glutamine, glycine and sucrose in water overnight at room temperature, followed by incubation in 2% tannic acid and guanidine hydrochloride for 2 hours at room temperature and then in 1% OsO_4 in water for an hour at room temperature, with washes in water between each solution. The samples were then transitioned to 100% ethanol, critical point dried from CO_2 and sputter coated with gold before imaging using a JEOL/FE JSM-7800F field emission scanning electron microscope. The stereocilia length and number measurements were analyzed using Fiji software.

Auditory Brainstem Response (ABR)

ABR waveforms were collected as previously described [60, 111] for frequencies of 4 kHz, 11 kHz, 16 kHz, 22kHz and 32 kHz. A Tucker-Davis Technologies System 3 was used to generate symmetrically shaped tone bursts 1 ms in duration with 300 μs raised cosine ramps that were delivered to a calibrated magnetic speaker starting at supra-threshold levels and decreasing in 5 dB steps to a sub-threshold level. Mice were anesthetized with Avertin and scalp potentials were recorded with subdermal electrodes with signals amplified 20,000 times, bandpass filtered between 0.03 and 10 kHz, digitized using a 20,000 kHz sampling rate and subjected to artifact rejection. The collected waveforms were stacked and the lowest level of stimulation that resulted in a definite waveform was considered as the threshold.

Fluorescence recovery after photobleaching (FRAP)

Middle turns of cochlea were dissected in DMEM:F12 media (Thermo Fisher Scientific) from P7 pups constitutively expressing EGFP-FSCN2 transgene and adhered to coverslips coated with

Matrigel (Thermo Fisher Scientific). The explants were incubated for 1.5 hours at 5% CO_2 and 37C before exchanging the media for DMEM (Thermo Fisher Scientific), 7% fetal bovine serum and 1 μg/ μl of ampicillin. Explants were incubated for overnight at the same conditions. The following day, explants were returned to DMEM:F12 media, inverted on a glass-bottom dish (Eppendorf) such that the coverslip was supported on spacers, suspending the explant with stereocilia oriented down and imaged with an inverted laser scanning confocal microscope (Olympus Fluoview1000, 40x NA1.1 water immersion objective). A rectangular region covering approximately half of the hair cell bundle was bleached using 488 nm laser at 100% power. Fluorescence recovery of EGFP-FSCN2 was monitored by imaging the same bundles at time points for 60 mins (OHCs), 5 hours (IHCs) or 65 mins (Utricular hair cells). Fluorescent intensities were determined in regions of interest (ROIs) using ImageJ software as previously described [28]. ROI1 is the bleached region of the bundle, ROI2 is the unbleached region of the bleached bundle and ROI3 is a region from an unbleached bundle in the same field. The plotted fractional fluorescence recovery values of EGFP-FSCN2 was calculated using the equation $[\{ROI1_x*(ROI3_{pre}/ROI3_x)\}-\{ROI1_0*(ROI3_{pre}/ROI3_0)\}]/(ROI1_{pre}-ROI_0)$ where $ROI1_{pre}$ is before bleaching, ROI_0 is immediately post bleach and $ROI1_x$ is at time x. Similarly, $ROI3_{pre}$ is before bleaching, $ROI3_0$ is immediately post bleach, $ROI3_x$ is at time x. ROI3 serves to correct the intensities of ROI1 and ROI2 for fading that occurred during timelapse imaging. The time until half-maximal recovery ($t_{1/2}$) was calculated from a fitted curve (one-phase decay function) in GraphPad Prism software. Fractional loss of fluorescence of EGFP-FSCN2 was calculated using the equation $1-[\{ROI2_{pre}-(ROI2_x *(ROI3_{pre}/ROI3_x)\}/ROI2_{pre}]$ where $ROI2_{pre}$ is before bleaching $ROI2_x$ is at time x.

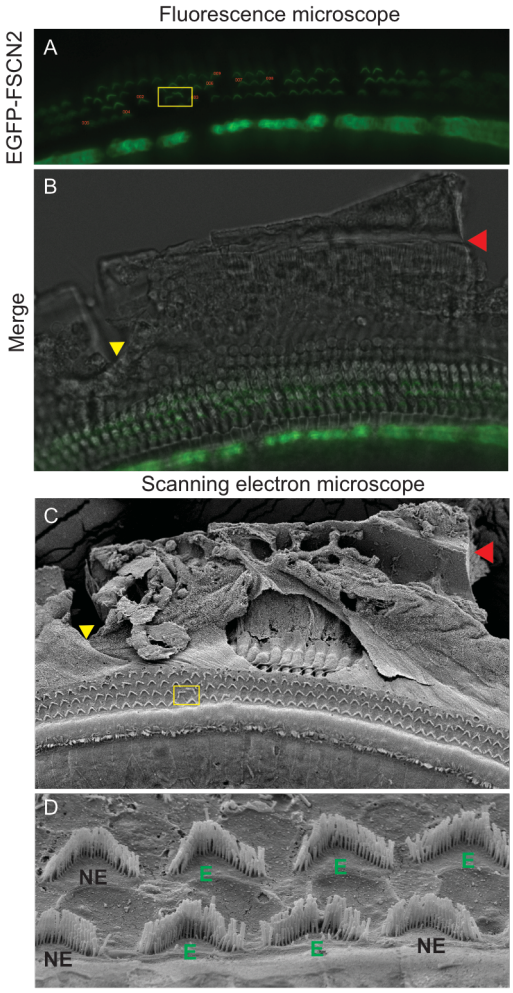

Figure 2.11 Correlative SEM**.** A) EGFP-FSCN2, marking several pairs of non-expressing and expressing EGFP-FSCN2 outer hair cells. B) Fluorescence merged with brightfield. C) SEM. Landmarks used to identify specific regions of the cochlear turn are indicated by yellow and red arrow heads while the yellow rectangle highlights distinctive stereocilia bundles.

CHAPTER 3. THE STABILITY OF STEREOCILIA ACTIN CORE IS DEPENDENT ON ACTIN CROSSLINKING PROTEINS

3.1 Introduction

Sensory hair cells in the inner ear require intricate actin-based structures called stereocilia that help in the detection of sound and motion induced vibrations. Stereocilia are arranged into bundles with 3 rows of increasing height giving the appearance of a staircase [62]. Deflection of the bundle towards the tallest row gates mechanotransduction channels located at the tips of stereocilia in the shorter rows, thereby depolarizing the hair cell in response to a physical force [116-118]. Stereocilia are formed from parallel actin filaments, with barbed ends at their tips and pointed ends at the base, extensively crosslinked by various actin crosslinking proteins. Since stereocilia are not regenerated, it is crucial that the length of stereocilia within each row is maintained for the entire life of an organism to sustain hearing ability.

The length of stereocilia depends on the dynamics of its actin core. Early work in GFP-actin transfected hair cell explants suggested that the stereocilia actin cores continuously treadmill [25]. According to this model, the steady state stereocilia length is maintained by an equal rate of actin monomer disassembly at the base and assembly at the tip. More recently, several studies have contradicted the actin treadmilling model and instead demonstrate that actin turnover primarily occurs at stereocilia tips with little to no actin turnover occurring along the remaining core. This tip turnover model has been supported by analyzing protein turnover through multi-isotope imaging mass spectrometry (MIMS), actin isoform ablation studies *in vivo* and studying GFP-actin dynamics *in vivo* [27-29]. The exceptional stability of actin core may be crucial for maintenance of stereocilia architecture over time.

Approximately 40% of the protein that is stable in the stereocilia actin core corresponds to actin [29]. This suggests that the remaining 60% of the proteins comprising of various actin crosslinkers including ESPN and FSCN2 are dynamically exchanged. We have previously shown that FSCN2 crosslinks are dynamic within mammalian stereocilia and compete with PLS1 and ESPN for actin binding, together demonstrating that actin crosslinkers can be dynamically remodeled [115]. These proteins link adjacent filaments together and also group crosslinked

filaments into larger bundles. Besides regulating bundle stiffness, dynamic crosslinks might be critical for reducing turnover of actin filaments in the stereocilia core. Consistent with this idea, fascin-crosslinked actin filaments depolymerize at a slower rate in biochemical assays [122] because dissociating actin monomers are held in close proximity, thereby favoring reassociation.

While ESPN and PLS1 are important for proper development of stereocilia, FSCN2 is thought to play a crucial role in stabilizing stereocilia once they are developed. An amino acid substitution of arginine to histidine at position 109 (R109H) of FSCN2 protein, which prevents actin crosslinking, results in hair bundle degeneration and progressive hearing loss in DBA/2J mice (expressing the $FSCN2^{R109H}$ mutation) [64]. FSCN2 is thus critical for maintenance of stereocilia structure and function during aging. Mutations in espin gene including the jerker mutation in mice, are associated with vestibular dysfunction and deafness [68]. The jerker mutation is a result of a frameshift mutation (caused by a deletion in guanine residue) in the espin gene. The auditory stereocilia of espin null mice (known as jerker mice because of their head-jerking movements) are abnormally thin and collapse by P10 [68] suggesting that espin is required to increase the number of actin filaments per stereocilia thus contributing to the increase in width of the stereociliary parallel actin bundles.

Although FSCN2 and ESPN crosslinkers play a critical role in stereocilia morphogenesis and maintenance, their effect on actin turnover is unknown. In this study, we generated novel transgenic mouse lines lacking ESPN or expressing mutant $FSCN2^{R109H}$ protein where actin-EGFP expression is induced irreversibly by cre recombinase, to study actin dynamics in stereocilia. We found that actin-EGFP incorporated along the entire utricular bundle in mice lacking ESPN in contrast to control mice where actin-EGFP incorporation was strictly limited to the stereocilia tips. Similarly, in mice expressing mutant $FSCN2^{R109H}$ protein, actin dynamics in mature stereocilia was different compared to that in control mice exemplified with an extended region of actin-EGFP incorporation from tip towards the base specifically in the apical row1 IHC stereocilia. Taken together, our study shows that ESPN-mediated crosslinking is required for the growth and stability of hair cell bundle while FSCN2 crosslinks are important for enhancing the stereocilia core stability and thus maintaining mature stereocilia length.

3.2 Results

3.2.1 Espin null utricular bundles have a dynamic stereocilia actin core

We obtained mice with a null mutation in the Espn gene (called the jerker allele, genotype $Espn^{je}$) on the CBA inbred strain background from Dr. James Bartles. $Espn^{je/+}$, which were crossed to B6 FLEx-actin-EGFP Cagg-creER mice. Resulting $Espn^{je/+}$ offspring carrying both transgenes were backcrossed for 5 consecutive generations to CBA $Espn^{je/+}$ mice. From these litters, we selected control mice ($Espn^{+/+}$ and $Espn^{je/+}$) and espin null ($Espn^{je/je}$) carrying both FLEx-actin-EGFP and Cagg-CreER. While stereocilia on both auditory and vestibular hair cells require espin for normal morphology, they are not equally affected. In contrast to auditory hair cell stereocilia of homozygous jerker mice ($Espn^{je/je}$) that are severely dysmorphic and are nearly absent by P10, vestibular hair cells in the extrastriolar region of the utricle are maintained until at least P40, though they are markedly thinner and shorter than in control mice [68]. Thus, we monitored actin-EGFP incorporation in the utricular extrastriolar stereocilia of $Espn^{je/je}$ mice by dosing with tamoxifen at P5, which irreversibly induced actin-EGFP expression by CreER recombinase, and tissue was harvested at P12. The espn null utricular bundles had actin-EGFP incorporation along the entire length of stereocilia in contrast to $Espn^{+/+}$ and $Espn^{je/+}$ mice, where actin-EGFP was predominantly restricted to the tips (Figure 3.1). We also imaged auditory hair cells but were unable to monitor actin-EGFP incorporation in $Espn^{je/je}$ mice since the apical surface were completely devoid of hair cells (Figure 3.2 G-I, Q-S). Whereas in $Espn^{+/+}$ and $Espn^{je/+}$ mice, actin-EGFP incorporation was restricted to the tips of OHC stereocilia and row 2/3 of IHC stereocilia (Figure 3.2 A-F, K-P). Row1 apical IHC stereocilia had an increased actin-EGFP incorporation extending from tip to base reporting stereocilia growth at this stage.

Previous study has shown that the jerker heterozygotes have reduced levels of ESPN (half that found in a normal WT mouse) resulting in a transient distal tapering evident between P0 and P10

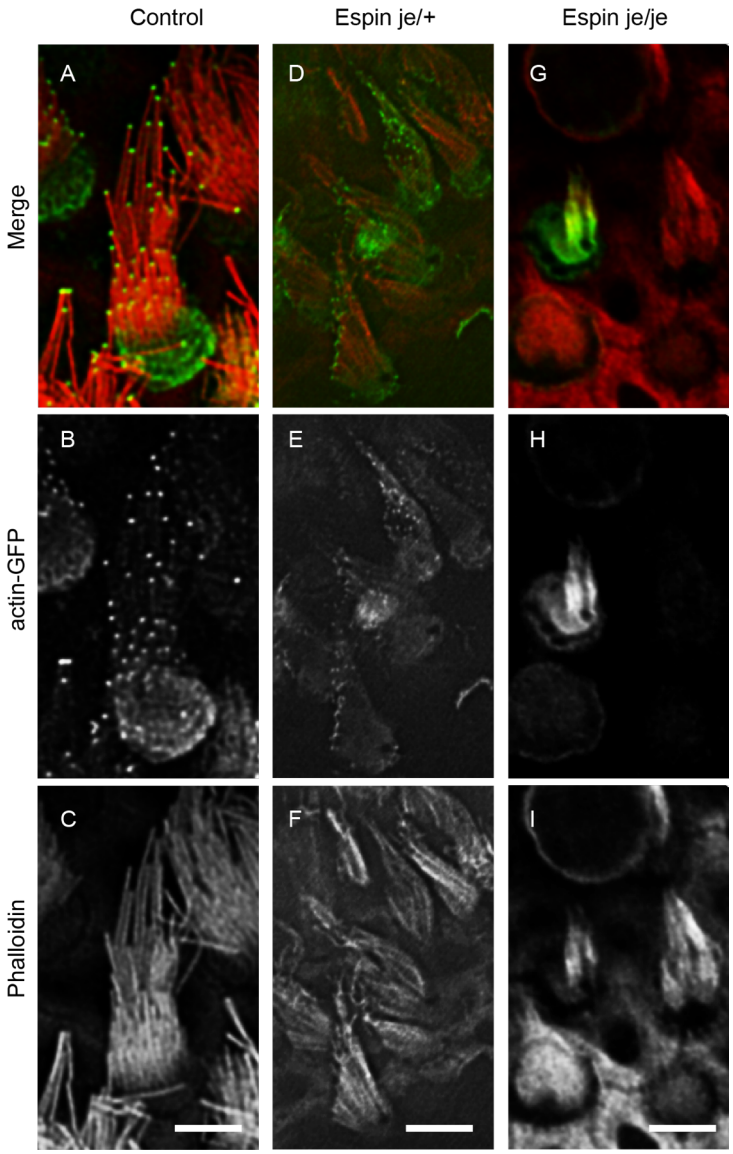

Figure 3.1 Actin-EGFP incorporation in espin null utricular hair cell stereocilia. Mice were dosed with tamoxifen at P5 and tissue was analyzed at P12. A-C) Control, D-F) Jerker heterozygote ($Espin^{je/+}$), G-I) Jerker homozygote ($Espin^{je/je}$). A, D, G) In merged images, actin-GFP is green while F-actin is red. B, E, H) actin-EGFP in grayscale. C, F, I) Phalloidin only. Actin-GFP localized to tips of control and $Espin^{je/+}$ stereocilia, but along the entire length of espin null stereocilia. Scale bar=1 μm.

in the auditory stereocilia [68]. To determine if this transient tapering at an early postnatal age has an impact on actin core stability in mature stereocilia, we utilized the actin-EGFP transgenic reporter to monitor actin incorporation in $Espn^{je/+}$ mice. Mice were dosed with tamoxifen at P21 and tissue was harvested at 5 months post-dosage. We found that actin-EGFP incorporation was

restricted to the row1 IHC stereocilia tips in both Espn$^{+/+}$ and espin$^{je/+}$ mice. Interestingly, there was a broader region of actin-EGFP incorporation in the shorter row stereocilia in espin$^{je/+}$ mice which was markedly different from that in control mice (Figure 3.3 A-F). The fluorescent intensity values of actin-EGFP at row 1 and row 2 stereocilia tips were plotted for both Espn$^{+/+}$ and espin$^{je/+}$ mice. The values for each stereocilium were normalized to the row1 average values

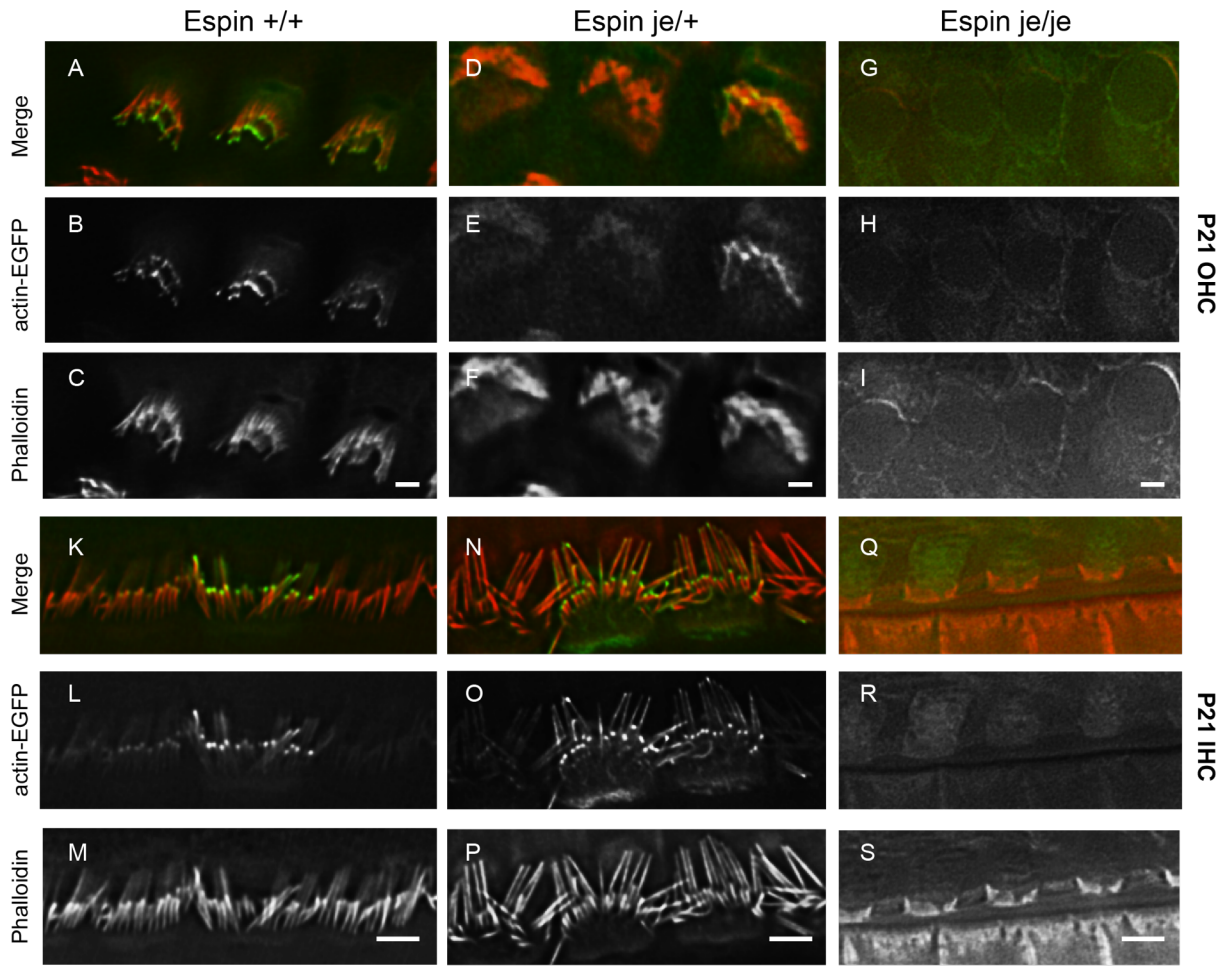

Figure 3.2 Actin-EGFP incorporation in espin null auditory hair cell stereocilia. Mice were dosed with tamoxifen at P5 and tissue was analyzed at P12. A-C) Espin$^{+/+}$ OHC, K-M) Espin$^{+/+}$ IHC, D-F) Jerker heterozygote (Espin$^{je/+}$) OHC, N-P) Espin$^{je/+}$ IHC, G-I) Jerker homozygote (Espin$^{je/je}$) OHC, Q-S) Espin$^{je/je}$ IHC. A, D, G, K, N, Q) In merged images, actin-EGFP is green while F-actin is red. B, E, H, L, O, R) actin-EGFP in grayscale. C, F, I, M, P, S) Phalloidin only. Actin-EGFP localized to tips of control and Espin$^{je/+}$ stereocilia, while not detected in Espin$^{je/je}$ bundles because the hair cells have degenerated. Scale bar=1 µm.

within an individual cell. Row 2 stereocilia tips in espin$^{je/+}$ mice had an increased and variable level of actin-EGFP incorporation in comparison to row1. In contrast, row 2 and row 1 stereocilia in control mice had comparable levels of actin-EGFP incorporation at their tips (Figure 3.3 G). This suggests that the reduced levels of ESPN does impact the stability of the mechanotransductive stereocilia core.

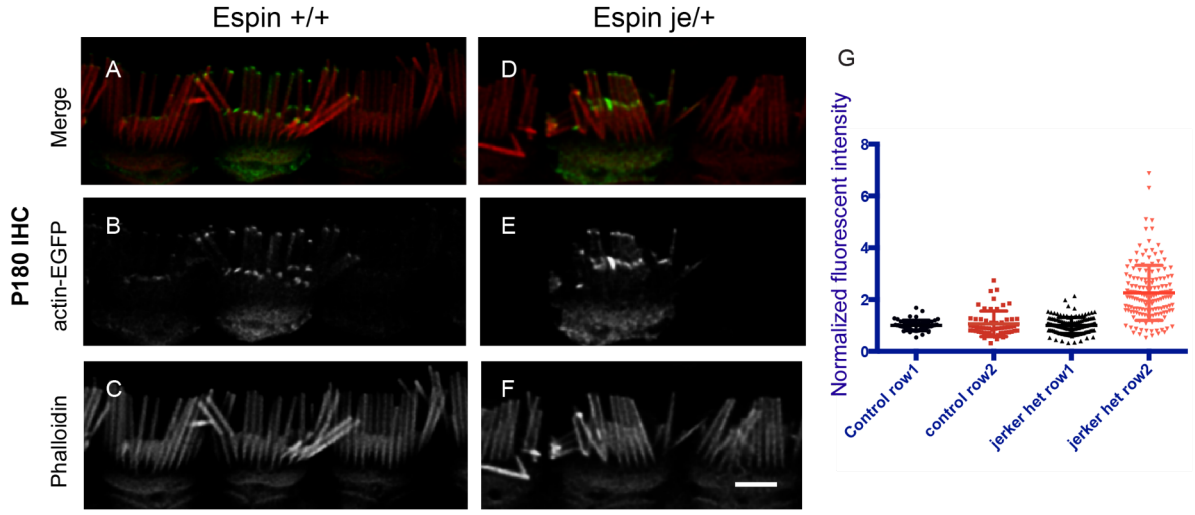

Figure 3.3 Actin-GFP incorporation in espin het inner hair cell stereocilia. Mice were dosed with tamoxifen at P21 and tissue was 5 months post dosage. A-C) Control, D-F) espin$^{je/+}$. A, D) In merged images, actin-EGFP is green while F-actin is red. B, E) actin-EGFP in grayscale. C, F) Phalloidin only. Actin-EGFP localized to tips of control as well as in espin$^{je/+}$ stereocilia. G) Plot showing fluorescent intensity values of actin-EGFP at the row 1 and row 2 stereocilia tips in control and jerker heterozygote mice. Row 2 stereocilia in jerker heterozygote mice incorporated increased and more variable levels of actin-EGFP compared to row1. The variability was much lower in row 2 of control mice. Scale bar=1 µm.

3.2.2 FSCN2^{R109H} mice have a diffused actin-EGFP incorporation in their stereocilia core

Next, we generated B6 mouse lines expressing both FLEx-actin-EGFP and Cagg-CreER transgenes with homozygous alleles of FSCN2^{R109H} (encoding the mutant FSCN2^{R109H}) for analyzing actin dynamics in mature stereocilia since FSCN2 is important for maintaining mature stereocilia length. Actin-EGFP expression was induced by dosing mice with tamoxifen at P21. Cochlear tissues were harvested at different time points following induction of expression. Actin

dynamics have been monitored at three different timepoints (4 weeks, 8 weeks and 20 weeks' post dosage). At 4 weeks post-dosage, actin-EGFP incorporation was restricted to the tips of stereocilia

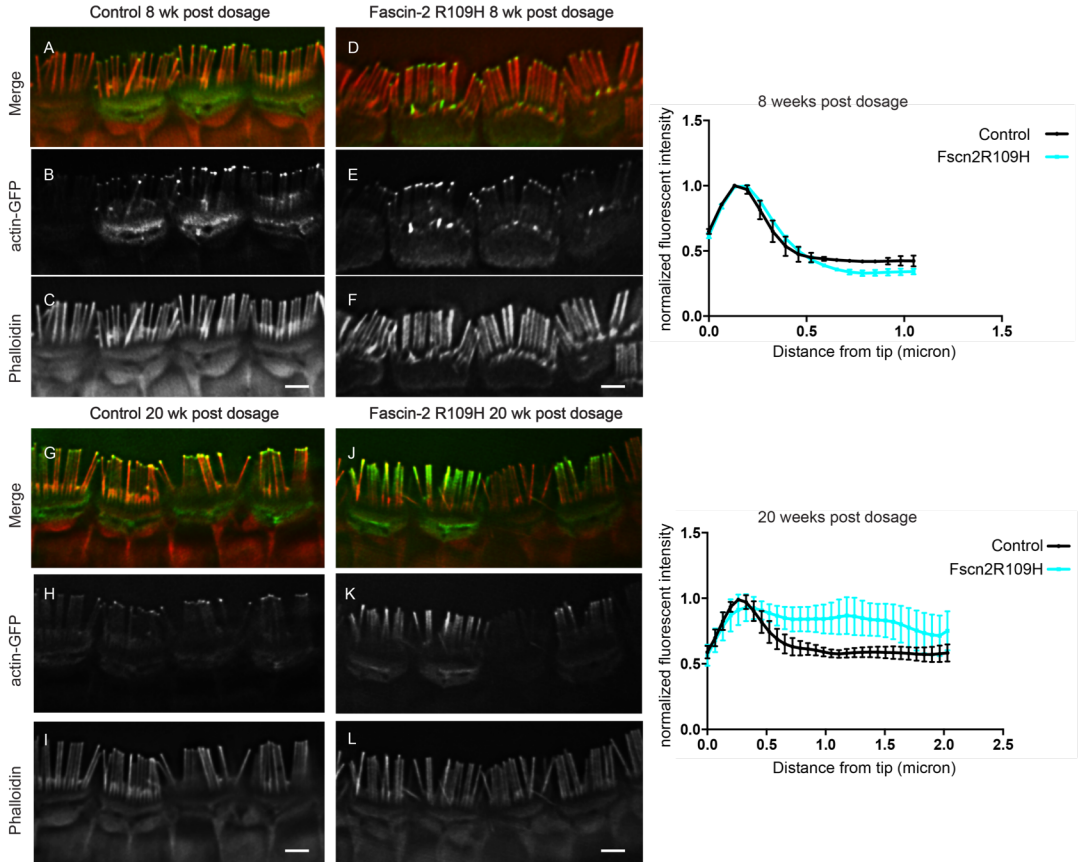

Figure 3.4 Actin-EGFP incorporation in FSCN2^{R109H} stereocilia. Actin-GFP incorporation in IHC stereocilia of control mice (A-C, G-I) and mice expressing FSCN2^{R109H} (D-F, J-L) 8 and 20 weeks' post dosage. A, D, G, J) F-actin is red while actin-GFP is green. B, E, H, K) Actin-GFP in grayscale. C, F, I, L) phalloidin only. Actin-GFP localized to the stereocilia tips in control while extended down to the shaft in mice expressing FSCN2^{R109H} 20 weeks post dosage. M, N) Actin-EGFP fluorescence intensity measured along the row1 stereocilia length from tip to the base 8 weeks and 20 weeks post induction respectively. Scale bar=1 µm.

in all the IHC bundles similar to that observed in control B6 mice (data not shown). From 8 weeks post dosage timepoint onwards, actin dynamics in FSCN2^{R109H} mice was different. Instead of being limited to tips, incorporation extended down to the shaft of row1 IHC stereocilia, suggesting the actin core was less stable (Figure 3.4 A-F). This pattern of incorporation became more pronounced by 20 weeks post-dosage where actin-EGFP was incorporated along a significant portion of the length of row1 stereocilia in almost all of the IHC bundles in the apical turn (Figure 3.4J-L). This is markedly different from control B6 stereocilia, where actin-EGFP incorporation is only evident at stereocilia tips at all the timepoints studied (Figure 3.4G-I). The region of actin-EGFP incorporation in row1 of FSCN2^{R109H} mice was quantified by measuring fluorescent intensity of actin-EGFP along the lines extending from the stereocilia tips towards the base which demonstrated an extended actin-EGFP incorporation in FSCN2^{R109H} mice compared to control mice (Figure 3.4 M, N). This broad region of actin incorporation phenotype was predominantly evident in the apical region of cochlea suggesting that cochlear positioning might affect stability of the core that becomes evident with age.

Shorter row stereocilia in some bundles had an increased actin-EGFP incorporation compared to control stereocilia, again suggesting that the actin core was less stable (Fig 3.4A-F). The quantification of actin-EGFP fluorescent intensity in shorter rows awaits better images from more samples. Previously it was reported that the length of row1 stereocilia is unaffected by the FSCN2^{R109H} mutation. Our data suggests that although the row1 length is not altered by the absence of FSCN2 crosslinking in contrast to the shorter rows, the stability of the core might be perturbed with age. This indicates that actin crosslinking by FSCN2 helps limit actin turnover in the stereocilia actin core.

3.2.3 A balanced crosslinker composition is important for proper stereocilia maintenance

The above data suggests that defective actin crosslinking in mice carrying FSCN2^{R109H} mutation results in an early onset age-related hearing loss due to destabilization of the actin core, resulting in the shortening of rows 2 and 3. Can overexpression of FSCN2 increase the stability of the core and prevent shortening? Our previous studies have shown that expression of EGFP-FSCN2 does not perturb auditory function in young mice[115]. EGFP-FSCN2 promotes growth in developing but not in mature stereocilia. EGFP-FSCN2 also competes with other abundant actin crosslinkers,

ESPN and PLS1, for binding sites in stereocilia, both when EGFP-FSCN2 is expressed constitutively from an early developmental stage and when its expression is induced in mature hair cells [115]. We thus wanted to determine if the altered crosslinker composition influence stereocilia function and structure when EGFP-FSCN2 is expressed for a longer timeframe than what has been previously studied. To this end, ABR thresholds of mice constitutively expressing EGFP-FSCN2 were analyzed following long-term expression of EGFP-FSCN2. While the ABR thresholds in these mice were comparable to control mice at 5 weeks and 3 months of age, they had slightly (though not significantly) elevated ABR thresholds at 6 and 9 months of age across almost all the frequencies tested (Figure 3.5 A, B). This suggests that EGFP-FSCN2 is unable to prevent age-related hearing loss.

Next, we analyzed stereocilia morphology of these mice at 9 months using scanning electron microscopy (SEM). Hair bundles expressing EGFP-FSCN2 were more dysmorphic than control mice at this age. This further suggests that overexpression of EGFP-FSCN2, which results in a corresponding decrease in PLS1 and ESPN levels, might be detrimental when expressed in hair cells for a prolonged time (Figure 3.5 C-F). We also observed irregular lengths within the same row in a bundle (Figure 3.5 C-F). Very occasionally, distal tapering was noted in some of the row 3 stereocilia (Figure 3.5 E, F). We also detected a reduction in the number of OHC row 3 stereocilia within a single bundle compared to control mice and some missing hair cells were evident (Figure 3.5 D). Our data suggest that increasing FSCN2 crosslinking does not improve stereocilia function and morphology. This is consistent with the idea that the stereocilia actin core is maximally stable in wild-type hair cells.

3.3 Discussion

Mammalian stereocilia are exceptionally stable as compared to other actin-based structures like microvilli or filopodia, where actin is known to continuously turnover. The reasoning behind this amazing stability is not known. Do actin crosslinkers in stereocilia have a role in conferring stability to the core? Actin crosslinking proteins including FSCN2 are important for long-term

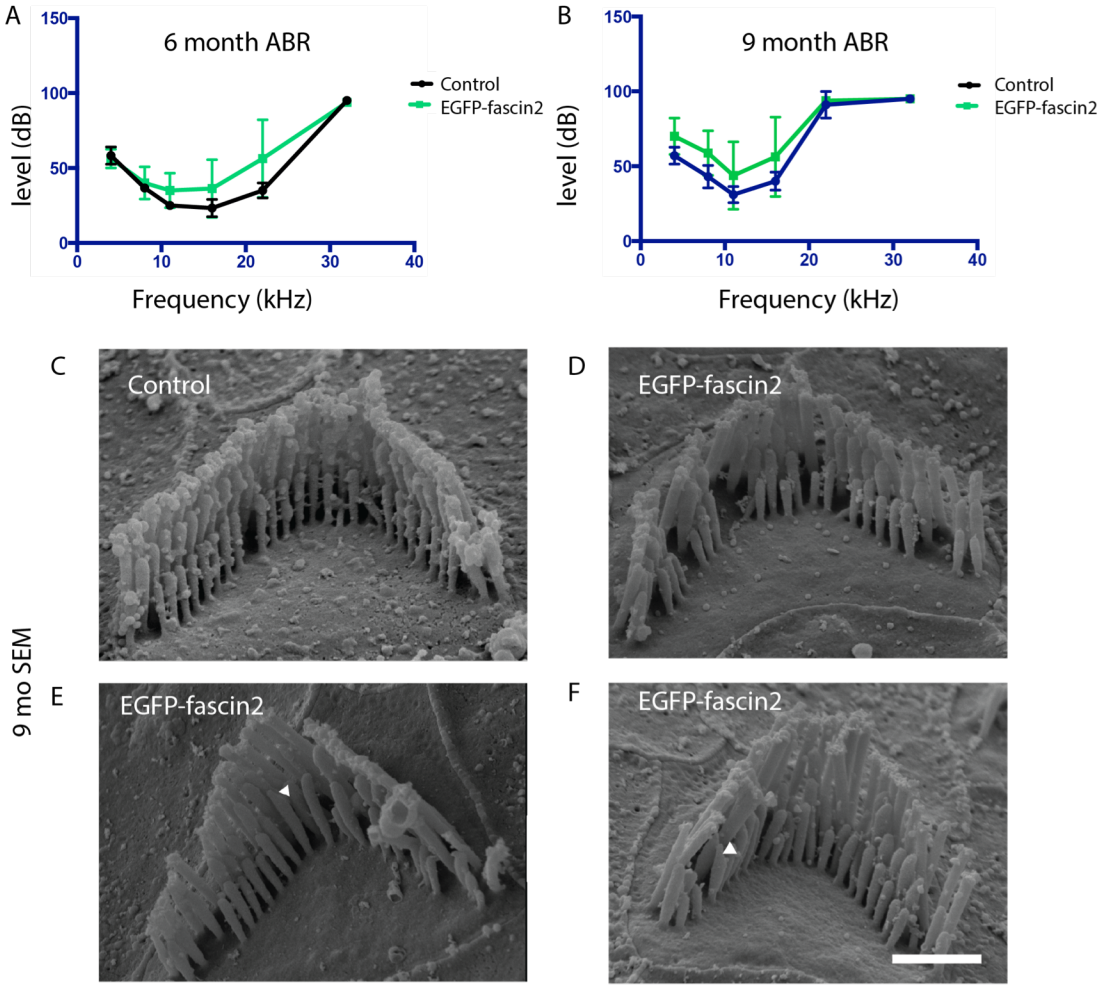

Figure 3.5 Effect of prolonged EGFP-FSCN2 expression on stereocilia function and morphology. ABR thresholds of mice expressing EGFP-FSCN2 at A) 6 and B) 9 months of age. ABR thresholds were obtained at 4, 8, 11, 16, 22 and 32 KHz. EGFP-FSCN2 elevates ABR thresholds at both the timepoints studied. Error bars indicate SD. P=0.192 (Student's *t* test). The Scanning electron micrographs of 9-month-old C) control B6 mice while D), E) and F) represent mice expressing EGFP-FSCN2 portraying irregular length and missing stereocilia. Distal tapering in row3 stereocilia is indicated with white triangle. Four mice were analyzed in ABR and SEM for each genotype. Scale bar=1 µm.

maintenance of stereocilia architecture since mutation in FSCN2 result in progressive hearing loss along with degeneration in stereocilia. In contrast, ESPN-mediated crosslinking is crucial for development of stereocilia as a null mutation of ESPN results in abnormally short, thin and unstable stereocilia. To better understand the role of FSCN2 and ESPN crosslinks in regulating actin stability, we studied actin dynamics in mice lacking ESPN and mice expressing mutant $FSCN2^{R109H}$ protein in mouse hair cells *in vivo*. We determined that in contrast to control mice where actin-EGFP incorporation is restricted to stereocilia tips, actin in the mutant mice was more dynamic, thus reporting an unstable core in absence of actin-crosslinking.

Earlier studies have suggested that actin treadmills in stereocilia but recent experiments using MIMS, conditional ablation of actin isoforms and conditional expression of GFP-actin in mice have refuted the treadmilling model [28, 29]. These studies have instead demonstrated that actin turnover occurs only at the stereocilia tips with a half-life time of 215 mins while actin remains stable along the stereocilia shaft over months long timeframe that has been studied so far [28]. The exceptional stability of the mammalian stereocilia actin core is attributed to the actin crosslinking proteins which are dynamic in contrast to actin. Each actin crosslinking protein contribute significantly to the stereocilia morphogenesis and maintenance. For example, stereocilia in mice lacking all espin isoforms are abnormally thin, suggesting that espin is required to increase the number of actin filaments per stereocilia. Correspondingly, cochlear hair cell stereocilia are unstable and they collapse, shorten and disappear around P10 [68]. Espin isoforms can also alter actin dynamics, shifting filaments in microvilli from a treadmilling behavior to a stable non-treadmilling array, potentially accounting for the phenotype of espin null stereocilia [86]. This suggests that actin treadmilling in stereocilia is blocked by espin isoforms, allowing stereocilia to grow and stabilize. Interestingly, in our study we noted actin-EGFP incorporation to extend down from tip to the base of stereocilia in espin null utricular bundles in contrast to the tip localization of actin-EGFP in control mice. Now the question is whether the actin turnover in espin null stereocilia occurs by a tip-to-base treadmilling mechanism or does it instead incorporate uniformly along the entire length of stereocilia? Uniform incorporation would mean that actin filaments are not continuous and instead consist of several filaments that start and end at multiple locations within the stereocilia actin core where actin can polymerize and depolymerize unless restricted by actin crosslinking proteins. There is

some evidence for uniform incorporation of actin in zebrafish stereocilia, though this has not been observed in mammalian systems.

Other crosslinkers, such as FSCN2, seem to be more important for stabilizing mature stereocilia. Stereocilia in mice expressing $FSCN2^{R109H}$ mutant protein, which cannot crosslink actin, develop normally but fail to maintain stereocilia lengths [60]. Considering that shorter row stereocilia stochastically incorporate actin-EGFP consistent with cycles of shortening and regrowth [28], we hypothesized that FSCN2 crosslinks normally function to stabilize row 2/3 actin cores and prevent shortening. In this study, we determined that defective crosslinks in these mice altered normal actin dynamics in adult mice as demonstrated by a broad region of actin-EGFP incorporation extending from tip towards the base in apical IHC stereocilia. This phenotype being mostly pronounced in the tallest row of stereocilia in older mice suggests that FSCN2 mediated crosslinking is critical to maintain stability of the core in mature stereocilia, an absence of which results in an unstable core. It is unclear how the length of row 1 stereocilia is maintained in the mutant mice in spite of having a less stable core whereas only the shorter rows degenerate. A combination of factors including tip-link defects, channel activity and defective crosslinking possibly contributes to the degeneration of the shorter row stereocilia.

Since reducing actin crosslinking when FSCN2 is mutated results in a less stable core, increasing crosslinking might have an opposite effect i.e, increase core stability, hence preventing stereocilia shortening. In contrast, when we overexpressed FSCN2, we didn't observe any beneficial effect. Instead prolonged expression of EGFP-FSCN2 caused an elevation in the ABR thresholds along with stereocilia morphology defects including missing stereocilia and irregular lengths within a bundle. Considering that EGFP-FSCN2 competes with ESPN and PLS1 for binding sites in stereocilia, decreased localization of these proteins could offset any benefit gained from increasing FSCN2 levels. Measuring actin incorporation in FSCN2 overexpressing cells would help resolve whether the core is actually stabilized.

Our current study provides an insight into the functional significance of actin stability in stereocilia development and maintenance. We illustrated here that crosslinkers confer stability to the stereocilia actin core. Efficient crosslinking by espin possibly converts treadmilling actin to a

stable, non-treadmilling array that is important for proper stereocilia development. Whereas, FSCN2 more likely help stabilize stereocilia core to maintain stereocilia length. An absence of crosslinking destabilizes the core resulting in stereocilia degeneration along with progressive hearing loss.

3.4 Materials and Methods

Mouse lines

To monitor actin dynamics in FSCN2^{R109H} mice, mice expressing FSCN2^{R109H} mutation (maintained on a C57BL/6 background) were crossed with FLEx-β-actin-EGFP Cagg-creER mice (generated previously in [28]. While to monitor actin dynamics in jerker mice, we obtained mice with a null mutation in the Espn gene (called the jerker allele, genotype Espn^{je}) on the CBA inbred strain background from Dr. James Bartles. Espn$^{je/+}$ mice were crossed to B6 FLEx-β-actin-EGF Cagg-creER mice and resulting Espn$^{je/+}$ offspring carrying both transgenes were backcrossed to Espn$^{je/+}$ mice. Mouse lines were maintained using standard husbandry practices in AALAC-accredited facilities. The Institutional Animal Care and Use Committee of Indiana University–Purdue University School of Science approved all experimental procedures.

Imaging by fluorescence microscopy

As described previously [115], dissected cochleae were fixed in 4% formaldehyde in phosphate-buffered saline (PBS) for 16 h at 4C before decalcification in 170 mM EDTA in PBS for 16 h at 4C. Cochlear turns and the utricle were dissected, incubated in 0.2% Triton X-100 for 10 min, and stained with phalloidin conjugated to Alexa-568 (ThermoFisher). Samples were mounted in Prolong Gold or prolong diamond and imaged either with a Nikon 90i epifluorescence microscope equipped with a Hamamatsu Orca Flash4-LT CMOS camera, a SOLA-SE II LED illuminator, and a 100X NA 1.45 objective or with a 63X NA 1.4 objective on a Leica SP8 confocal microscope operating in resonant mode. Images were subsequently deconvolved using Huygens X11 Essentials deconvolution software.

Scanning electron microscopy

Cochleae were dissected from mice. After removing the round and oval window membranes and making a small hole in the apex, the tissue was fixed by immersing in a solution of 2.5%

glutaraldehyde, 1mM CaCl2 and 0.1M sodium cacodylate for 4 h at room temperature before decalcification in 170mM EDTA at 4C for 16 h. As previously described in [115], the organ of Corti was dissected and to reduce surface charging, tissue was incubated overnight at room temperature in 2% each of arginine, glutamine, glycine, and sucrose in water, followed by incubation in 2% tannic acid and guanidine hydrochloride for 2 h at room temperature and then in 1% OsO4 in water for 1 h at room temperature, with washes in water between each solution. The samples were then transitioned to 100% ethanol, critical point dried from CO2, and sputter coated with gold before imaging using a JEOL/FE JSM-7800F field emission scanning electron microscope. The stereocilia length and number measurements were analyzed using Fiji software.

Auditory brainstem response

ABR waveforms were collected as previously described [60, 111] for frequencies of 4, 11, 16, 22, and 32 khz. a tucker-davis technologies system 3 was used to generate symmetrically shaped tone bursts 1 ms in duration with 300-µs raised cosine ramps that were delivered to a calibrated magnetic speaker starting at suprathreshold levels and decreasing in 5-db steps to a subthreshold level. mice were anesthetized with avertin and scalp potentials were recorded with subdermal electrodes with signals amplified 20,000 times, bandpass filtered between 0.03 and 10 khz, digitized using a 20,000-khz sampling rate, and subjected to artifact rejection. the collected waveforms were stacked and the lowest level of stimulation that resulted in a definite waveform was considered as the threshold**.**

CHAPTER 4. ESSENTIAL NUCLEOTIDE AND PROTEIN DEPENDENT FUNCTIONS OF ACTB/β-ACTIN

This chapter has been published in reference [123]. Figures 5-9 were generated by me while the remaining data was generated by other co-authors.

4.1 Abstract

The highly similar cytoplasmic β- and γ-actins actins differ by only four functionally similar amino acids, yet previous *in vitro* and *in vivo* data suggest that they support unique functions due to striking phenotypic differences between *Actb* and *Actg1* null mouse and cell models. To determine if the four amino acid variances were responsible for the functional differences between cytoplasmic actin, we gene-edited the endogenous mouse *Actb* locus to translate γ-actin protein. The resulting mice and primary embryonic fibroblasts completely lacked β-actin protein, but were viable and did not present with the most overt and severe cell and organismal phenotypes observed with gene knockout. Nonetheless, the edited mice exhibited progressive high frequency hearing loss and degeneration of actin-based stereocilia as previously reported for hair cell-specific *Actb* knockout mice. Thus β-actin protein is not required for general cellular functions, but is necessary to maintain auditory stereocilia.

4.2 Significance Statement

Actin is required for many general and specialized cellular functions. Two isoforms, β-actin and γ-actin, are ubiquitously expressed and 99% identical in amino acid sequence, yet previous studies indicated only β-actin is indispensable for life. The nucleotide sequence of each gene also varies, providing additional regulation that may make β-actin indispensable. To separate the effects of protein and nucleotide sequences, the β-actin gene was edited to encode γ-actin protein, while retaining any regulation contained in the nucleotide sequence. The mice, which lack β-actin protein, are viable and appear to be normal. However, they develop progressive hearing loss as

auditory sensory cells degenerate. Together, these results show that β-actin function depends on both its nucleotide and protein sequence.

4.3 Introduction

The actin cytoskeleton contributes to a wide range of cellular functions such as muscle contraction, cytokinesis, migration, chromatin remodeling, transcriptional regulation and regulating cell shape [124]. Though often thought of as a single protein, there are actually six actin isoforms encoded by separate genes. Four actins are considered muscle specific while the cytoplasmic β- and γ-actin isoforms are ubiquitously expressed. The cytoplasmic actins are highly similar at the level of both gene and protein: the coding sequences of *Actb and Actg1* are 89% identical and β- and γ-actin differ at just 4 out of 375 amino acid residues. Furthermore, human and mouse *Actb* coding sequences are 90% identical and β- and γ-actin primary sequences are identical across birds and mammals [100]. The fact that selective pressure has maintained these seemingly slight differences for hundreds of millions of years has confounded cell biologists since the cytoplasmic actins were initially cloned four decades ago: why do cells apparently require two such highly similar proteins?

Corresponding to the evolutionary conservation of β- and γ-actin, several lines of evidence demonstrate that both isoforms are required for normal cellular function. In humans, point mutations in *ACTB* and *ACTG1* cause a spectrum of developmental defects as well as progressive hearing loss, demonstrating lack of compensation between the isoforms [125-127] . In mice, genetic ablation of each isoform results in different phenotypes. Loss of *Actb* results in embryonic lethality and severe cellular proliferation and migration defects in null fibroblasts, while *Actg1* knockouts survive, though with decreased fitness [108-110]. Finally, ablation of each isoform in auditory sensory hair cells causes different patterns of progressive hearing loss and degeneration of actin-based protrusions [111].

The phenotypes arising from conventional gene knockout may result from loss of isoform specific transcript or protein. Most notably, the *Actb* transcript has a 3'UTR "zipcode" sequence not found

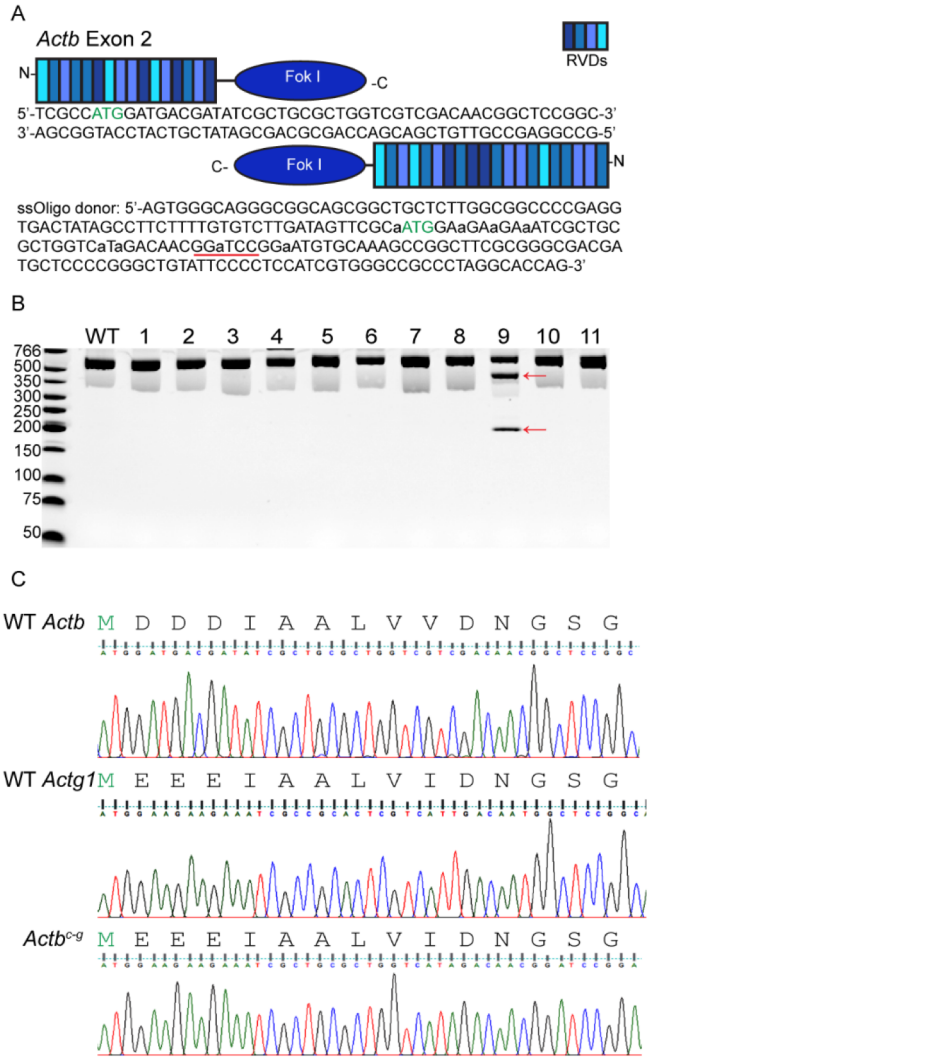

Figure 4.1 Genetically engineered *Actb*$^{c\text{-}g}$ mice via TALENs and a single-strand oligo donor. (A) Schematic of TALEN target sequence within WT mouse *Actb* exon 2 and the ssOligo homologous repair donor sequence. The start codon is labeled in green, BamHI restriction enzyme site is underlined in red, edited nucleotides are denoted in lowercase letters. (B) RFLP results of WT and live born F0 pups using the BamHI restriction enzyme digestion. Red arrows indicate the correct digested fragments. (C) Sanger sequence results for WT mouse pup number 9. Aspartic acids 2-4 and Valine 10 in WT β-actin have been changed to glutamic acids 2-4 and isoleucine 10 in the corresponding location in γ-actin.

in *Actg1* transcripts that targets the transcript to subcellular regions and regulates translation [102, 128]. In addition, the transcripts differ in ribosome density and translation rate [129]. On the protein level, purified β- and γ-actin have slightly different polymerization rates and differentially interact with a subset of actin binding proteins [103, 130]. Considering that nucleotide and amino acid sequences are evolutionally maintained, both may contribute to critical cellular functions.

To separate the effects of non-coding regulation from differences in β- and γ-actin protein, we edited the *Actb* gene encoding β-actin to instead encode γ-actin while retaining all the endogenous *Actb* regulatory elements. We found the resulting mice, despite lacking β-actin protein, were born in Mendelian ratios and that the mice and derived fibroblasts appeared phenotypically normal. These results, together with those of a recent study using a similar approach [129] demonstrate that the nucleotide sequence is a critical determinant of actin isoform specific function. However, we also found that β-actin protein is required to maintain the shape and function of auditory hair cells, demonstrating that other functions of cytoplasmic actins are defined by their amino acid sequences.

4.4 Results

4.4.1 *Actb*$^{c\text{-}g}$ mice coding γ-actin instead of β-actin protein are grossly normal

We designed transcription activator-like effector nucleases (TALENs) and a single-stranded oligo (ssOligo) donor template to edit the endogenous *Actb* locus within the mouse genome (Fig. 4.1A). A single founder was edited so the *Actb* exon 2 encoded E2-4 and I10 instead of D2-4 and V10, thus producing γ-actin protein instead of β-actin (Fig. 4.1 B-C). We named the edited allele as *Actb*$^{c\text{-}g}$ for *Actb* **c**oding **g**amma. Whereas conventional cre-mediated knockout of *Actb* results in embryonic lethality[108], homozygous *Actb*$^{c\text{-}g}$ mice were born in Mendelian ratios (27% *Actb*$^{+/+}$, 50% *Actb*$^{c\text{-}g/+}$, 23% *Actb*$^{c\text{-}g/c\text{-}g}$; chi-squared = 0.80) and in normal litter sizes (average of 7 pups/litter; 17 litters). In addition, homozygous *Actb*$^{c\text{-}g}$ mice were visibly indistinguishable from

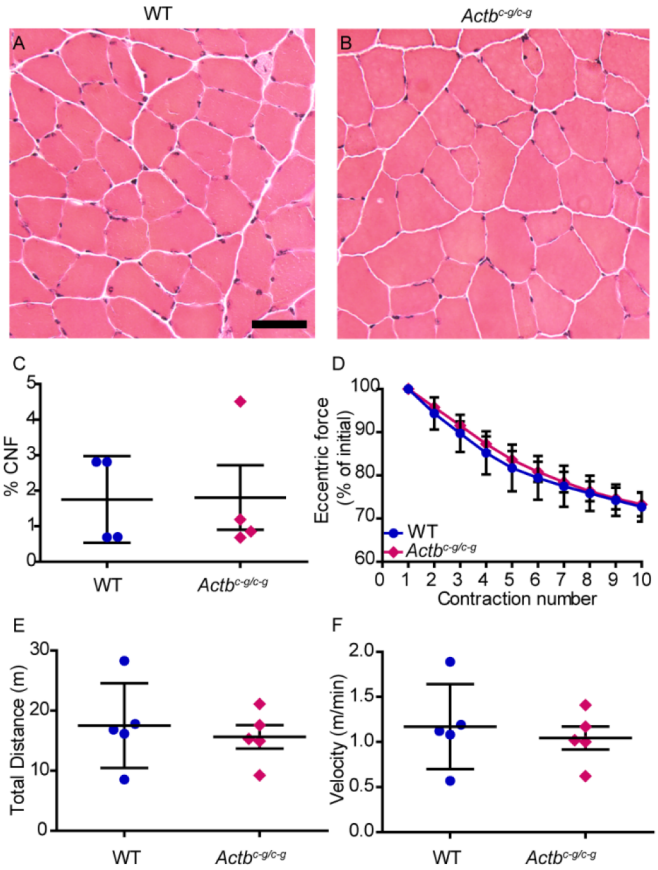

Figure 4.2 *Actb*$^{c\text{-}g}$ mice display CNF percentage and open field activity not different than WT. (A-B) Representative H&E images of WT and homozygous *Actb*$^{c\text{-}g}$ mice quadricep muscle. (C) Calculated CNF % of WT and homozygous *Actb*$^{c\text{-}g}$ mice quadricep. N=4 mice, n≥400 fibers per mouse. (D) Graph of eccentric force drop as a percentage of initial force N=5. (E) Total distance traveled during an open field activity assay. (F) Average velocity of each mouse during an open field activity assay. N=5. Error bars are S.D.

Actb$^{+/+}$ littermates, grew at the same rate as their littermates and exhibited no perinatal or early onset death out to six months of age (n=30).

Cre-mediated knockout of *Actb* in skeletal muscle or the central nervous system resulted in a mild myopathy or hyperactivity, respectively[131, 132]. These phenotypes were not detected in homozygous *Actb*$^{c\text{-}g}$ mice. *Actb*$^{c\text{-}g}$ homozygous mice displayed no evidence of histopathology in quadriceps muscles at 6 months of age (Fig. 4.2A-C), had no defects in muscle contractile function (Fig. 4.2D, Table 4.1) and behaved normally in an Open Field assay (Fig. 4.2E-F). Overall, these results suggest that β-actin protein is dispensable for mouse viability if γ-actin protein is expressed from the endogenous *Actb* locus.

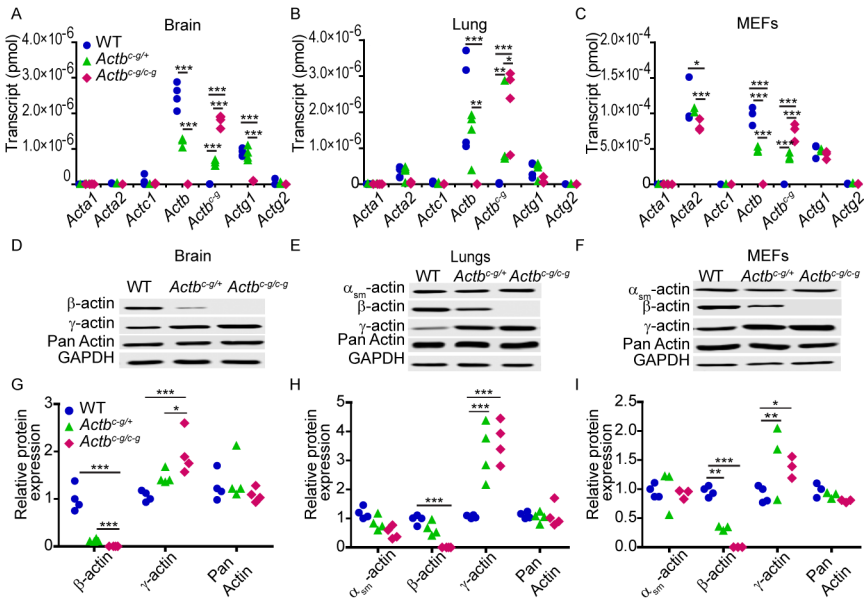

Figure 4.3 *Actb*$^{c\text{-}g}$ transcript is synthesized from the edited *Actb* locus and correlates with a 2-fold increase in γ-actin protein expression. (A-C) Calculated quantity of isoactin transcript via qRT-PCRs in brain (N=4), lung tissues (N=4) and MEFs (N=3). X-axis denotes actin isoform. Y-axis denotes transcript in pmol. (D-F) Representative western blots in brain, lung and MEFs. (G-I) Calculated relative isoactin protein expression in WT, heterozygous and homozygous *Actb*$^{c\text{-}g}$ mice brain (N=4), lung (N=4) and MEFs (N≥3). X-axis denotes actin isoform. Y-axis denotes relative protein expression which were normalized to GAPDH and relative to a WT sample. Two-way ANOVA with Bonferroni post-test. *p<0.05, **p<0.01, ***p<0.001

4.4.2 *Actg1*/γ-actin responds to loss of β-actin protein in *Actb*$^{c\text{-}g}$ mice

We next measured transcript and protein levels for each actin isoform in tissue and cells from *Actb*$^{c\text{-}g}$ mice to determine how the actin isoform composition changed without β-actin expression. *Actb* transcript and β-actin protein in brain, lung and primary MEFs were decreased in *Actb*$^{c\text{-}g}$ heterozygotes and absent in homozygous mice. Correspondingly, the edited *Actb*$^{c\text{-}g}$ transcript

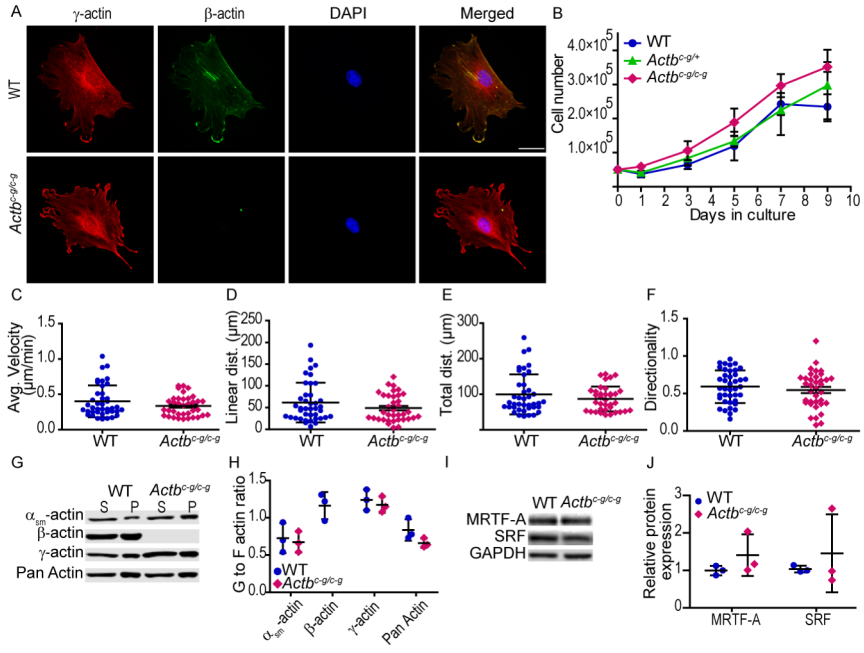

Figure 4.4 Actb$^{c\text{-}g}$ MEFs display cell proliferation and random migration rates not different than WT. (A) Representative immunofluorescence images of WT MEFs and Actb$^{c\text{-}g}$ MEFs. γ-actin is labeled in red, β-actin is labeled in green, nucleus is labeled in blue and the merged image is on the right. Scare bar = 50μm. (B) MEFs growth curve analysis, cultured from 0-9 days. N=3 (C-F) Calculated average velocity, linear distance, total distance, and directionality from random migration assay. N≥4, n≥40 cells per genotype. (G-H) G- to F-Actin ratio in WT and Actb$^{c\text{-}g}$ MEFs. X-axis denotes actin isoform. Y-axis denotes G-to-F actin ratio. N=3. (I-J) Representative and calculated relative isoactin protein expression in WT, homozygous Actb$^{c\text{-}g}$ MEFs for SRF and MRTF-A. N=3. X-axis denotes actin isoform. Y-axis denotes relative protein expression which were normalized to GAPDH and relative to a WT sample. Error bars are S.D.

increased in parallel (Fig. 4.3A-C), which correlated with increased γ-actin protein expression (Fig. 4.3D-I). Transcripts and protein levels for muscle-specific actin isoforms were largely unchanged (Fig. 4.3A-I). *Acta2* transcript, encoding α_{sm}-actin, was decreased in $Actb^{c\text{-}g/c\text{-}g}$ MEFs, which contrasts with *Acta2* upregulation previously observed following cre-mediated knockout of *Actb* [108, 109, 133]. Interestingly, WT *Actg1* transcripts were significantly decreased in $Actb^{c\text{-}g}$ homozygous brain (Fig. 4.3A), suggesting cells can distinguish β- and γ-actin proteins, and downregulate.endogenous *Actg1* transcription to compensate for increased expression of γ-actin protein from the edited $Actb^{c\text{-}g}$ locus (Fig. 4.3D,G).

4.4.3 $Actb^{c\text{-}g}$ MEFs proliferate and migrate normally

We previously demonstrated that MEFs with cre-mediated knockout of *Actb* failed to proliferate and migrated less efficiently than control cells [108]. $Actb^{c\text{-}g/c\text{-}g}$ MEFs, as gauged by immunostaining with actin isoform specific antibodies, localize γ-actin to stress fibers and the periphery of lamellipodial protrusions, and do not express β-actin (Fig. 4.4A). Despite lacking β-actin, heterozygous and homozygous $Actb^{c\text{-}g}$ MEFs proliferated similarly to control cells in culture (Fig. 4.4B). Similarly, $Actb^{c\text{-}g}$ homozygous MEFs migrated normally, displaying average velocity, linear distance, total distance and directionality persistence comparable to WT MEFs (Fig. 4.4C-F). Thus, β-actin protein is not required for cell proliferation or migration.

Finally, actin exists both as a monomer (G-actin) and as filaments (F-Actin); and the G-to F-actin dynamic plays a key role in the serum response (SRF)/myocardin related transcription factor (MRTF) signaling pathway[133]. Cre-mediated β-actin knockout in primary MEFs caused a significant decrease in G-actin which correlated with altered gene expression[110]. In contrast, we found α_{sm}-, γ- and total actin G- to F-actin ratios were not altered in $Actb^{c\text{-}g}$ homozygous MEFs (Fig. 4.4G, H). Expression of SRF and MRTF-A proteins were also not altered when compared to WT MEFs (Fig. 4.4I, J). Overall, these results suggest that γ-actin and β-actin are functionally redundant for G-actin mediated regulation of gene expression.

4.4.4 Progressive hearing loss and stereocilia degeneration in *Actb*$^{c\text{-}g}$ mice

We previously demonstrated that cre-mediated knockout of *Actb* resulted in progressive, high-frequency hearing loss corresponding to inappropriate shortening of stereocilia, which are actin-based protrusion on auditory hair cells that detect sound [60, 111]. We therefore assessed hearing in *Actb*$^{c\text{-}g}$ mice by measuring auditory brainstem responses (ABRs) to a range of pure frequency tones. At 6 weeks of age, control and *Actb*$^{c\text{-}g}$ mice had comparable thresholds, except at 32 kHz,

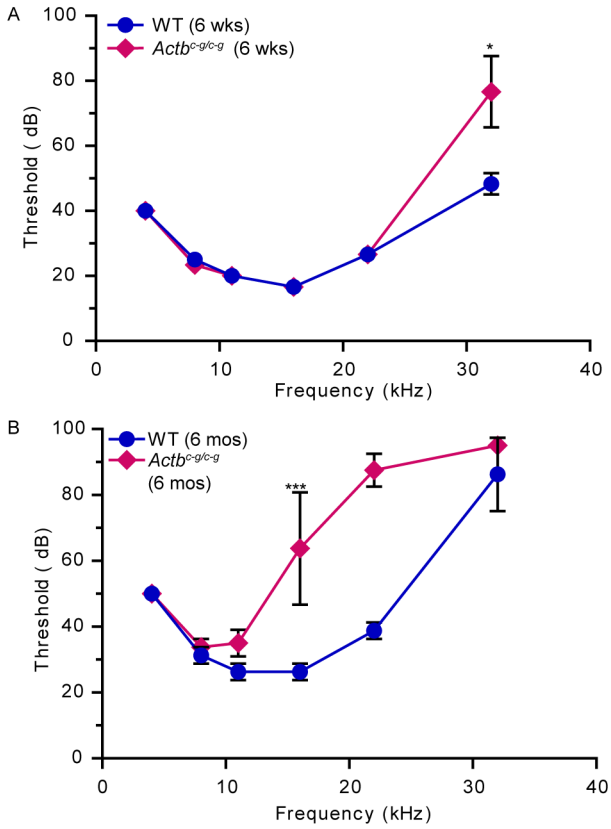

Figure 4.5 *Actb*$^{c\text{-}g}$ mice suffer from progressive hearing loss. (A) ABR of 6-week-old WT and homozygous *Actb*$^{c\text{-}g}$ mice. N=3 mice. (B) ABR of 6-month-old WT and homozygous *Actb*$^{c\text{-}g}$ mice. N=4 mice. X-axis denotes defined frequency in kHz, y-axis denotes threshold (dB) sound that elicit an ABR. Student T-Test. *P<0.05, ***P<0.001. Error bars are S.D.

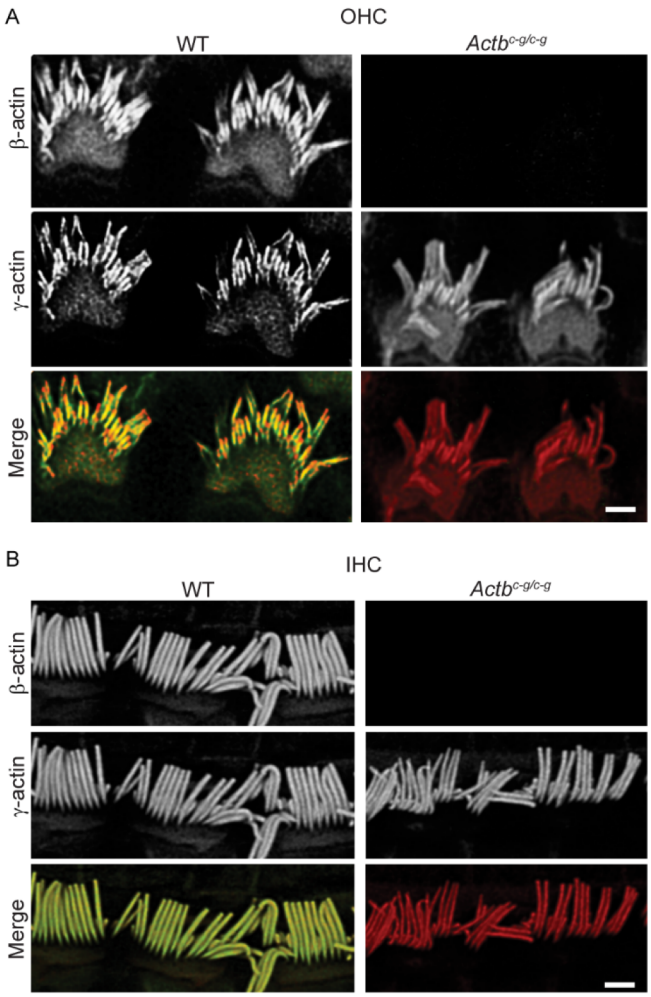

Figure 4.6 β--actin protein is not localized to stereocilia in *Actb*$^{c\text{-}g}$ mice. (A) Representative immunofluorescent images of β-actin (green), γ-actin (red) and merged image in the OHC between WT and homozygous *Actb*$^{c\text{-}g}$ mice. (B) Representative immunofluorescent images of β -actin (green), γ -actin (red) and merged image in the IHC between WT and homozygous *Actb*$^{c\text{-}g}$ mice. Scare bar = 1μm. N=3 mice

the highest frequency tested, where *Actb*$^{c\text{-}g}$ mice had some hearing loss as demonstrated by their higher ABR threshold (Fig. 4.5A). This high frequency hearing loss was more advanced by 6 months of age, with significant elevation of ABR thresholds at and above 16 kHz in *Actb*$^{c\text{-}g}$ mice as compared to control mice (Fig. 4.5B). We immunostained cochlear tissue to assess the distribution of β and γ-actin in stereocilia on inner hair cells (IHCs) and outer hair cells (OHCs), which both detect sound but have different stereocilia morphologies. As expected, β-actin was not detected in *Actb*$^{c\text{-}g}$ stereocilia (Fig. 4.6). In wild type hair cells at P7, when bundles are developing, β-actin and γ-actin are colocalized to the OHC stereocilia. However, β-actin was reduced and γ-actin markedly enriched at the tips of OHC stereocilia in mature P21-P40 mice, where stereocilia

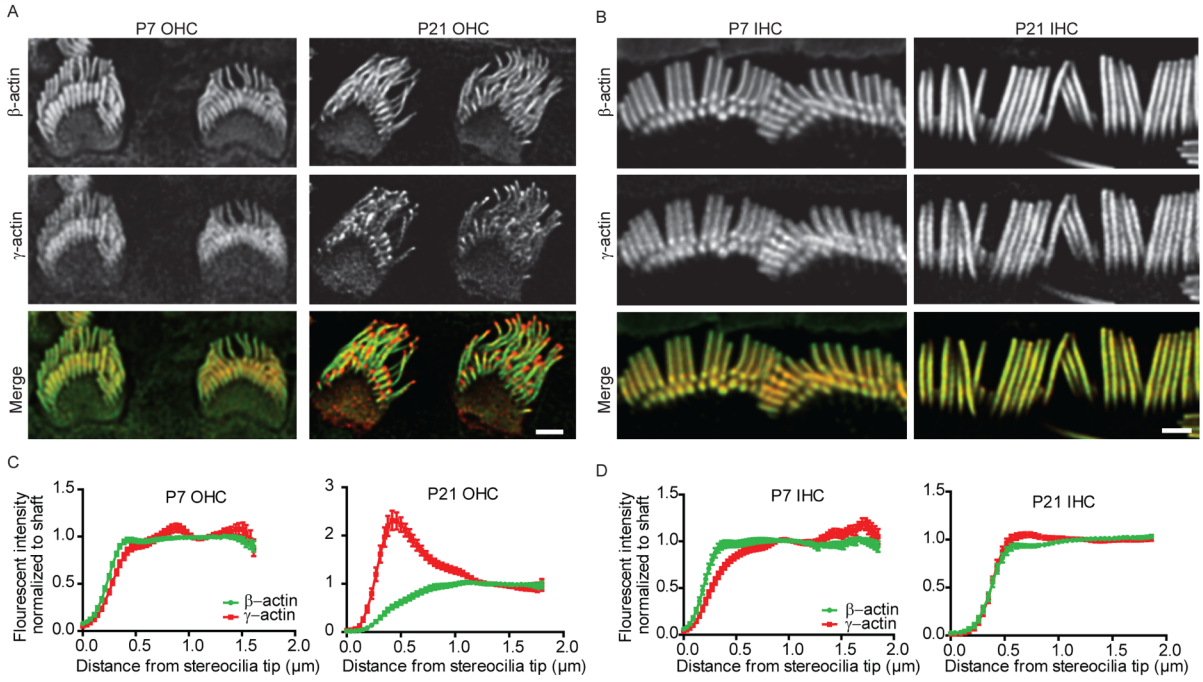

Figure 4.7 β-actin and γ-actin colocalized in developing OHC stereocilia. (A) Representative immunofluorescent images of the OHC in P7 and P21 C57BL/6 mice. β-actin is labeled in green, γ-actin is labeled in red. (B) Representative immunofluorescent images of the IHC in P7 and P21 C57BL/6 mice. β-actin is labeled in green, γ-actin is labeled in red. (C) Calculated fluorescent intensity of β- and γ-actin normalized to the shaft in the OHC. N=3 mice, n≥40 stereocilia. (D) Calculated fluorescent intensity of β- and γ-actin normalized to the shaft in the IHC. Scare bar = 1μm. N=3 mice, n≥40 stereocilia. Error bars are S.E.M

lengths are unchanging (Fig. 4.7A, C). IHC stereocilia showed a similar trend, with a higher proportion of β-actin the at tips of developing stereocilia (Fig. 4.7B, D). Thus, increased levels of β-actin at stereocilia tips correlates with growth, suggesting that β-actin protein drives stereocilia growth.

The morphology of stereocilia bundles is closely associated with their mechanotransductive function (Fig. 4.8C). We used scanning electron microscopy (SEM) to examine OHC stereocilia from the middle turn of the cochlea, which corresponds to the frequency range where ABR thresholds in $Actb^{c\text{-}g}$ mice are normal at 6 weeks of age, but elevated at 6 months of age. Six-week-old control and $Actb^{c\text{-}g}$ mice had OHC bundles that appeared normal, featuring similar numbers of stereocilia that were of similar height (Fig. 4.8A, D). In contrast, at 6 months of age, the mechanotransducing stereocilia in $Actb^{c\text{-}g}$ mice had started to degenerate and were shorter and fewer in number than in control OHCs. In addition, some OHCs stereocilia bundles were missing in $Actb^{c\text{-}g}$ mice (Fig. 4.8B, D). Towards the base of the cochlea where higher pitch sounds are detected, a similar phenotype was observed in $Actb^{c\text{-}g}$ OHC stereocilia at 6 weeks of age (Fig. 4.9). Together, these data suggest that $Actb^{c\text{-}g}$ mechanotransducing OHC stereocilia selectively and progressively degenerate, leading to hearing loss. Notably, this pattern of hearing loss and stereocilia degeneration is similar to that previously observed in hair cell specific *Actb* knockout mice [60, 111], demonstrating that this protein isoform is required for stereocilia length maintenance.

4.5 Discussion

To distinguish the relative contributions of nucleotide and amino acid sequences to the unique functions of closely-related cytoplasmic actins, we used TALENs to engineer the endogenous *Actb* gene to express γ-actin instead of β-actin. This approach edited only the nucleotides required to substitute the β-actin N-terminal amino acids D2-4, and V10 for γ-actin residues E2-4, and I10 The resulting mice and cells, which produce no β-actin protein, lacked the most severe and overt phenotypes of previously characterized *Actb* knockouts. These findings demonstrate that many functions of the highly conserved and expressed *Actb* gene reside in the nucleotide sequence and

do not depend on the protein sequence. However, homozygous *Actb*$^{c\text{-}g}$ mice did develop progressive hearing loss due to degeneration of actin-rich protrusions on sensory cells. Therefore,

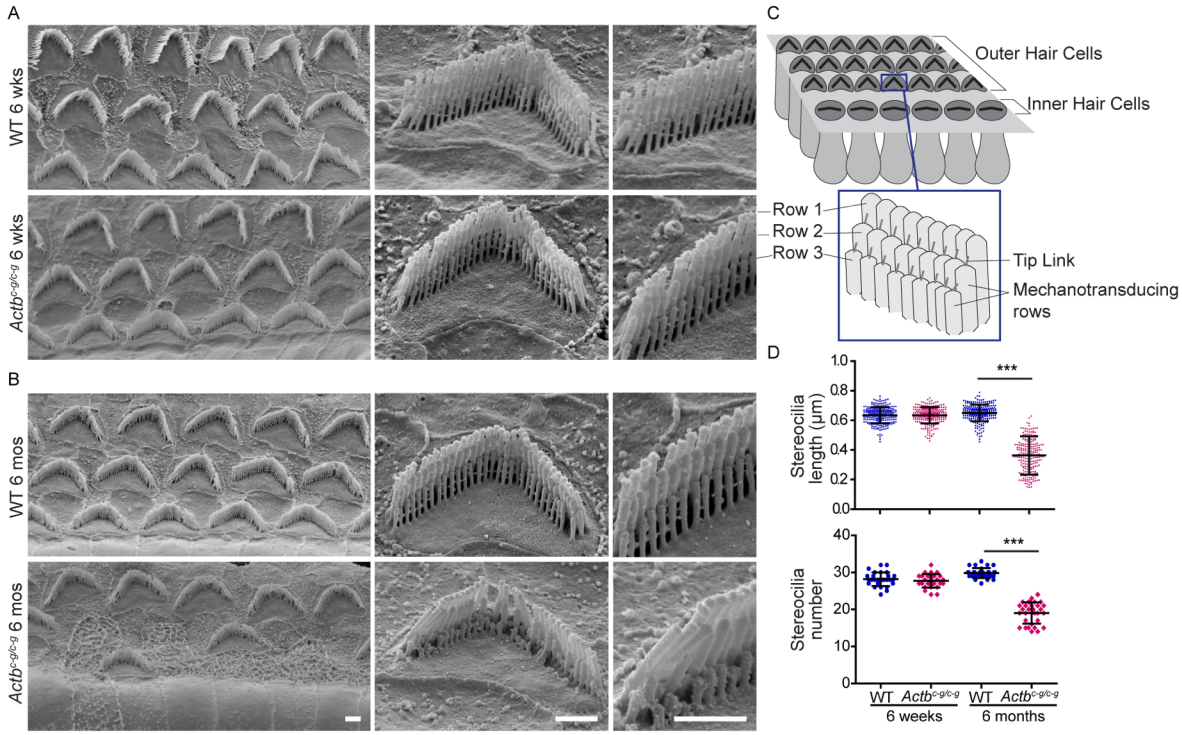

Figure 4.8 Actb$^{c\text{-}g}$ mice show evidence of stereocilia degeneration**.** Representative scanning electron microcopy images of (A) 6-week-old, and (B) 6-month-old OHC stereocilia from the middle turn of the cochlea**.** Scare bar = 1µm. (C) Cartoon image of the stereocilia. (D) Length (µm) of stereocilia in row 3 of OHC bundles in 6-week-old and 6-month-old WT and homozygous Actb$^{c\text{-}g}$ mice**.** N=4 mice, n≥200 stereocilia. Number of stereocilia in row 3 of OHC bundles in 6-week-old and 6-month-old WT and homozygous Actb$^{c\text{-}g}$ mice**.** N=4 mice, n≥28 cells. One-way ANOVA with Tukey's post-test. ***P<0.001. Error bars are S.D.

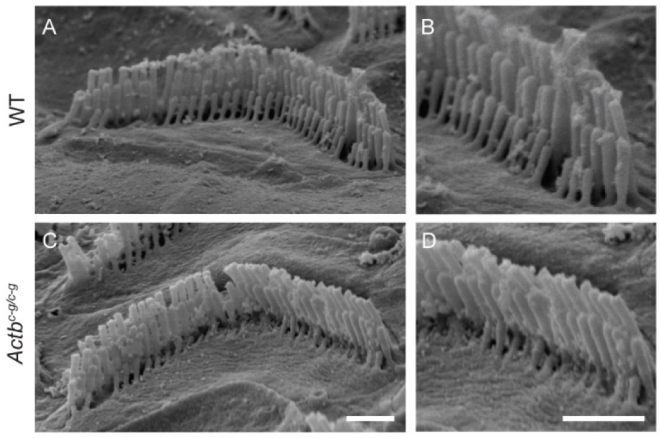

Figure 4.9 6 week old *Actb*$^{c\text{-}g}$ mice display stereocilia degeneration. (A-D) Representative scanning electron microscopy images of 6 week old OHC stereocilia from the base of the cochlea. Scare bars = 1µm. N=4 mice.

β-actin protein has functions in some specialized cell types that cannot be compensated for by γ-actin. A recent study using clustered regularly interspaced short palindromic repeats (CRISPR)/Cas9 methodology also edited the endogenous *Actb* locus to express γ-actin protein [129], and the resulting mouse line is nearly identical to the one we independently generated and characterized here. Several of the same phenotypes were assessed, and very similar results were obtained. In particular, *Actb*$^{c\text{-}g}$ mice are viable and appear to develop normally without evidence of premature mortality [129]. In addition, *Actb*$^{c\text{-}g}$ MEFs also have proliferation and migration rates similar to WT (Fig. 4.2 [129]. We further show that *Actb*$^{c\text{-}g}$ muscle viability and physiology, as well as the activity level of the mice, was comparable to wild type. Overall, these two independent studies are highly consistent and support the major finding that β-actin protein is dispensable for most cellular functions.

The *Actb* gene-edited mice (herein, [129]) contrast with conventional cre-mediated knockout of a floxed *Actb* allele, where exons 2 and 3 were deleted, and which caused embryonic lethality in mice [110]. Tissue-specific knockout of the same allele also resulted in a variety of phenotypes

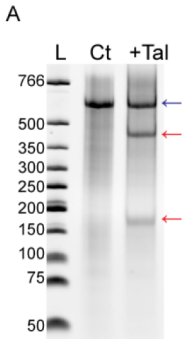

Figure 4.10 TALEN activity validation in NIH3T3 fibroblasts. (A) Control and TALEN nucleofected fibroblast gDNA post the Surveyor Assay. Blue arrow indicates the WT band, red arrows indicate the Surveyor nuclease digested bands

with muscle showing progressive myofiber degeneration/regeneration, muscle weakness, impaired mitochondrial fission [132, 134], and the CNS showing tissue morphology defects that correlated with hyperactivity and cognitive behavior impairments [131]. Additionally, isolated MEFs failed to divide or migrate, suggesting β-actin was required for fundamental cellular processes [109, 110]. None of these phenotypes were observed in *Actb*$^{c\text{-}g}$ mice. It is possible that some of the phenotypes observed following cre-mediated deletion of *Actb* exons 2-3 are independent of normal *Actb* function. For example, there may be an essential element in the intervening intron. It is also possible that recombination produces toxic transcript and/or truncated protein. However, differences between cre-mediated knockouts and *Actb*$^{c\text{-}g}$ mice most likely suggest that regulatory information embedded in the nucleotide sequence is critical, as this would be altered in the *Actb* floxed knockout but not in the *Actb*$^{c\text{-}g}$ mice.

Singer and colleagues first discovered and established the *Actb* zipcode as a key difference between *Actb* and *Actg1* gene and transcript [135], which is conserved from birds to mammals [136]. ZBP1 binds to this sequence to regulate both transcript localization and translation of β-actin [128]. Consistent with well-regulated temporal and spatial β-actin protein translation, *Actb* transcript is more abundant than *Actg1* transcript in primary MEFs even when β- and γ- actin protein levels are similarly expressed [109]. Based on [129] and our findings that the 4 amino acid variances between

β- and γ- actin protein are not critical to most cellular functions, it seems likely that transcript targeting and regulated translation via the zipcode is the essential feature of *Actb*. A similar gene-editing approach can potentially address the importance of the *Actb* zipcode *in vivo*.

While β-actin protein is not essential to the function of many cell types, some tissues nonetheless seem to specifically detect and regulate the levels of β- and γ-actin. As $Actb^{c\text{-}g}$ transcript increased in heterozygous and homozygous brain tissue, the level of γ-actin protein increased as it was produced both from the engineered *Actb* locus and the endogenous *Actg1* locus. (Fig. 4.3A-C). Interestingly, as γ-actin protein concentration increased, the amount of transcript from the endogenous *Actg1* alleles decreased. In $Actb^{c\text{-}g}$ cells, as well as in most cells and tissues where *Actb* or *Actg1* were knocked out, total actin protein levels remained constant across all genotypes even as transcript levels varied [108, 110]. Thus, most cell and tissue types appear to maintain actin homeostasis via a protein-based feedback mechanism.

Clinically, spontaneous missense mutations in both *ACTB* and *ACTG1* have been associated with Baraitser-Winter syndrome, a rare disease with complex phenotypes including facial dysmorphism, learning disabilities and deafness [137]. Some of the mutations affect the polymerization properties of actin or interaction with actin binding proteins to cause a gain-of-function or a dominant-negative effect [138-140]. Interestingly, the more severe forms of Baraitser-Winter syndrome are associated with mutations in *ACTB* over *ACTG1* [126]. Loss-of-function mutations in human *ACTB* also cause developmental delays, intellectual disability, internal organ malformations, hearing loss and facial malformations [125]. Together, these studies suggest that loss or mutation of cytoplasmic actins, though not necessarily lethal, perturbs a variety of specialized cells or cellular processes and decrease organismal fitness.

Stereocilia maintenance is one such specialized process that requires β-actin protein, which likely relates to deafness observed in humans with mutations in *ACTB* and *ACTG1* [140]. $Actb^{c\text{-}g}$ hair cells, like cre-mediated *Actb* knockout hair cells characterized previously, have a particular pattern of degeneration where the shorter rows of the bundle shorten irregularly as mice age, but the tallest row of the bundle is largely unaffected [111]. In contrast, *Actg1* knockout hair cells have a different phenotype where individual stereocilia are lost from bundles [111, 114]. Together, these data point

to a particular requirement for β-actin in maintaining stereocilia length. As with *Actb* knockout, blocking mechanotransduction also results in degeneration of the shorter rows of stereocilia, which can subsequently regrow when mechanotransduction is restored [141]. Considering that the mechanotransductive apparatus is under constant mechanical stress, one possibility is that damage and repair during aging results in cycles of stereocilia shortening and regrowth [28]. Efficient regrowth likely requires β-actin. Indeed, preferential localization of β-actin to the growing tips of

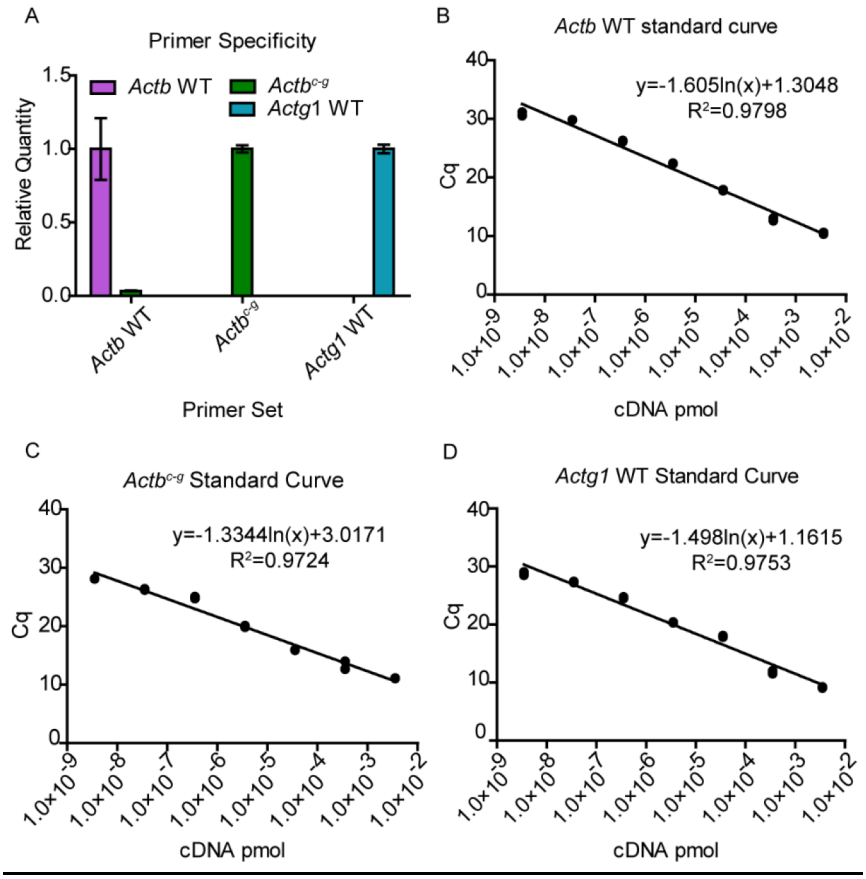

Figure 4.11 Mouse actin isoform standard curves and primer specificity analysis.

(A) Representative graph of qRTPCR primer specificity. Two new primer sets were designed to specifically amplify WT *Actb* and *Actb*$^{c\text{-}g}$ edited transcript. Each primer set was used to amplify WT *Actb*, edited *Actb*$^{c\text{-}g}$, and WT *Actg1* control constructs to calculate relative quantity. Color bars represent individual actin isoform, y-axis denotes relative quantity, x-axis denotes primer set. (B-D) Representative standard curves generated using specific actin isoform primers with the corresponding control actin construct in a ten-fold dilution.

developing stereocilia further supports a role for β-actin over γ-actin elongating stereocilia. The ability of β-actin to lengthen stereocilia may be because it has a faster polymerization rate than γ-actin [103] under calcium bound conditions, which may reasonably occur in mechanotransducing stereocilia. Besides polymerization kinetics, multiple actin binding proteins may also differentially interact with β- and γ-actin. For example, non-muscle myosinIIa and myosinVIIa both exhibit higher ATPase activity with γ- actin filaments [142]. MyosinVIIa is a particularly interesting candidate for mediating actin isoform specific effects since it is also localized to stereocilia. Finally, the actin filament severing protein cofilin regulates β- and γ-actin differently [130], which is intriguing since mice lacking the severing protein actin depolymerizing factor (ADF) phenocopy the pattern of stereocilia degeneration seen in $Actb^{c\text{-}g}$ mice [28] .

Whether through polymerization kinetics or differential binding partners, differences in β- and γ-actin function in stereocilia depend on the four amino acid differences in the N-terminus. One substitution is a valine for an isoleucine, while the other three substitutions are in an acidic block (DDD in β- and EEE in γ-actin). Auditory function in mice expressing β-actin from the *Actg1* locus seem likely to phenocopy *Actg1* nulls, while swapping the EEE acidic block or the isoleucine from *Actg1* into the *Actb* locus would help resolve the relative contributions of each feature to β-actin protein function.

Regardless of the mechanism by which β-actin protein contributes to stereocilia maintenance, this isoform has a cellular function that is not met by γ-actin protein. Therefore, it is likely that other cell types also depend on β-actin protein to form or maintain specialized features. However, this scenario is considerably less common than previously appreciated and, in agreement with Vedula *et al.*, 2017, we conclude that the nucleotide sequence rather than amino acid sequence determines the majority of the divergent phenotypes previously associated with *Actb* gene disruption.

Table 4-1 Physiological parameters of isolated EDL muscles used in *ex vivo* force measurements

Parameter	WT	*Actb*$^{c\text{-}g/c\text{-}g}$	P value
EDL mass (mg)	13.4 ± 1.1	13.8 ± 1.1	0.587
L_o (mm)	13.7 ± 0.3	13.5 ± 0.4	0.397
CSA (mm^2)	2.1 ± 0.2	2.2 ± 0.2	0.500
Passive stiffness (N/m)	13.3 ± 1.0	14.6 ± 2.9	0.367
P_o (mN)	451 ± 67	452 ± 45	0.979
Specific P_o (N/cm^2)	21.6 ± 3.1	20.7 ± 1.7	0.592
ΔP_0 (%)	16.6 ± 5.9	18.4 ± 12.1	0.772
Peak eccentric force (mN)	857 ± 138	834 ± 74	0.752
Specific eccentric force (N/cm^2)	40.9 ± 5.7	38.3 ± 2.3	0.378
Eccentric force loss (%)	27.3 ± 3.4	26.7 ± 2.7	0.763
Active stiffness (N/m)	866 ± 106	844 ± 59	0.696
Peak twitch (mN)	133 ± 20	130 ± 11	0.777
Twitch Force development time (ms)	16.9 ± 2.5	16.4 ± 1.2	0.690
Twitch ½ relaxation time (ms)	17.1 ± 3.1	16.7 ± 3.2	0.845
Tetanic Maximal rate of contraction (mN/s)	14.4 ± 1.6	14.3 ± 1.0	0.910
Tetanic Maximal rate of relaxation (mN/s)	21.8 ± 4.4	21.9 ± 2.7	0.966

Values are mean ± SD.

L_o = optimal muscle length, CSA = physiological cross-sectional area, P_o = maximal isometric tetanic force. ΔP_o = change in P_o after eccentric contractions. n=5 for each line. Statistics were performed using unpaired *t*-test analyses with $p < 0.05$ considered significant.

4.6 Materials and Methods

Animal care

Animals were housed and treated in accordance with the standards set by the University of Minnesota Institutional Animal Care and Use Committee.

Statistics

All statistical analysis was analyzed using the GraphPad Prism software

TALEN construction and purification: TALEN constructs were generated using the Golden Gate TALEN assembly method (1) into RCIscript-GoldyTALEN backbone (Addgene #38142, Carlson *et al.*, 2012). TALEN DNA constructs were transformed into DH5α cells, miniprepped

with Wizard ® *Plus* SV Minipreps DNA Purification System (Promega, Cat. #A1460), linearized with the BamHI restriction enzyme (New England Biolabs Inc. Cat. #R3136S), and then phenol/chloroform purified. TALEN RNAs were *in-vitro* transcribed from purified linearized DNA using the mMESSAGE mMACHINE® T3 Transcription Kit. (Thermo Fisher Scientific, Cat. #AM1348) and then purified using the MEGAclear™ Kit. (Thermo Fisher Scientific, Cat. #AM1908M) following manufacture protocols. Purified RNAs were stored at -80°C until use.

TALEN activity validation. TALEN RNA pairs (15µg each arm) were nucleofected (Amaxa® Cell Line Nucleofector® Kit R, Amaxa® Nucleofector® II) into $1x10^6$ NIH3T3 fibroblasts. 3-days post nucleofection, gDNA was harvested from the cells with the PureLink® Genomic DNA Mini Kit, Invitrogen according to manufacture protocols. TALEN activity was assayed via the Surveyor Mutation Detection Kit (Transgenomic, Cat. #706020.) (Figure S5). Primers: *Actb* Exon2 F 5'-GGTAATAATGCGGCCGGTCT-3', *Actb* Exon2 R 5' TACCCGGGATACTGACCTGG-3'. Additionally, *in-silico* off-target analysis using https://tale-nac.cornell.edu with the most stringent cutoff showed that the most similar potential off-target sequences had a minimum of 7 nucleotides that differed between the on- and off-targets.

Generating genome engineered mice and validation

TALEN RNA pairs (25ng/µL) and the corresponding Exon 2 PAGE Ultramer ssOligo donor (15ng/µL) template (Integrated DNA Technologies) were sent to the Murine Genetics Core at The Scripps Research Institute for pronuclear microinjection into fertilized C57BL/6 blastocysts, which were then implanted into pseudo-pregnant female mice. The donor template contained 8 nucleotide alterations to exchange the translation of β-actin D2-4, V10 to the γ-actin E2-4, I10, to disrupt TALEN re-binding to the edited locus, and to insert a BamHI site for restriction fragment length polymorphism (RFLP) analysis. Genomic DNA from all F0 mouse pup tail samples was purified (PureLink® Genomic DNA Mini Kit) and assessed by RFLP assay with the BamHI restriction enzyme (New England Biolabs Inc. Cat. #R3136S) and Sanger sequenced for donor template integration. Primers used for RFLP: *Actb* Exon2 F 5'-GGTAATAATGCGGCCGGTCT-3', *Actb* Exon2 R 5'-TACCCGGGATACTGACCTGG-3'.

Cell Culture: Primary MEFs were cultured from E13.5 WT, *Actb*$^{c\text{-}g}$ heterozygous and homozygous mouse embryos as described previously (3). Cells were grown to 80% confluency on 10-cm plates and frozen down at passage 1 at $1x10^6$ cells/mL in MEF freezing media (95% FBS and 5% dimethyl sulfoxide). Primary MEFs from individual embryos were thawed and cultured in MEF media (DMEM supplemented with 10% FBS, 1% Pen/Strep, 0.5ug/mL Fungizone), grown to 80% confluency. NIH3T3 fibroblasts were cultured in 3T3 media (DMEM supplemented with 10% BS, 1% Pen/Strep, 0.5ug/mL Fungizone).

Open Field Activity Assay

Activity was measured using an AccuScan system by Columbus Instruments, Inc. Total horizontal distance (meters) was determined by measuring infrared beam breaks. Mice were placed in the open-field apparatus and horizontal distance was measured for 15 minutes.

Muscle histology and physiology

Quadriceps muscles from each mouse line were cryopreserved in melting isopentane for 30 seconds and 10 μm transverse cryosections were obtained (Leica CM3050 S). For histology, sections were stained with hematoxylin and eosin and imaged on a Leica DM5500 B microscope equipped with a Leica HC PLAN APO 20x objective. Centrally nucleated fibers (CNFs) were counted using the Cell Counter plugin on ImageJ software (NIH) and expressed as a percentage of the total number of myofibers (%CNFs). For *ex-vivo* force analysis, mice were anesthetized with sodium pentobarbital and extensor digitorum longus (EDL) muscles dissected. Silk suture was used to attach the distal tendon to a static structure and the proximal tendon to a force transducer (Model 300B-LR, Aurora Scientific). The EDL was incubated in Krebs-Ringer bicarbonate buffer [120.5 mM NaCl, 4.8 mM KCl, 1.2 mM $MgSO_4$ 1.2 mM Na_2HPO_4, 20.4 mM $NaHCO_3$, 10 mM glucose, 10 mM pyruvate, 1.5 mM $CaCl_2$], oxygenated with 95% O_2/5% CO_2. Muscles were set to their anatomic length (L_o) which was measured from myotendonous junction to myotendonous junction using digital calipers. Muscles remained quiescent for 5 min before passive stiffness was determined by passively stretching the muscles sinusoidally from 97.5% L_o to 102.5% L_o at 0.5 Hz while measuring the resulting force. Isometric tetanic contractions separated by 2 min followed 30s later until a plateau was attained (within 5 mN) and –dP/dt and +dP/dt were measured. EDL muscles were stimulated for 200 ms at 175 Hz. Peak twitch force was then measured 2 min later

using a 0.5 ms pulse at 150 V (Grass S48 stimulator delivered through a SIU5D stimulus isolation unit; Grass Telefactor, Warwick, RI) before active stiffness was calculated using a sinusoidal length oscillation of 0.01% at 500 Hz during a tetanic isometric contraction(4, 5). Two minutes later, the muscle completed 10 eccentric contractions in which muscles were passively shortened to 90 % L_o and then stimulated for 200ms while being simultaneously lengthened to 110 % L_o at 1.0 L_o/s. Each eccentric contraction was separated by 3 min of rest to prevent fatigue[143][141]. Immediately following the 10^{th} contraction, muscles were readjusted to L_o before a post P_o was measured and compared to pre P_o as a percentage.

Primary MEFs fixation, staining and immunofluorescent imaging

MEFs were plated on 5 μg/ml fibronectin coated coverslips at a density of 1×10^4 cells/coverslip and incubated in MEF culturing media. The next day, cells were fixed with fresh 4% paraformaldehyde in PBS for 15 min at room temperature, washed in phosphate-buffered saline (1xPBS) 3x5min, and blocked in 5% Bovine serum albumin (BSA) for 30 min. Coverslips were incubated with 1° antibodies for β-actin (AC15; Sigma-Aldrich) and γ-actin (affinity purified γ-cyto actin rabbit 7577) in 5% BSA at 4°C overnight, washed in 1xPBS 3x5min and incubated with Alexa-488- or 568-conjugated 2° antibodies (Life Technologies). Coverslips were mounted in Prolong (P36931; Life Technologies) mounting medium prior to imaging. All images were obtained were acquired using a 20x/NA0.75 objective on a Delta Vision personalDV microscope using softWoRx 3.7.1 software (GE Technologies).

Cochlea Immunofluorescent microscopy

Dissected cochlea were fixed in 4% paraformaldehyde (PFA) in PBS for 4 hours at room temperature before decalcification in 170 mM EDTA in PBS for 16 hrs at 4°C. Organ of Corti was dissected, incubated in methanol for 10 mins at -20°C, permeabilized with 0.2% triton X-100 for 10 minutes at room temperature and blocked with 5% goat serum in PBS before incubation with Alexa-546 conjugated monoclonal anti γ-actin antibody clone 1-37 and FITC conjugated anti-β-actin antibody clone AC-15 (AbCam, 1:400) overnight at 4°C. Samples were mounted either in Prolong Gold or Prolong Diamond anti-fade reagent (P36930 or P36965, Life Technologies) imaged with a 63X NA 1.4 objective on a Leica SP8 confocal microscope operating in resonant mode. Images were deconvolved using Huygens X11 Essentials software. Fluorescence intensities

of actin immunostaining along the stereocilia length were measured using the line function in Leica LasX software.

Scanning electron microscopy

Dissected cochlea were fixed in 2.5% glutaraldehyde, 0.1 M sodium cacodylate, 2 mM $CaCl_2$ overnight at 4°C and then decalcified in 170 mM EDTA in PBS for 16 hours at 4°C. Dissected organ of Corti was incubated in 2% each of arginine, glutamine, glycine and sucrose in water overnight at room temperature, followed by incubation in 2% tannic acid and guanidine hydrochloride for 2 hours at room temperature and 1% $Os0_4$ in water for 1 hour at room temperature, with extensive water washes between steps. The samples were transitioned to 100% ethanol, critical point dried from CO_2 and sputter coating with gold. Samples were imaged using a JEOL JSM-7800F field emission scanning electron microscope. The stereocilia length and number measurements were analyzed using Fiji software (National Institutes of health, Bethesda, MD).

Auditory Brainstem Response (ABR)

ABR waveforms were collected for mice using a Tucker Davis Technologies System 3 at frequencies of 4 kHz, 11 kHz, 16 kHz, 22kHz and 32 kHz as described previously (6). Mice were anesthetized with Avertin following which scalp potentials were recorded using subdermal electrodes. Waveforms for each frequency were collected starting at 90 dB, decreasing in 5 dB to a sub-threshold level. The collected waveforms were stacked and the lowest level of stimulation that resulted in a definite waveform was considered as the threshold.

Live cell imaging

$10x10^4$ MEFs were plated on a Nunc™ Glass Base Dish (Thermo Scientific) and cultured overnight in regular MEF media. Second day, the dish was sealed with vacuum grease and a glass coverslip. MEF culture media containing 25 mM 4-(2-hydroxyethyl)-1-piperazineethanesulfonic acid (HEPES) was used to stabilize the pH, and the cells were maintained at 37°C by an environmental chamber enclosing the microscope. For random migration assay, images were captured on a Delta Vision personalDV (GE Technologies) with a 10x/NA0.25 objective with phase contrast illumination. Images were captured at 10-minute intervals for 4 hours, and cells

were tracked using the Manual Tracking plugin for ImageJ software (National Institutes of health, Bethesda, MD). Cells that divided or contacted other cells during the experiment were excluded for data analysis. Velocity was calculated as the total track distance divided by the total time (240 min), and directionality (D/T) was calculated as the linear distance (D) divided by the total track distance (T).

qRT-PCR

Generation of WT mouse isoactin control constructs were previously described in Patrinostro *et al.*, 2017. *Actb*$^{c\text{-}g}$ control construct was generated by site-directed mutagenesis using the QuikChange II XL kit (Agilent Technologies, Cat# 200521) according to manufacture protocols from the WT pENTR/D-TOPO-*Actb* vector generated in Patrinostro *et al.*, 2017. Each actin isoform qRT-PCR primer set was tested for amplification of all control constructs to assess primer specificity (7) and Figure S6. Total RNA was extracted from WT, *Actb*$^{c\text{-}g}$ heterozygous and homozygous MEF samples using the Bio-Rad-Aurum Total RNA Mini Kit following the manufacturer's instructions. RNA concentration and purity (260/280 ratio) were determined using a NanoDrop spectrophotometer (Wilmington, DE). First-strand cDNA was synthesized with a Bio-Rad iScript Advanced cDNA Synthesis Kit for qRT-PCR using the same initial RNA amount for all samples. Individual control constructs were used in a 10-fold dilution to generate a standard curve, and MEF samples were amplified in parallel with each specific qRT-PCR primer set using Bio-Rad SsoAdvanced Universal SYBR polymerase on the Bio-Rad CFX96 Real Time System C1000 Touch Thermal Cycler to profile each actin isoform transcript amount (picomoles).

G- to F- Actin ratio

WT and *Actb*$^{c\text{-}g}$ homozygous primary MEFs were counted and equal number of cells from each genotype were pelleted prior to the experiment. G-to F-actin ratio as assed by the commercially available G-Actin/F-Actin In Vivo Assay Biochem Kit (Cytoskeleton, Cat# BK037) according to manufacture protocols and then Westered blotted. Please see Western blotting methods for list of antibodies. LiCor fluorescence intensity for each Western blot fraction band is used to determine the ratio of G-to F-actin in each embryo.

Western blotting

MEF and tissue protein was extracted with 1% SDS buffer in 1x PBS and a cocktail of protease inhibitors (100 μM aprotinin, 0.79 mg/ml benzamide, 10 nM E-64, 10 μM leupeptin, 0.1 mg/ml pepstatin, 1 mM phenylmethylsulfonyl fluoride), sonicated (Model 150V/T Ultrasonic homogenizer; BioLogics), boiled, and centrifuged to remove the insoluble fraction. Equal amounts of cleared total lysate protein (25 μg) were blotted with antibodies β-actin (AC-15; Sigma-Aldrich), γ-actin (mAb 1-17), α_{sm}-actin (A14; Sigma-Aldrich), Pan-actin (C4), SRF (G-20; Santa Cruz Biotechnology), MRTF-A (H-140; Santa Cruz Biotechnology), with glyceraldehyde 3-phosphate dehydrogenase (GAPDH; G9545 or G8795; Sigma-Aldrich) as loading control.

CHAPTER 5. FINAL DISCUSSION AND FUTURE DIRECTIONS

Age-related hearing loss is a major health problem affecting people worldwide. One of the leading causes for age-related hearing loss is the gradual degeneration or dysfunction of inner ear sensory hair cells that occurs with increasing age. Since hair cells lack the potential to regenerate stereocilia, it is important that stereocilia homeostasis be properly maintained to preserve auditory function throughout an individual's lifetime. It is therefore critical that efforts are made to understand the molecular mechanisms behind stereocilia development and maintenance to prevent and possibly reverse deafness.

To understand stereocilia morphogenesis and homeostasis, it is imperative to clearly decipher the structural components of stereocilia and their dynamics. The stereocilia actin core is exceptionally stable and is extensively crosslinked by actin crosslinking proteins, which are required for stereocilia development and maintenance. Previous studies have elucidated that, in mammals, actin is dynamic only at the stereocilia tip while remaining stable along the core for at least several months [28, 29]. The F-actin cores of mammalian stereocilia are much more stable than those in zebrafish, where the actin turnover occurs in few hours, along the entire length of stereocilia [76]. One possibility is that zebrafish can tolerate a less stable core since they can regenerate their sensory hair cells. In contrast, mammals cannot regenerate auditory hair cells and may therefore have evolved a way to stabilize their stereocilia actin core so that the length and longevity of stereocilia is preserved to maintain hearing. These suggests that zebrafish stereocilia might have different mechanisms regulating their actin core compared to mammalian stereocilia. This raises interesting questions about the role of actin core stability in the long-term maintenance of stereocilia.

Although actin dynamics has been studied extensively in mammalian systems, not much is known about the dynamics of actin crosslinkers, which are nearly as abundant as actin in stereocilia. In chapter 2 using a novel transgenic reporter mouse line, we determined that in contrast to actin, EGFP-FSCN2 is dynamic within the stereocilia core. Additionally, we determined in this study that EGFP-FSCN2 competes with two other abundant crosslinkers, ESPN and PLS1, for binding sites in stereocilia, both when EGFP-FSCN2 is expressed constitutively from an early

developmental stage and when its expression is induced in mature hair cells, suggesting that other crosslinkers are also dynamic within the core [115]. However, the advantage conferred by the dynamism of actin crosslinkers with respect to stereocilia homeostasis is still largely unknown. The reversible crosslinking might be necessary for the regulation of actin in response to small breaks that arise due to prolonged mechanical stimulation for years within the core. The dynamic crosslinks could perhaps allow for actin assembly and disassembly transiently at the areas of mechanical damage while maintaining the integrity of the structure at the same time. This is a possible mechanism by which mammals allow for repair of otherwise stable structures to preserve hearing ability.

The need for multiple crosslinkers in hair cells and their roles in regulating actin dynamics remains a mystery. Each crosslinker is indispensable as loss-of-function mutations cause distinct phenotypes. For example, mutations in FSCN2 causes stereocilia degeneration along with progressive hearing loss [60], while mutations in ESPN prevents stereocilia from developing properly [68]. In chapter 3, we monitored actin dynamics in mice expressing deafness-causing mutations in FSCN2 and ESPN to see if they altered actin behavior in different ways. While actin is stable along the stereocilia core in normal mice, actin was dynamic in mice expressing mutant $FSCN2^{R109H}$ or lacking ESPN. But the onset of this phenotype differed in each case. In espin null stereocilia, actin-EGFP incorporation extended down from the tip to the base in early postnatal ages, suggesting role of ESPN in stabilizing bundles while they are growing. Whereas FSCN2 seem to be more important in maintaining the stability of mature stereocilia as reflected by the broad and diffused actin incorporation in the stereocilia of 6-month-old $FSCN2^{R109H}$ mice. Thus crosslinkers, though themselves dynamic [115], distinctly act to maintain actin filaments in a stable array. Even relatively subtle changes in crosslinker composition induced by expressing EGFP-FSCN2, which decreased PLS1 and ESPN levels, seemed to result in stereocilia maintenance defects. Previous studies have shown that mutations in PLS1 and Xirp2 result in similar phenotype as that in $FSCN2^{R109H}$ mice [63, 66]. The questions that remain to be addressed in future are: Why does stereocilia require so many different crosslinkers with similar function? How do each individual crosslinker contribute to the actin core stability and repair? What are the specific roles of FSCN2, PLS1 and XIRP2 in mature stereocilia length maintenance? This is important because

it may be that transiently varying crosslinker levels would provide a means to stimulate a desired repair mechanism in the case of stereocilia damage.

Exploring specific roles of each espin isoform in stereocilia core stability is a potential area of research. The Espn gene is alternatively spliced to produce several protein products including long and short isoforms. The longer isoforms, Espin 1 and Espin 2 include an additional xAB domain, which is lacking in the shorter isoforms (Espin 3A and espin 4) and is thought to drive the formation of large bundles [82-84]. Espin 1, when expressed in cultured cells is known to convert treadmilling actin in microvilli to a stable non-treadmilling array [86]. This could potentially be a part of the mechanism by which espin stabilizes actin core in stereocilia. While this is observed in vitro, in vivo results surprisingly demonstrate milder and cell-type specific functions of espin 1. For example, loss of espin 1 results in disruption of staircase organization restricted solely to the extrastriolar utricular bundles, but not in the organ of Corti and other regions of the vestibular system [90]. Perhaps Espin2 compensates, but this isoform is not detected in normal stereocilia, which raises the possibility that the shorter isoforms are primarily responsible for slowing actin turnover and driving stereocilia growth. It will be interesting to determine if the expression of other espin isoforms is upregulated in the auditory hair cells when espin 1 is knocked out. Furthermore, it will be important to determine whether xAB domain of the longer isoforms is even necessary for rendering stability to the stereocilia actin core. Additionally, in jerker mice which lack espin, stereocilia in the organ of Corti degenerate by P10 while the extrastriolar stereocilia of the utricle though thin and short, remains upright at least till P40 [68]. Since, espin 1 localizes at the stereocilia tips while the other isoforms, including espin 3A, are detected in the stereocilia shaft and that espin 3A is the most abundant isoform along the stereocilia shaft until P15 [89], it will be indeed promising to explore if espin 3A can rescue the jerker phenotype. The other interesting espin isoform, espin 4, which in fact is the smallest isoform, accumulates in stereocilia between P6 and P10, suggesting its role in bundle maturation [89]. Thus, it is imperative to determine the relative importance of these other isoforms of espin, which do not have the additional xAB domain, in stereocilia morphogenesis in these regions.

Stereocilia have some capacity for maintenance, but complete regeneration following severe damage does not generally occur even if the hair cell body remains viable. For example, following

aminoglycoside antiobiotic gentamycin damage, a subset of utricular hair cells lost their stereocilia yet remained viable [144]. These cells did not grow a new bundle. Similarly, when bundles were physically sheared off of auditory hair cells in postnatal explants the hair cell body survived for several days without any evidence of bundle regrowth [145]. These observations suggest that after the stereocilia bundle forms, the hair cell losses the ability to form new stereocilia, perhaps because of changes in gene expression, loss of instructive cues or changes to the apical surface of the hair cell that prevent formation of new protrusions. This is consistent with our data where we found that EGFP-FSCN2 expression, increased stereocilia length and width only when it was initiated early in development. In contrast, when expression was initiated at P21 after hair cells were fully mature with fully elongated stereocilia, there was no discernable effect of stereocilia dimensions. While stereocilia are growing, additional FSCN2 presumably slightly increases the growth rate, but not the developmental timing of growth. After a developmental shift, perhaps due to increased capping of actin filaments, that prevents further growth, crosslinking itself cannot restart growth. This suggests that stereocilia structure can be modulated only while it's still growing. This justifies the pivotal observation that stereocilia cannot be regenerated, in case they are damaged, but maintaining its homeostasis is the main objective to maintain optimal hearing ability.

Given the obstacles to hair cell replacement and bundle regeneration, hair cells must maintain existing stereocilia. This requires a means to keep each protrusion at its original length by regulating the actin core so that the bundles meet the geometric requirements necessary to detect nanoscale deflections. Stabilizing actin to prevent new actin incorporation seems to be the cornerstone for stereocilia maintenance. However, regulation of actin is also required, particularly to maintain the length of the shorter row stereocilia. As mentioned earlier, stereocilia tips have a zone of dynamic actin in contrast to the highly stable F-actin along the remainder of the stereocilia shaft [28, 29]. The relatively dynamic actin at stereocilia tips is by far the best candidate for mediating repair, such as regrowth following tip link loss. This dynamic tip zone might be critical for rebuilding stereocilia. It will be highly interesting to determine if different crosslinkers impact this dynamic tip region and whether this correspondingly influences regrowth following shrinkage.

Stereocilia maintenance seems to depend on several other factors, including tip links that connect adjacent stereocilia. Mutations in a tip link transmembrane protein CDH23 results in shortening of

shorter row stereocilia, which house mechanosensitive channels at their tip. The same rows degenerate in FSCN2^{R109H} mutation, without impacting the tallest row. Previously it was noted that the mechanotransducive stereocilia of the bundle sometimes have extended tip regions of new actin incorporation that may reflect instances where stereocilia shortened and then regrew following tip ink loss [28]. Thus, tip link loss could be another mechanism that causes shortening of mechanotransducive stereocilia. To gain insight into how tip link integrity impacts actin core stability, it will be interesting to monitor actin-EGFP incorporation in FSCN2^{R109H} mice expressing Cdh23^{+}. The expression of wild type Cdh23^{+} allele largely suppresses high frequency hearing loss in FSCN2^{R109H} mice, which normally expresses Cdh23^{ahl}. [60]. Thus Cdh23^{+} might also prevent instability in the core reflected by the broad and increased region of actin-EGFP incorporation that we observed in row 1 and row 2 stereocilia in these mice (in chapter 3). However, the phenotype might still exist suggesting that FSCN2 crosslinks are necessary to stabilize actin core. This result would suggest that shortening of mechanotransducive stereocilia probably occurs when tip link loss put pressure on the compromised core. This would provide further evidence that cytoskeletal instability is exacerbated by tip link perturbation.

Taken together, our current work has significantly deepened our understanding of the functions of actin cytoskeletal proteins in hair cells. Additionally, we have gained valuable information about possible mechanisms of stereocilia degeneration. An additional challenge will be to use this information to correct bundle defects or augment normal maintenance programs to restore or prevent hearing loss. Understanding the mechanisms regulating actin are important for identifying potential therapeutic approaches to promoting stereocilia length maintenance. There can be two different approaches that seem possible therapeutic remedies to ameliorate hearing loss stemming from stereocilia degeneration. One way would be to try to repair damaged hair cells while the other would be to altogether replace them by stem cells having the regenerative capacity to initiate new stereocilia morphogenesis. Out of the two, the former seems simpler, given the complications associated with engineering stem cells to initiate a specific cell type like hair cells and to insert them in an already established complicated tissue system. Nevertheless, devising repair methods to revive damaged hair cells still represents a steep research curve, which depends on deciphering the regulatory mechanism governing stereocilia actin dynamics.

REFERENCES

1. Dalton, D.S., et al., *The impact of hearing loss on quality of life in older adults.* Gerontologist, 2003. **43**(5): p. 661-8.
2. Bielefeld, E.C., et al., *Age-related hearing loss: is it a preventable condition?* Hear Res, 2010. **264**(1-2): p. 98-107.
3. Henry, K.R. and R.A. Chole, *Genotypic differences in behavioral, physiological and anatomical expressions of age-related hearing loss in the laboratory mouse.* Audiology, 1980. **19**(5): p. 369-83.
4. Johnson, K.R., et al., *A major gene affecting age-related hearing loss in C57BL/6J mice.* Hear Res, 1997. **114**(1-2): p. 83-92.
5. Hequembourg, S. and M.C. Liberman, *Spiral ligament pathology: a major aspect of age-related cochlear degeneration in C57BL/6 mice.* J Assoc Res Otolaryngol, 2001. **2**(2): p. 118-29.
6. Mikaelian, D.O., *Development and degeneration of hearing in the C57/b16 mouse: relation of electrophysiologic responses from the round window and cochlear nucleus to cochlear anatomy and behavioral responses.* Laryngoscope, 1979. **89**(1): p. 1-15.
7. Wang, J., et al., *Over-expression of X-linked inhibitor of apoptosis protein slows presbycusis in C57BL/6J mice.* Neurobiol Aging, 2010. **31**(7): p. 1238-49.
8. Willott, J.F., *Effects of aging, hearing loss, and anatomical location on thresholds of inferior colliculus neurons in C57BL/6 and CBA mice.* J Neurophysiol, 1986. **56**(2): p. 391-408.
9. Spongr, V.P., et al., *Quantitative measures of hair cell loss in CBA and C57BL/6 mice throughout their life spans.* J Acoust Soc Am, 1997. **101**(6): p. 3546-53.
10. Li, H.S. and E. Borg, *Age-related loss of auditory sensitivity in two mouse genotypes.* Acta Otolaryngol, 1991. **111**(5): p. 827-34.
11. Zheng, Q.Y., K.R. Johnson, and L.C. Erway, *Assessment of hearing in 80 inbred strains of mice by ABR threshold analyses.* Hear Res, 1999. **130**(1-2): p. 94-107.
12. Kane, K.L., et al., *Genetic background effects on age-related hearing loss associated with Cdh23 variants in mice.* Hear Res, 2012. **283**(1-2): p. 80-8.
13. Johnson, K.R., et al., *A locus on distal chromosome 11 (ahl8) and its interaction with Cdh23 ahl underlie the early onset, age-related hearing loss of DBA/2J mice.* Genomics, 2008. **92**(4): p. 219-25.
14. Johnson, K.R., C.M. Longo-Guess, and L.H. Gagnon, *A QTL on Chr 5 modifies hearing loss associated with the fascin-2 variant of DBA/2J mice.* Mamm Genome, 2015. **26**(7-8): p. 338-47.
15. Raviv, D., A.A. Dror, and K.B. Avraham, *Hearing loss: a common disorder caused by many rare alleles.* Ann N Y Acad Sci, 2010. **1214**: p. 168-79.
16. McGrath, J., P. Roy, and B.J. Perrin, *Stereocilia morphogenesis and maintenance through regulation of actin stability.* Semin Cell Dev Biol, 2017. **65**: p. 88-95.
17. Fettiplace, R., *Hair Cell Transduction, Tuning, and Synaptic Transmission in the Mammalian Cochlea.* Compr Physiol, 2017. **7**(4): p. 1197-1227.

18. Cunningham, C.L. and U. Muller, *Molecular Structure of the Hair Cell Mechanoelectrical Transduction Complex.* Cold Spring Harb Perspect Med, 2018.
19. Pickles, J.O. and D.P. Corey, *Mechanoelectrical transduction by hair cells.* Trends Neurosci, 1992. **15**(7): p. 254-9.
20. Barr-Gillespie, P.G., *Assembly of hair bundles, an amazing problem for cell biology.* Mol Biol Cell, 2015. **26**(15): p. 2727-32.
21. Burns, J.C. and J.S. Stone, *Development and regeneration of vestibular hair cells in mammals.* Semin Cell Dev Biol, 2017. **65**: p. 96-105.
22. Moravec, W.J. and E.H. Peterson, *Differences between stereocilia numbers on type I and type II vestibular hair cells.* J Neurophysiol, 2004. **92**(5): p. 3153-60.
23. Pollard, T.D., *Actin and Actin-Binding Proteins.* Cold Spring Harb Perspect Biol, 2016. **8**(8).
24. Flock, A. and H.C. Cheung, *Actin filaments in sensory hairs of inner ear receptor cells.* J Cell Biol, 1977. **75**(2 Pt 1): p. 339-43.
25. Rzadzinska, A.K., et al., *An actin molecular treadmill and myosins maintain stereocilia functional architecture and self-renewal.* J Cell Biol, 2004. **164**(6): p. 887-97.
26. Schneider, M.E., et al., *Rapid renewal of auditory hair bundles.* Nature, 2002. **418**(6900): p. 837-8.
27. Drummond, M.C., et al., *Live-cell imaging of actin dynamics reveals mechanisms of stereocilia length regulation in the inner ear.* Nat Commun, 2015. **6**: p. 6873.
28. Narayanan, P., et al., *Length regulation of mechanosensitive stereocilia depends on very slow actin dynamics and filament-severing proteins.* Nat Commun, 2015. **6**: p. 6855.
29. Zhang, D.S., et al., *Multi-isotope imaging mass spectrometry reveals slow protein turnover in hair-cell stereocilia.* Nature, 2012. **481**(7382): p. 520-4.
30. Belyantseva, I.A., et al., *Myosin-XVa is required for tip localization of whirlin and differential elongation of hair-cell stereocilia.* Nat Cell Biol, 2005. **7**(2): p. 148-56.
31. Delprat, B., et al., *Myosin XVa and whirlin, two deafness gene products required for hair bundle growth, are located at the stereocilia tips and interact directly.* Hum Mol Genet, 2005. **14**(3): p. 401-10.
32. Manor, U., et al., *Regulation of stereocilia length by myosin XVa and whirlin depends on the actin-regulatory protein Eps8.* Curr Biol, 2011. **21**(2): p. 167-72.
33. Zampini, V., et al., *Eps8 regulates hair bundle length and functional maturation of mammalian auditory hair cells.* PLoS Biol, 2011. **9**(4): p. e1001048.
34. Fang, Q., et al., *The 133-kDa N-terminal domain enables myosin 15 to maintain mechanotransducing stereocilia and is essential for hearing.* Elife, 2015. **4**.
35. Furness, D.N., et al., *Progressive hearing loss and gradual deterioration of sensory hair bundles in the ears of mice lacking the actin-binding protein Eps8L2.* Proc Natl Acad Sci U S A, 2013. **110**(34): p. 13898-903.
36. Schafer, D.A., P.B. Jennings, and J.A. Cooper, *Dynamics of capping protein and actin assembly in vitro: uncapping barbed ends by polyphosphoinositides.* J Cell Biol, 1996. **135**(1): p. 169-79.
37. Avenarius, M.R., et al., *Correlation of actin crosslinker and capper expression levels with stereocilia growth phases.* Mol Cell Proteomics, 2014. **13**(2): p. 606-20.
38. Peng, A.W., et al., *Twinfilin 2 regulates actin filament lengths in cochlear stereocilia.* J Neurosci, 2009. **29**(48): p. 15083-8.

39. Rzadzinska, A.K., et al., *MyosinVIIa interacts with Twinfilin-2 at the tips of mechanosensory stereocilia in the inner ear.* PLoS One, 2009. **4**(9): p. e7097.
40. Kitajiri, S., et al., *Actin-bundling protein TRIOBP forms resilient rootlets of hair cell stereocilia essential for hearing.* Cell, 2010. **141**(5): p. 786-98.
41. Pataky, F., R. Pironkova, and A.J. Hudspeth, *Radixin is a constituent of stereocilia in hair cells.* Proc Natl Acad Sci U S A, 2004. **101**(8): p. 2601-6.
42. Zhao, H., et al., *Large membrane domains in hair bundles specify spatially constricted radixin activation.* J Neurosci, 2012. **32**(13): p. 4600-9.
43. Marcotti, W., et al., *The acquisition of mechano-electrical transducer current adaptation in auditory hair cells requires myosin VI.* J Physiol, 2016. **594**(13): p. 3667-81.
44. Zhao, B., Z. Wu, and U. Muller, *Murine Fam65b forms ring-like structures at the base of stereocilia critical for mechanosensory hair cell function.* Elife, 2016. **5**.
45. Goodyear, R.J., et al., *Hair bundle defects and loss of function in the vestibular end organs of mice lacking the receptor-like inositol lipid phosphatase PTPRQ.* J Neurosci, 2012. **32**(8): p. 2762-72.
46. Salles, F.T., et al., *CLIC5 stabilizes membrane-actin filament linkages at the base of hair cell stereocilia in a molecular complex with radixin, taperin, and myosin VI.* Cytoskeleton (Hoboken), 2014. **71**(1): p. 61-78.
47. !!! INVALID CITATION !!! {Fettiplace, 2006 #86;Fettiplace, 2017 #62;Gillespie, 2009 #185}.
48. Kazmierczak, P., et al., *Cadherin 23 and protocadherin 15 interact to form tip-link filaments in sensory hair cells.* Nature, 2007. **449**(7158): p. 87-91.
49. Alagramam, K.N., et al., *Mutations in protocadherin 15 and cadherin 23 affect tip links and mechanotransduction in mammalian sensory hair cells.* PLoS One, 2011. **6**(4): p. e19183.
50. Siemens, J., et al., *Cadherin 23 is a component of the tip link in hair-cell stereocilia.* Nature, 2004. **428**(6986): p. 950-5.
51. Holme, R.H. and K.P. Steel, *Progressive hearing loss and increased susceptibility to noise-induced hearing loss in mice carrying a Cdh23 but not a Myo7a mutation.* J Assoc Res Otolaryngol, 2004. **5**(1): p. 66-79.
52. Gillespie, P.G. and U. Muller, *Mechanotransduction by hair cells: models, molecules, and mechanisms.* Cell, 2009. **139**(1): p. 33-44.
53. Grati, M. and B. Kachar, *Myosin VIIa and sans localization at stereocilia upper tip-link density implicates these Usher syndrome proteins in mechanotransduction.* Proc Natl Acad Sci U S A, 2011. **108**(28): p. 11476-81.
54. Caberlotto, E., et al., *Coupling of the mechanotransduction machinery and F-actin polymerization in the cochlear hair bundles.* Bioarchitecture, 2011. **1**(4): p. 169-174.
55. Grillet, N., et al., *Harmonin mutations cause mechanotransduction defects in cochlear hair cells.* Neuron, 2009. **62**(3): p. 375-87.
56. Verpy, E., et al., *A defect in harmonin, a PDZ domain-containing protein expressed in the inner ear sensory hair cells, underlies Usher syndrome type 1C.* Nat Genet, 2000. **26**(1): p. 51-5.
57. Boeda, B., et al., *Myosin VIIa, harmonin and cadherin 23, three Usher I gene products that cooperate to shape the sensory hair cell bundle.* Embo j, 2002. **21**(24): p. 6689-99.
58. Indzhykulian, A.A., et al., *Molecular remodeling of tip links underlies mechanosensory regeneration in auditory hair cells.* PLoS Biol, 2013. **11**(6): p. e1001583.

59. Miyasaka, Y., et al., *Compound heterozygosity of the functionally null Cdh23(v-ngt) and hypomorphic Cdh23(ahl) alleles leads to early-onset progressive hearing loss in mice.* Exp Anim, 2013. **62**(4): p. 333-46.
60. Perrin, B.J., et al., *beta-Actin and fascin-2 cooperate to maintain stereocilia length.* J Neurosci, 2013. **33**(19): p. 8114-21.
61. Shin, J.B., et al., *Molecular architecture of the chick vestibular hair bundle.* Nat Neurosci, 2013. **16**(3): p. 365-74.
62. Tilney, L.G., D.J. Derosier, and M.J. Mulroy, *The organization of actin filaments in the stereocilia of cochlear hair cells.* J Cell Biol, 1980. **86**(1): p. 244-59.
63. Taylor, R., et al., *Absence of plastin 1 causes abnormal maintenance of hair cell stereocilia and a moderate form of hearing loss in mice.* Hum Mol Genet, 2015. **24**(1): p. 37-49.
64. Shin, J.B., et al., *The R109H variant of fascin-2, a developmentally regulated actin crosslinker in hair-cell stereocilia, underlies early-onset hearing loss of DBA/2J mice.* J Neurosci, 2010. **30**(29): p. 9683-94.
65. Francis, S.P., et al., *A short splice form of Xin-actin binding repeat containing 2 (XIRP2) lacking the Xin repeats is required for maintenance of stereocilia morphology and hearing function.* J Neurosci, 2015. **35**(5): p. 1999-2014.
66. Scheffer, D.I., et al., *XIRP2, an actin-binding protein essential for inner ear hair-cell stereocilia.* Cell Rep, 2015. **10**(11): p. 1811-8.
67. Zheng, L., et al., *The deaf jerker mouse has a mutation in the gene encoding the espin actin-bundling proteins of hair cell stereocilia and lacks espins.* Cell, 2000. **102**(3): p. 377-85.
68. Sekerkova, G., C.P. Richter, and J.R. Bartles, *Roles of the espin actin-bundling proteins in the morphogenesis and stabilization of hair cell stereocilia revealed in CBA/CaJ congenic jerker mice.* PLoS Genet, 2011. **7**(3): p. e1002032.
69. Jansen, S., et al., *Mechanism of actin filament bundling by fascin.* J Biol Chem, 2011. **286**(34): p. 30087-96.
70. Sedeh, R.S., et al., *Structure, evolutionary conservation, and conformational dynamics of Homo sapiens fascin-1, an F-actin crosslinking protein.* J Mol Biol, 2010. **400**(3): p. 589-604.
71. Aramaki, S., et al., *Filopodia formation by crosslinking of F-actin with fascin in two different binding manners.* Cytoskeleton (Hoboken), 2016. **73**(7): p. 365-74.
72. Courson, D.S. and R.S. Rock, *Actin cross-link assembly and disassembly mechanics for alpha-Actinin and fascin.* J Biol Chem, 2010. **285**(34): p. 26350-7.
73. Winkelman, J.D., et al., *Fascin- and alpha-Actinin-Bundled Networks Contain Intrinsic Structural Features that Drive Protein Sorting.* Curr Biol, 2016. **26**(20): p. 2697-2706.
74. Yang, S., et al., *Molecular mechanism of fascin function in filopodial formation.* J Biol Chem, 2013. **288**(1): p. 274-84.
75. Krey, J.F., et al., *Plastin 1 widens stereocilia by transforming actin filament packing from hexagonal to liquid.* J Cell Biol, 2016. **215**(4): p. 467-482.
76. Hwang, P., et al., *The Stereociliary Paracrystal Is a Dynamic Cytoskeletal Scaffold In Vivo.* Cell Rep, 2015. **13**(7): p. 1287-1294.
77. Otani, T., et al., *IKKepsilon inhibits PKC to promote Fascin-dependent actin bundling.* Development, 2016. **143**(20): p. 3806-3816.
78. Lin, S., et al., *Monoubiquitination Inhibits the Actin Bundling Activity of Fascin.* J Biol Chem, 2016. **291**(53): p. 27323-27333.

79. Noben-Trauth, K., Q.Y. Zheng, and K.R. Johnson, *Association of cadherin 23 with polygenic inheritance and genetic modification of sensorineural hearing loss.* Nat Genet, 2003. **35**(1): p. 21-3.
80. Chou, S.W., et al., *Fascin 2b is a component of stereocilia that lengthens actin-based protrusions.* PLoS One, 2011. **6**(4): p. e14807.
81. Bartles, J.R., A. Wierda, and L. Zheng, *Identification and characterization of espin, an actin-binding protein localized to the F-actin-rich junctional plaques of Sertoli cell ectoplasmic specializations.* J Cell Sci, 1996. **109 (Pt 6)**: p. 1229-39.
82. Chen, B., et al., *Espin contains an additional actin-binding site in its N terminus and is a major actin-bundling protein of the Sertoli cell-spermatid ectoplasmic specialization junctional plaque.* Mol Biol Cell, 1999. **10**(12): p. 4327-39.
83. Sekerkova, G., et al., *Espins are multifunctional actin cytoskeletal regulatory proteins in the microvilli of chemosensory and mechanosensory cells.* J Neurosci, 2004. **24**(23): p. 5445-56.
84. Sekerkova, G., et al., *Espins and the actin cytoskeleton of hair cell stereocilia and sensory cell microvilli.* Cell Mol Life Sci, 2006. **63**(19-20): p. 2329-41.
85. Salles, F.T., et al., *Myosin IIIa boosts elongation of stereocilia by transporting espin 1 to the plus ends of actin filaments.* Nat Cell Biol, 2009. **11**(4): p. 443-50.
86. Zheng, L., D.M. Beeler, and J.R. Bartles, *Characterization and regulation of an additional actin-filament-binding site in large isoforms of the stereocilia actin-bundling protein espin.* J Cell Sci, 2014. **127**(Pt 6): p. 1306-17.
87. Bartles, J.R., et al., *Small espin: a third actin-bundling protein and potential forked protein ortholog in brush border microvilli.* J Cell Biol, 1998. **143**(1): p. 107-19.
88. Loomis, P.A., et al., *Targeted wild-type and jerker espins reveal a novel, WH2-domain-dependent way to make actin bundles in cells.* J Cell Sci, 2006. **119**(Pt 8): p. 1655-65.
89. Sekerkova, G., et al., *Differential expression of espin isoforms during epithelial morphogenesis, stereociliogenesis and postnatal maturation in the developing inner ear.* Dev Biol, 2006. **291**(1): p. 83-95.
90. Ebrahim, S., et al., *Stereocilia-staircase spacing is influenced by myosin III motors and their cargos espin-1 and espin-like.* Nat Commun, 2016. **7**: p. 10833.
91. Shepherd, G.M., B.A. Barres, and D.P. Corey, *"Bundle blot" purification and initial protein characterization of hair cell stereocilia.* Proc Natl Acad Sci U S A, 1989. **86**(13): p. 4973-7.
92. Namba, Y., et al., *Human T cell L-plastin bundles actin filaments in a calcium-dependent manner.* J Biochem, 1992. **112**(4): p. 503-7.
93. Daudet, N. and M.C. Lebart, *Transient expression of the t-isoform of plastins/fimbrin in the stereocilia of developing auditory hair cells.* Cell Motil Cytoskeleton, 2002. **53**(4): p. 326-36.
94. Bretscher, A. and K. Weber, *Fimbrin, a new microfilament-associated protein present in microvilli and other cell surface structures.* J Cell Biol, 1980. **86**(1): p. 335-40.
95. Pacholsky, D., et al., *Xin repeats define a novel actin-binding motif.* J Cell Sci, 2004. **117**(Pt 22): p. 5257-68.
96. Wang, Q., et al., *Xin proteins and intercalated disc maturation, signaling and diseases.* Front Biosci (Landmark Ed), 2012. **17**: p. 2566-93.
97. Cherepanova, O., et al., *Xin-repeats and nebulin-like repeats bind to F-actin in a similar manner.* J Mol Biol, 2006. **356**(3): p. 714-23.

98. Avenarius, M.R., et al., *Heterodimeric capping protein is required for stereocilia length and width regulation.* J Cell Biol, 2017. **216**(11): p. 3861-3881.
99. Mburu, P., et al., *Gelsolin plays a role in the actin polymerization complex of hair cell stereocilia.* PLoS One, 2010. **5**(7): p. e11627.
100. Perrin, B.J. and J.M. Ervasti, *The actin gene family: function follows isoform.* Cytoskeleton (Hoboken), 2010. **67**(10): p. 630-4.
101. Buxbaum, A.R., B. Wu, and R.H. Singer, *Single beta-actin mRNA detection in neurons reveals a mechanism for regulating its translatability.* Science, 2014. **343**(6169): p. 419-22.
102. Zhang, F., et al., *Differential arginylation of actin isoforms is regulated by coding sequence-dependent degradation.* Science, 2010. **329**(5998): p. 1534-7.
103. Bergeron, S.E., et al., *Ion-dependent polymerization differences between mammalian beta- and gamma-nonmuscle actin isoforms.* J Biol Chem, 2010. **285**(21): p. 16087-95.
104. Karakozova, M., et al., *Arginylation of beta-actin regulates actin cytoskeleton and cell motility.* Science, 2006. **313**(5784): p. 192-6.
105. Condeelis, J. and R.H. Singer, *How and why does beta-actin mRNA target?* Biol Cell, 2005. **97**(1): p. 97-110.
106. Hill, M.A. and P. Gunning, *Beta and gamma actin mRNAs are differentially located within myoblasts.* J Cell Biol, 1993. **122**(4): p. 825-32.
107. Kislauskis, E.H., X. Zhu, and R.H. Singer, *beta-Actin messenger RNA localization and protein synthesis augment cell motility.* J Cell Biol, 1997. **136**(6): p. 1263-70.
108. Bunnell, T.M., et al., *beta-Actin specifically controls cell growth, migration, and the G-actin pool.* Mol Biol Cell, 2011. **22**(21): p. 4047-58.
109. Patrinostro, X., et al., *Relative importance of betacyto- and gammacyto-actin in primary mouse embryonic fibroblasts.* Mol Biol Cell, 2017. **28**(6): p. 771-782.
110. Bunnell, T.M. and J.M. Ervasti, *Delayed embryonic development and impaired cell growth and survival in Actg1 null mice.* Cytoskeleton (Hoboken), 2010. **67**(9): p. 564-72.
111. Perrin, B.J., K.J. Sonnemann, and J.M. Ervasti, *beta-actin and gamma-actin are each dispensable for auditory hair cell development but required for Stereocilia maintenance.* PLoS Genet, 2010. **6**(10): p. e1001158.
112. Shmerling, D., et al., *Strong and ubiquitous expression of transgenes targeted into the beta-actin locus by Cre/lox cassette replacement.* Genesis, 2005. **42**(4): p. 229-35.
113. Shawlot, W., et al., *Restricted beta-galactosidase expression of a hygromycin-lacZ gene targeted to the beta-actin locus and embryonic lethality of beta-actin mutant mice.* Transgenic Res, 1998. **7**(2): p. 95-103.
114. Belyantseva, I.A., et al., *Gamma-actin is required for cytoskeletal maintenance but not development.* Proc Natl Acad Sci U S A, 2009. **106**(24): p. 9703-8.
115. Roy, P. and B.J. Perrin, *The stable actin core of mechanosensory stereocilia features continuous turnover of actin cross-linkers.* Mol Biol Cell, 2018. **29**(15): p. 1856-1865.
116. Schwander, M., B. Kachar, and U. Muller, *Review series: The cell biology of hearing.* J Cell Biol, 2010. **190**(1): p. 9-20.
117. Beurg, M., et al., *Localization of inner hair cell mechanotransducer channels using high-speed calcium imaging.* Nat Neurosci, 2009. **12**(5): p. 553-8.
118. Kazmierczak, P. and U. Muller, *Sensing sound: molecules that orchestrate mechanotransduction by hair cells.* Trends Neurosci, 2012. **35**(4): p. 220-9.

119. Schnutgen, F., et al., *A directional strategy for monitoring Cre-mediated recombination at the cellular level in the mouse.* Nat Biotechnol, 2003. **21**(5): p. 562-5.
120. Schnutgen, F. and N.B. Ghyselinck, *Adopting the good reFLEXes when generating conditional alterations in the mouse genome.* Transgenic Res, 2007. **16**(4): p. 405-13.
121. Matei, V., et al., *Smaller inner ear sensory epithelia in Neurog 1 null mice are related to earlier hair cell cycle exit.* Dev Dyn, 2005. **234**(3): p. 633-50.
122. Schmoller, K.M., C. Semmrich, and A.R. Bausch, *Slow down of actin depolymerization by cross-linking molecules.* J Struct Biol, 2011. **173**(2): p. 350-7.
123. Patrinostro, X., et al., *Essential nucleotide- and protein-dependent functions of Actb/beta-actin.* Proc Natl Acad Sci U S A, 2018. **115**(31): p. 7973-7978.
124. Pollard, T.D. and J.A. Cooper, *Actin, a central player in cell shape and movement.* Science, 2009. **326**(5957): p. 1208-12.
125. Cuvertino, S., et al., *ACTB Loss-of-Function Mutations Result in a Pleiotropic Developmental Disorder.* Am J Hum Genet, 2017. **101**(6): p. 1021-1033.
126. Di Donato, N., et al., *Severe forms of Baraitser-Winter syndrome are caused by ACTB mutations rather than ACTG1 mutations.* Eur J Hum Genet, 2014. **22**(2): p. 179-83.
127. Riviere, J.B., et al., *De novo mutations in the actin genes ACTB and ACTG1 cause Baraitser-Winter syndrome.* Nat Genet, 2012. **44**(4): p. 440-4, s1-2.
128. Ross, A.F., et al., *Characterization of a beta-actin mRNA zipcode-binding protein.* Mol Cell Biol, 1997. **17**(4): p. 2158-65.
129. Vedula, P., et al., *Diverse functions of homologous actin isoforms are defined by their nucleotide, rather than their amino acid sequence.* Elife, 2017. **6**.
130. Kapustina, M., T.A. Read, and E.A. Vitriol, *Simultaneous quantification of actin monomer and filament dynamics with modeling-assisted analysis of photoactivation.* J Cell Sci, 2016. **129**(24): p. 4633-4643.
131. Cheever, T.R., B. Li, and J.M. Ervasti, *Restricted morphological and behavioral abnormalities following ablation of beta-actin in the brain.* PLoS One, 2012. **7**(3): p. e32970.
132. Prins, K.W., et al., *Quadriceps myopathy caused by skeletal muscle-specific ablation of beta(cyto)-actin.* J Cell Sci, 2011. **124**(Pt 6): p. 951-7.
133. Olson, E.N. and A. Nordheim, *Linking actin dynamics and gene transcription to drive cellular motile functions.* Nat Rev Mol Cell Biol, 2010. **11**(5): p. 353-65.
134. O'Rourke, A.R., et al., *Impaired muscle relaxation and mitochondrial fission associated with genetic ablation of cytoplasmic actin isoforms.* Febs j, 2018. **285**(3): p. 481-500.
135. Kislauskis, E.H., X. Zhu, and R.H. Singer, *Sequences responsible for intracellular localization of beta-actin messenger RNA also affect cell phenotype.* J Cell Biol, 1994. **127**(2): p. 441-51.
136. Artman, L., et al., *Planning your every move: the role of beta-actin and its post-transcriptional regulation in cell motility.* Semin Cell Dev Biol, 2014. **34**: p. 33-43.
137. Ampe, C. and M. Van Troys, *Mammalian Actins: Isoform-Specific Functions and Diseases.* Handb Exp Pharmacol, 2017. **235**: p. 1-37.
138. Jepsen, L., et al., *Two Deafness-Causing Actin Mutations (DFNA20/26) Have Allosteric Effects on the Actin Structure.* Biophys J, 2016. **111**(2): p. 323-332.
139. Johnston, J.J., et al., *Functional analysis of a de novo ACTB mutation in a patient with atypical Baraitser-Winter syndrome.* Hum Mutat, 2013. **34**(9): p. 1242-9.

140. Rubenstein, P.A. and K.K. Wen, *Insights into the effects of disease-causing mutations in human actins.* Cytoskeleton (Hoboken), 2014. **71**(4): p. 211-29.
141. Velez-Ortega, A.C., et al., *Mechanotransduction current is essential for stability of the transducing stereocilia in mammalian auditory hair cells.* Elife, 2017. **6**.
142. Muller, M., et al., *Distinct functional interactions between actin isoforms and nonsarcomeric myosins.* PLoS One, 2013. **8**(7): p. e70636.
143. Lowe, D.A., et al., *Eccentric contraction-induced injury of mouse soleus muscle: effect of varying [Ca2+] o.* Journal of Applied Physiology, 1994. **76**(4): p. 1445-1453.
144. Gale, J.E., et al., *Survival of bundleless hair cells and subsequent bundle replacement in the bullfrog's saccule.* J Neurobiol, 2002. **50**(2): p. 81-92.
145. Jia, S., et al., *Fate of mammalian cochlear hair cells and stereocilia after loss of the stereocilia.* J Neurosci, 2009. **29**(48): p. 15277-85.